KONINKLIJK BELGISCH INSTITUUT VOOR NATUURWETENSCHAPPEN
OD NATUUR – BEHEERSEENHEID VAN HET MATEMATISCH MODEL

MOnitoring en MOdellering van het cohesieve sedimenttransport en evaluatie van de effecten op het mariene ecosysteem ten gevolge van bagger- en stortoperatie (MOMO)

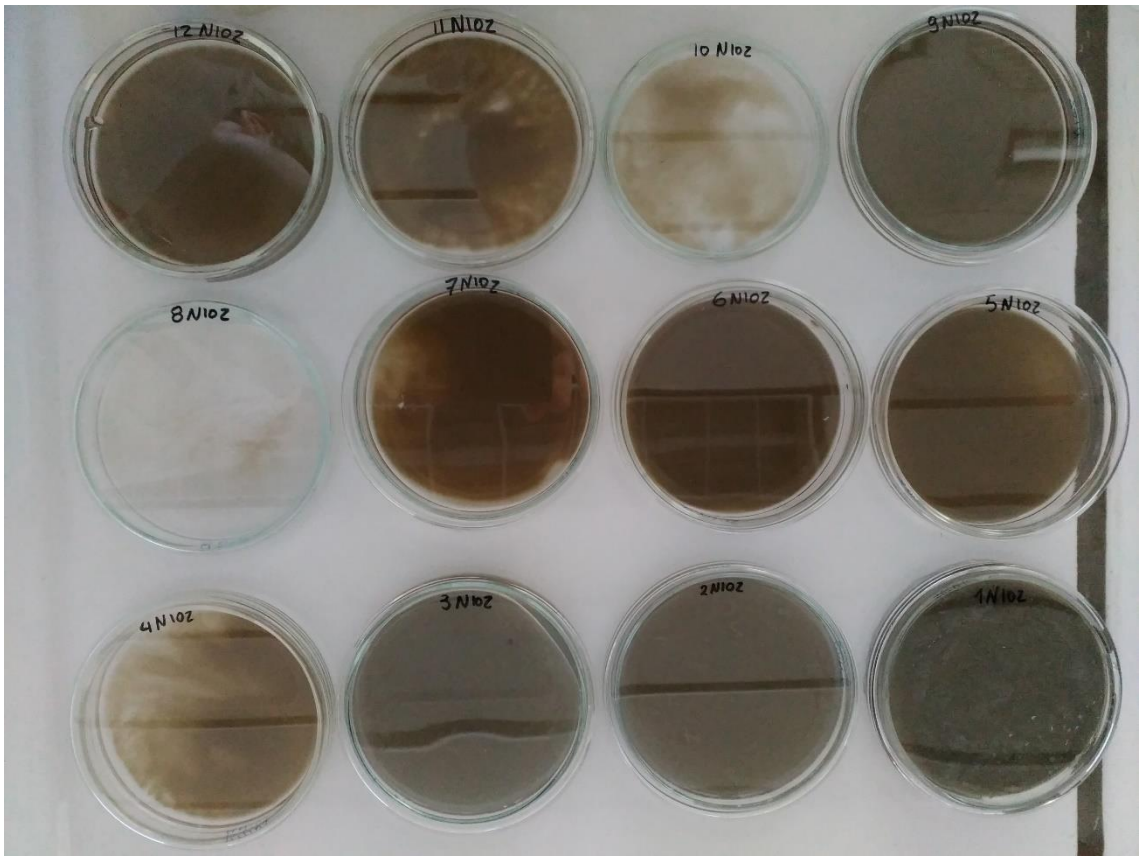

Activiteitsrapport (1 januari - 30 juni 2020)

Michael Fettweis, Argiro Adamopoulou, Matthias Baeye, Koen Parmentier, Dries Van den Eynde

MOMO/9/MF/202010/NL/AR/3

KBIN-OD Natuur - BMM
Vautierstraat 29
B–1000 Brussel
België

Inhoudstafel

1. Inleiding

1.1. Voorwerp van deze opdracht

Het MOMO-project (monitoring en modellering van het cohesieve sedimenttransport en de evaluatie van de effecten op het mariene ecosysteem ten gevolge van bagger- en stortoperatie) maakt deel uit van de algemene en permanente verplichtingen van monitoring en evaluatie van de effecten van alle menselijke activiteiten op het mariene ecosysteem waaraan België gebonden is overeenkomstig het verdrag inzake de bescherming van het mariene milieu van de noordoostelijke Atlantische Oceaan (1992, OSPAR-Verdrag). De OSPAR Commissie heeft de objectieven van haar Joint Assessment and Monitoring Programme (JAMP) gedefinieerd tot 2021 met de publicatie van een holistisch "quality status report" van de Noordzee en waarvoor de federale overheid en de gewesten technische en wetenschappelijke bijdragen moeten afleveren ten laste van hun eigen middelen.

De menselijke activiteit die hier in het bijzonder wordt beoogd, is het storten in zee van baggerspecie waarvoor OSPAR een uitzondering heeft gemaakt op de algemene regel "alle stortingen in zee zijn verboden" (zie OSPAR-Verdrag, Bijlage II over de voorkoming en uitschakeling van verontreiniging door storting of verbranding). Het algemene doel van de opdracht is het bestuderen van de cohesieve sedimenten op het Belgisch Continentaal Plat (BCP) en dit met behulp van zowel numerieke modellen als het uitvoeren van metingen. De combinatie van monitoring en modellering zal gegevens kunnen aanleveren over de transportprocessen van deze fijne fractie en is daarom fundamenteel bij het beantwoorden van vragen over de samenstelling, de oorsprong en het verblijf ervan op het BCP, de veranderingen in de karakteristieken van dit sediment ten gevolge van de bagger- en stortoperaties, de effecten van de natuurlijke variabiliteit, de impact op het mariene ecosysteem in het bijzonder door de wijziging van habitats, de schatting van de netto input van gevaarlijke stoffen op het mariene milieu en de mogelijkheden om deze laatste twee te beperken.

Een samenvatting van de resultaten uit de vergunningsperioden 2017-2021 kan gevonden worden in het "Vooruitgangsrapport (juni 2019) over de effecten op het mariene milieu van baggerspeciestortingen" (Lauwaert et al. 2019) dat gepubliceerd werden conform art. 10 van het K.B. van 12 maart 2000 ter definiëring van de procedure voor machtiging van het storten in de Noordzee van bepaalde stoffen en materialen. Een tussentijdsrapport voor de vergunningsperiode

1.2. Algemene doelstellingen

Het onderzoek kadert in de algemene doelstellingen om de baggerwerken op het BCP en in de kusthavens te verminderen en om een gedetailleerd inzicht te verwerven van de fysische processen die plaatsvinden in het mariene kader waarbinnen deze baggerwerken worden uitgevoerd. Dit impliceert enerzijds beleidsondersteunend onderzoek naar de vermindering van de sedimentatie op de baggerplaatsen en het evalueren van alternatieve stortmethoden. Anderzijds is onderzoek naar knelpunten voor het plannen en schatten van de effecten van de baggerwerken vereist. Dit is specifiek gericht op het dynamische gedrag van silb in de waterkolom en op de bodem en zal uitgevoerd worden met behulp van modellen en in situ metingen. De specifieke acties die binnen dit onderzoek uitgevoerd worden om de algemene doelstellingen in te vullen zijn:

1. Streven naar een efficiënter stortbeleid door een optimalisatie van de stortlocaties.

2. Continue monitoring van het fysisch-sedimentologische milieu waarbinnen de baggerwerken worden uitgevoerd (Taak 1) en aanpassing van de monitoring aan de nog op te stellen targets voor het bereiken van de goede milieutoestand (GES), zoals gedefinieerd zal worden binnen MSFD;

3. Uitbouw en optimalisatie van het numerieke modelinstrumentarium, ter ondersteuning van het onderzoek (Taak 2.1).

1.3. Algemeen Onderzoek 2017-2021

Voor de vergunningsperiode 2017-2021 werden volgende taken voorzien:

1) In situ en remote sensing metingen en data-analyse
De monitoring van effecten van baggerspeciestortingen gebeurd met behulp van een vast meetstation in de nabijheid van MOW1, en met meetcampagnes met de RV Belgica (een 4-tal meetcampagnes voor het verzamelen van traject informatie, profielen en de calibratie van sensoren; en een 10-tal campagnes voor het onderhoud van het meetstation te MOW1). De geplande monitoring is gericht op het begrijpen van processen, zodoende dat de waargenomen variabiliteit en de effecten van baggerspeciestortingen in een correct kader geplaatst kunnen worden. Een belangrijk deel is daarom gericht op zowel het uitvoeren van de in situ metingen, het garanderen van kwalitatief hoogwaardige data en het archiveren, rapporteren en interpreteren ervan. Remote sensing data afkomstig van onder andere satellieten worden gebruikt om een ruimtelijk beeld te bekomen.

2) Uitbouw en optimalisatie van het modelinstrumentarium
Het tijdens de voorbije jaren verbeterde en aangepaste slibtransportmodel zal verder worden ontwikkeld. Dit zal parallel gebeuren met de nieuwe inzichten die voorvloeien uit de metingen en de procesgerichte interpretatie van de metingen.

3) Ondersteunend wetenschappelijke onderzoek
Monitoring gebaseerd op wetenschappelijke kennis is essentieel om de effecten van menselijke activiteiten (hier het storten van baggerspecie) te kunnen inschatten en beheren. Om te kunnen voldoen aan de door OSPAR opgelegde verplichtingen van monitoring en evaluatie van de effecten van menselijke activiteiten is het ontwikkelen van nieuwe monitorings- en modelleractiviteiten nodig. Dit houdt in dat onderzoek dat de actuele stand van de wetenschappelijke kennis weerspiegelt wordt uitgevoerd en dat de hieruit voortvloeiende nieuwe ontwikkelingen geïntegreerd zullen worden in zowel de verbetering van het modelinstrumentarium als voor het beter begrijpen van het fysisch milieu.

1.4. Onderzoek Januari 2019 – December 2021

Het onderzoek uitgevoerd tijdens de periode 2017-2018 werd gerapporteerd in Fettweis et al. (2017, 2018a, 2018b, 2019). Voor de periode 2019-2021 werd in overleg met de ambtelijke werkgroep baggeren een nieuw takenpakket opgesteld waarbij rekening gehouden werd met de aanbevelingen voor de minister ter ondersteuning van de ontwikkeling van een versterkt milieubeleid zoals geformuleerd in het “Syntheserapport over de effecten op het mariene milieu van baggerspeciestortingen (2016)” dat uitgevoerd werd conform art. 10 van het K.B. van 12 maart 2000 ter definiëring van de procedure voor machtiging van het storten in de Noordzee van bepaalde stoffen en materialen.

Taak 1: In situ en remote sensing metingen en data-analyse

Taak 1.1 Langdurige metingen

Sinds eind 2009 worden er continue metingen uitgevoerd te MOW1 met behulp van een meetframe (tripode). Met dit frame worden stromingen, slibconcentratie, korrelgrootteverdeling van het suspensiemateriaal, saliniteit, temperatuur, waterdiepte en zeebodem altimetrie gemeten. Om een continue tijdreeks te hebben, wordt gebruik gemaakt van 2 tripodes. Na ongeveer 1 maand wordt de verankerde tripode voor onderhoud aan wal gebracht en wordt de tweede op de meetlocatie verankerd. Op de meetdata wordt een kwaliteitsanalyse uitgevoerd, zodat de goede data onderscheiden kunnen worden van slechte of niet betrouwbare data.

Taak 1.2 Calibratie van sensoren tijdens in situ metingen

Tijdens 11 meetcampagnes per jaar met de R/V Belgica zullen een 13-uursmetingen uitgevoerd worden met doel het calibreren van optische of akoestische sensoren en het verzamelen van verticale profielen. De metingen zullen plaatsvinden in een drietal punten gelegen op het BCP (zie Taak 3.1). De optische metingen (Optical Backscatter Sensor) zullen gecalibreerd worden met de opgemeten hoeveelheid materie in suspensie (gravimetrische bepalingen na filtratie) om te komen tot massa concentraties. Naast de totale hoeveelheid

aan suspensiemateriaal (SPM) wordt ook de concentratie aan POC/PON, chlorophyl (Chl-a, Chl-b), phaeofytine (a, b) en Transparante Exoploimerische Partikels (TEP) bepaald. Stalen van suspensiemateriaal zullen genomen worden met de centrifuge om de samenstelling ervan te bepalen.

Taak 1.3: Data archivering en rapportage

De meetdata worden gearchiveerd en er wordt een kwaliteitsanalyse uitgevoerd, zodat de goede data onderscheiden kunnen worden van slechte of niet betrouwbare data. Slechte data kunnen bv optreden doordat het instrument slecht heeft gewerkt en verkeerd werd ingesteld. Niet betrouwbare data zijn typisch geassicieerd met bv biofouling. De data en metadata worden gearchiveerd.

Taak 1.4: Verwerking en interpretatie van metingen

De metingen vergaard tijdens de 13-uursmetingen aan boord van de Belgica en met de tripode worden verwerkt en geïnterpreteerd. Hiervoor werden in het verleden reeds heel wat procedures (software) toegepast of ontwikkeld, zoals de berekening van de bodemschuifspanning uit turbulentiemetingen, entropieanalyse op partikelgrootteverdelingen, de opsplitising van multimodale partikelgrootteverdeling in een som van lognormale verdelingen, het groeperen van de data volgens getij, meteorologie, klimatologie en seizoenen. Deze methodes (zullen opgenomen worden) zijn opgenomen in de standaardverwerking van de data. De aldus verwerkte data dienen als basis voor het verder gebruik binnenin wetenschappelijke vragen (zie taak 2.2, 2.3 en 4.2, 4.4).

Taak 2: Uitbouw en optimalisatie van het modelinstrumentarium

Taak 2.1: Opstellen van een slibtransportmodel voor het BCP met Coherens V2

Ondertussen is de nieuwe implementatie van het Noordzeemodel (inclusief een submodel van de Belgische kustzone) gerealiseerd voor de hydrodynamica. In een volgende fase zal op basis van dit model het slibtransportmodel worden geïmplementeerd en gevalideerd. Verdere ontwikkelingen aan het model parallel met nieuwe inzichten die voorvloeien uit de metingen en de process gerichte interpretatie van de metingen zullen worden geïmplementeerd in het model.

Taak 2.2: Validatie van het slibtransportmodel voor het jaar 2013 (stortproef)

Een eerste toepassing van het model kan het jaar 2013 zijn, waarin de terreinproef voor alternatieve stortplaats alsook een intensieve monitoring plaatsvond. Deze laatste zal gebruikt worden voor de validatie van het model.

Taak 3: Ondersteunend wetenschappelijk onderzoek

Monitoring gebaseerd op wetenschappelijke kennis is essentieel om de effecten van menselijke activiteiten (hier het storten van baggerspecie) te kunnen inschatten en beheren. Om te kunnen voldoen aan de door OSPAR opgelegde verplichtingen van monitoring en evaluatie van de effecten van menselijke activiteiten is een verdere implementatie van huidige en het ontwikkelen van nieuwe monitoringsactiviteiten nodig. Meer specifiek gericht op de activiteit ‘storten van baggerspecie’ worden hier – wat het fysische milieu betreft - turbiditeit, samenstelling van de zeebodem, bathymetrie en hydrografische condities beoogt. Deze taak speelt hierop in door de ontwikkeling en de implementatie van nieuwe tools die de actuele stand van de wetenschappelijke kennis weerspiegelen teneinde de mathematische modellen te optimaliseren en verfijnen.

Taak 3.1: Intensieve bio-geo-chemische monitoring van het SPM in de overgangszone kust – offshore in 2019

Een sleutelelement in het functioneren van kustnabije ecosystemen is de aanwezigheid van biotische en abiotische partikels. Verticale en dus ook horizontale fluxen van particulair suspensiemateriaal (verder afgekort als SPM) worden bepaald door hun valsnelheid, die afhangt van de capaciteit van de deeltjes om te flocculeren. Flocculatie beïnvloed de grootte van de gesuspendeerde deeltjes en bepaald daardoor ook de depositie van het slib in onder andere havens en vaargeulen. Op zijn beurt wordt flocculatie gestuurd door turbulentie,

SPM concentratie en de oppervlakte eigenschappen van de deeltjes, die van electrochemische of biologische oorsprong kunnen zijn.

SPM bestaat uit minerale deeltjes van fysicochemische (b.v. kleimineralen, kwarts, veldspaat) en biogene oorsprong (b.v. calciet, aragoniet, opaal), levend (bacteriën, fyto- en zooplankton) en niet-levend organisch materiaal (b.v. fecale pellets, detritus, exopolymeren), en partikels van menselijke oorsprong (microplastiek). Het SPM kan door hydrofobe organische polluenten of metalen gecontamineerd zijn. De samenstelling en concentratie van het SPM inclusief de hydrofobe polluenten en de metalen verandert in functie van de tijd en de locatie. Deze variaties worden beïnvloed door de interacties tussen de fysische processen (getij, meteo, klimaat), biologische cycli (algenbloei), chemische processen (koolstofcyclus) en menselijke activiteiten (aanvoer van nutriënten en polluenten, bagger- en stortactiviteiten, offshore constructies). Het doel van deze taak is om een integrale monitoring uit te voeren in 2019 van de belangrijkste parameters die betrokken zijn bij de SPM-dynamica.

Een nieuw geïntegreerd monitoringsprogramma zal worden opgezet in vier stations (MOW1, W03, W05, W08), zie Figuur 1.1. Deze stations worden aanzien als zijnde representatief voor de belangrijkste gradiënten vanaf de kustzone (invloed van de Schelde) naar offshore (invloed van het Engels Kanaal) en zullen maandelijks bemonsterd worden. Gedurende 13 uur zullen om het uur waterstalen genomen worden aan de oppervlakte en bodem in stations MOW1, W05 en W08. De monitoring bevat alle parameters die nu reeds worden bepaald (maar niet noodzakelijk samen) op waterstalen (SPM, POC/PON, DOC/DON, Chl, TEP, nutriënten, pH) en met behulp van sensoren (CTD, OBS, ABS, LISST), en zullen aangevuld worden met Chl in sedimenten, de hydrofobe chemische polluenten (b.v. PAHs, PCBs) Verder wordt een monitoring voorzien van fysische parameters (ADCP/tripode) in de stations W05 en W08.

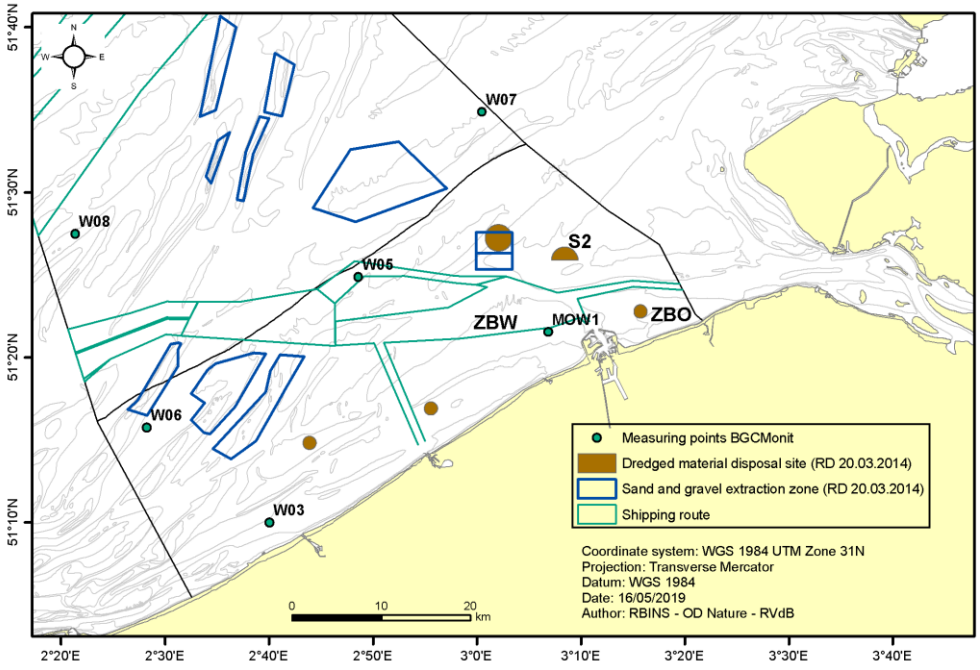

Figuur 1.1: BGC monitorings stations MOW1, W03, W05 en W08.

Door de verschillende monitoringsactiviteiten van OD Natuur/BMM (MOMO, WFD, MSFD, OSPAR en satellietvalidatie) te combineren en de monitoringsfrequentie en stations aan te passen worden de inspanningen geoptimaliseerd, blijven de legale verplichtingen en validatieprotocollen verzekerd, komen state-of-the-art wetenschappelijke vragen aan bod en wordt een bevattelijk dataset bekomen die alle gemeten parameters met elkaar verbindt. Na een eerste jaar van intensieve monitoring in 2019 zal het staalname schema geevalueerd worden voor alle parameters om aldus tot een kwalitatieve sprong in monitoringsstrategie te komen die tijdsgebonden veranderingen, invariante eigenschappen en ruimtelijke gradiënten kan identificeren. De belangrijkste wetenschappelijk vragen die aan

de grondslag liggen van deze monitoring zijn:

1. Hoe variëren de fysische, biologisch en chemische parameters in de waterkolom tijdens een getijcyclus en tijdens de seizoenen.
2. Waarom is het kustgebied troebel en wat is hierbij de link met de cross-shore gradiënten in fysische, biologische en chemische parameters.
3. Hoe beïnvloedt de SPM-concentratie de algenbloei (lichtreductie) en vice versa (TEP-productie)? Hoe moet het modelinstrumentarium (flocculatiemodule) worden aangepast om deze seizoenaliteit te kunnen modelleren.
4. Wat is de variabiliteit van de concentratie aan chemische polluenten in het SPM? Hoe beïnvloed de variabiliteit in SPM-concentratie en samenstelling de variabiliteit van de chemische polluenten?
5. Verbetering van remote sensing producten (SPM, Chl) door in situ validatie.

Taak 3.2: Monitoring stortplaats ZBW

De concentratie en samenstelling van het suspensie- en bodemmateriaal zal gemonitoord worden in de nabijheid van de nieuwe stortplaats ZBW. Afhankelijk van de keuze van de stortplaats kan de langdurige meetlocatie MOW1 hiervoor in aanmerking komen of kan een andere locatie gekozen worden als de veiligheid van de meetapparatuur kan gegarandeerd worden. Details hiervan zullen op een vergadering van de technische werkgroep besproken worden.

Taak 3.3: Ondersteuning kader rond Passende Beoordeling van stortactiviteiten

Ondersteuning zal gegeven worden voor het opstellen van de passende beoordeling voor de vergunningsplichtige stortactiviteiten. Dit houdt in het meewerken aan een schriftelijk verslag waarin aan de hand van gemotiveerde argumenten uitgelegd wordt of de Europese natuurwaarden in het vogelrichtlijngebied nabij Zeebrugge al dan niet betekenisvol worden aangetast door het storten van baggerspecie in zee. Meer specifiek zal onderzoek worden uitgevoerd over de verstoring van het eetgedrag van zeevogels door de verhoging van de turbiditeit die gepaard gaat met de baggerspeciestortingen.

Taak 3.4: Trends in SPM concentratie

Om significante statistische trends te kunnen documenteren in SPM concentratie over de laatste decades, zijn kwalitatief hoogstaande metingen nodig die een lange tijdspanne omvatten en over een groot gebied verdeeld zijn. Deze data zijn helaas niet beschikbaar. Wat er wel beschikbaar is zijn de tripode metingen te MOW1 (vanaf 2005) en op andere locaties, de puntmetingen verzamelt met onderzoeksschepen in het Belgisch Deel van de Noordzee sinds ongeveer 1970 (cf. Belspo 4DEMON project) en satellietbeelden (vanaf 1997). De tripode data geven de temporele variabiliteit weer, maar zijn heel beperkt wat ruimtelijke spreiding betreft. De 4DEMON en satellietbeelden zijn beschikbaar over een lange periode en over een groot gebied, maar kunnen de temporele schaal niet oplossen. Om deze heterogene datasets samen te kunnen gebruiken, zal gekeken worden naar de statistische verschillen tussen de datasets en naar een manier om deze te combineren. Doel is om mogelijke trends in de SPM concentratie te identificeren en deze te linken aan natuurlijke veranderingen of aan menselijke activiteiten.

Taak 4: Rapportage en outreach

Om de zes maanden zal er een activiteitenrapport worden opgesteld dat de onderzoeksresultaten beschrijft. Jaarlijks wordt er een 'factual data' rapport opgesteld van de verzamelde meetgegevens. De resultaten uit het onderzoek zullen tevens worden voorgesteld op workshops, conferenties en in de wetenschappelijke literatuur.

1.5. Gerapporteerde en uitgevoerde taken

Periode Januari 2019 – Juni 2019

Taak 1.1: De meetreeks te MOW1 werd verdergezet.

Taak 1.2: Calibratie van OBS sensoren werd uitgevoerd tijdens RV Begica campagnes 2019/01, 2019/03, 2019/07, 2019/11, 2019/14 en 2019/17.

Taak 2.1: Het 2 klassen population balance model van Lee at al. (2011) werd geïmplementeerd in Coherens V2 en gevalideerd met testcases.

Taak 3.1: Intensieve bio-geochemische monitoring werd uitgevoerd te MOW1 (RV Belgica campagnes 2019/01, 2019/03, 2019/07, 2019/11, 2019/14, 2019/17), W03 (RV Belgica campagnes 2019/03, 2019/11, 2019/14, 2019/17), W05 (2019/01, 2019/03, 2019/11, 2019/14, 2019/17) en W08 (2019/01, 2019/03, 2019/14, 2019/17).
De methode voor de TEP-analyse werd opgesteld en gevalideerd.

Periode Juli 2019 – December 2019

Taak 1.1: De meetreeks te MOW1 werd verdergezet.

Taak 1.2: Calibratie van OBS sensoren werd uitgevoerd tijdens RV Begica campagnes 2019/18, 2019/22, 2019/25, 2019/29 en 2019/32.

Taak 1.3: Data archivering en rapportage werd uitgevoerd.

Taak 1.4: Verwerking en interpretatie van de tripode meetdata 2016-2018.

Taak 2.1: Een op Baeysiaanse statistiek gebaseerde methode werd toegepast op de MOW1 data om de parameters van het 2 klassen populatiemodel te bepalen en voorgesteld op de INTERCOH conferentie.

Taak 3.1: Intensieve bio-geochemische monitoring werd uitgevoerd te MOW1 (RV Belgica campagnes 2019/20, 2019/22, 2019/25, 2019/29, 2019/32), W03 RV Belgica campagnes 2019/20, 2019/22, 2019/25, 2019/29, 2019/32), W05 (2019/20, 2019/22, 2019/25, 2019/29, 2019/32) en W08 (2019/20, 2019/22, 2019/25, 2019/29, 2019/32).
Een eerste interpretatie van de bio-geochemische meetresultaten werd voorgesteld op de INTERCOH conferentie.

Periode Januari 2020 – Juni 2020

Taak 1.1: De meetreeks te MOW1 werd verdergezet, zover dit mogelijk was onder Covid maatregelen. Metingen met de tripode zijn beschikbaar van januari t.e.m. ongeveer en van 12 juni t.e.m 8 juli.

Taak 1.2: Calibratie van OBS sensoren werd uitgevoerd tijdens RV Begica campagnes 2020/01 (21-24/01), 2020/04 (18-20/02) en 2020/19a. Wegens Covid maatregelen konden de campagnes 2020/08 (16-20/03), 2020/12 (27-30/04), 2020/14 (25-29/05) niet worden uitgevoerd. Campagne 2020/19a (22-24/06) is de eerste campagne na de lockdown. Staalnames werden beperkt tot 3 ½ getijcycli.

Taak 2.1: Ondanks de grote hoeveelheid aan data en modellerstudies, zijn de mechanismen die het turbiditeitstmaximum in de Belgisch-Nederlandse kustzone ter hoogte van Zeebrugge instand houden nog onvoldoende gekend. Om de dynamica ervan beter te begrijpen werd de rol van barocline (saliniteit en sediment geïnduceerde) processen en lokale sedimentbronnen onderzocht met een numeriek model, zie van Maren et al. (2020) in appendix 1.

Taak 3.1: Intensieve bio-geochemische monitoring werd uitgevoerd te MOW1 (RV Belgica campagnes 2020/01, 2020/04,2020/19a), W03 (RV Belgica campagnes 2020/01), W05 (2020/01, 2020/19a) en W08 (2020/01, 2020/19a), zie ook taak 1.2.
Een overzicht van de biogeochemische data verzameld vanaf 2018 tot heden wordt gegeven in Hoofdstuk 2.
De analyse van stalen genomen met sedimenttraps bevestigd aan de tripode (MOW) worden beschreven en geëvalueerd in Hoofdstuk 3.

1.6. Publicaties (januari 2019 – juni 2020)

Hieronder wordt een overzicht gegeven van publicaties met directe betrokkenheid van het KBIN waar resultaten en data uit het MOMO project in werden gebruikt.

Activiteits-, Meet- en Syntheserapporten

Fettweis M, Adamapoulou A, Baeye M, Parmentier K, van den Eynde D. 2020. MOMO activiteitsrapport (1 januari – 30 juni 2020). BMM-rapport MOMO/9/MF/202010/NL/AR/3, 42pp + app.

Fettweis M, De Ville de Goyet N, Francken F, Van den Eynde D. 2020. MOMO activiteitsrapport (1 juli – 31 december 2019). BMM-rapport MOMO/9/MF/202005/NL/AR/2, 59pp + app.

Fettweis M, Baeye M, Francken F, Jespers N, Knockaert M, Montereale-Gavazzi G, Parmentier K, Van den Eynde D. 2019. MOMO activiteitsrapport (1 januari – 30 juni 2019). BMM-rapport MOMO/9/MF/201911/NL/AR/1, 21pp + app.

Lauwaert B, Fettweis M, De Witte B, Van Hoei G, Timmermans S, Hermans L. 2019. Vooruitgangsrapport (juni 2019) over de effecten op het mariene milieu van baggerspeciestortingen (Vergunningsperiode 01/01/2017 – 31/12/2021). RBINS-ILVO-AMT-CD rapport. BL/2019/01, 28pp.

Backers J, Hindryckx K, Vanhaverbeke W. 2019. Rapport van de RV Belgica Meetcampagnes en Verankering van Meetsystemen MOMO – 2018. BMM-rapport BMM-MDO/2019-05/MOMO/2018, 169pp.

Conferenties/Workshops

Fettweis M, Riethmüller R, Schartau M, Verney R, Lee BJ. 2019. The composition of suspended particulate matter in coastal areas. JJ Mehta Award lecture at Intercoh, 13-17 October, Istanbul (Turkey).

Lee BJ, Bi Q, Toorman E, Fettweis M, Lee BK, 2019. Application of a Bayesian Method for Investigating the Probability and Uncertainty of a Two-Class Flocculation Kinetic Model. Intercoh, 13-17 October, Istanbul (Turkey).

Shen X, Toorman E, Fettweis M, Lee BJ. 2019. A population balance model for multi-class floc size distributions of cohesive sediments in Belgian coastal zones. EGU, 7-12 April, Vienna (Austria).

Fettweis M. 2019. Schwebstoff in Küstenmeeren – Flockige Fracht in ständigem Wandel: Gut zu sehen und doch schwer genau zu messen. Invited lecture at HZG Institute for Coastal Research, 31 January, Geesthacht (Germany).

Peer reviewed artikels

Fettweis M, Riethmüller R, Verney R, Becker M, Backers J, Baeye M, Chapalain M, Claeys S, Claus J, Cox T, Deloffre J, Depreiter D, Druine F, Flöser G, Grünler S, Jourdin F, Lafite R, Nauw J, Nechad B, Röttgers R, Sotollichio A, Vanhaverbeke W, Vereecken H. 2019. Uncertainties associated with in situ long-term observations of suspended particulate matter concentration using optical and acoustic sensors. Progress in Oceanography, 178, 102162. doi:10.1016/j.pocean.2019.102162

Montereale-Gavazzi G, Roche M, Degrendele K, Lurton X, Terseleer N, Baeye M, Francken F, Van Lancker V. 2019. Insight into short term tidal variability of multibeam backscatter from field experiments on different seafloor types. Geosciences 2019, 9, 34; doi:10.3390/geosciences9010034

Shen X, Toorman EA, Lee BJ, Fettweis M. 2019. Effects of aquatic biofilms on flocculation processes of cohesive sediments: A modeling approach. Journal of Geophysical Research, 124, 4098-4116. doi:10.10290/2018JC014493

Vanlede J, Dujardin A, Fettweis M, Van Hoestenberghe T, Martens C. 2019. Mud dynamics in the port of Zeebrugge. Ocean Dynamics, 69, 1085-1099. doi:10.1007/s10236-019-01273-3

van Maren DS, Vroom J, Fettweis M, Vanlede J. 2020. Formation of the Zeebrugge coastal turbidity maximum: The role of uncertainty in near-bed exchange processes. Marine Geology 425, 106186. doi:10.1016/j.margeo.2020.1061

Thesis, eindwerk

Demilde C. 2019. Analyse van transparante exopolymeerpartikels (TEP) optimaliseren en valideren. Bachelorproef, Bachelor in de agro- en biotechnologie, Afstudeerrichting biotechnologie, VIVES Hogeschool, 66pp + bijlagen

2. Biogeochemsche monitoring van het SPM: Overzicht data 2018-2020

Een grondige kennis over de dynamica van het gesuspendeerd materiaal (Suspended Particulate Matter, SPM) is nodig in veel oceanografische disciplines. SPM is een basisparameter voor waterkwaliteitsmonitoring wegens zijn belangrijke rol in aquatische ecosystemen (b.v. troebelheid van het water, contaminanten). Het bestaat uit een mengsel van verschillende partikel met verschillende origine. Enerzijds zijn er de minerale deeltjes die een fysicochemische (b.v. kleimineralen, kwarts, veldspaat) of een biogene oorsprong hebben (b.v. calciet, aragoniet, opaal). Anderzijds is er het organisch materiaal, dat levend (bacteriën, phyto - en zoöplankton) of niet-levend kan zijn (fecale partikel, detritus en de afbraakproducten van microbiële activiteiten, zoals mucus en exopolymeren). Het SPM kan gecontamineerd zijn met hydrofobe organische polluenten en/of zware metalen. De SPM concentratie en haar samenstelling varieert in de tijd en in de ruimte. Deze variaties worden beïnvloed door de interacties tussen fysische krachten (getij, meteo, klimaat), biologische cycli (b.v. algenbloei), chemische processen (koolstof cyclus, nutriëntencyclus) en menselijke activiteiten (bagger en stortactiviteiten, toevoer van een overmaat aan voedingsstoffen, offshore constructies, zandextractie). Verticale en dus ook horizontale fluxen van het SPM worden bepaald door hun valsnelheid, die afhangt van de capaciteit van de deeltjes om te flocculeren. Flocculatie beïnvloed de grootte van de gesuspendeerde deeltjes en bepaald daardoor ook de depositie van het slib in onder andere havens en vaargeulen. Op zijn beurt wordt flocculatie gestuurd door turbulentie, SPM concentratie en de oppervlakte eigenschappen van de deeltjes, die van elektrochemische of biologische oorsprong kunnen zijn. Om de dynamica van het SPM beter te begrijpen en te kunnen voorspellen werd een integrale monitoring opgezet voor een hele reeks fysische, biologische en chemische parameters. Deze aanpak groepeert verschillende monitoringsactiviteiten van het KBIN, die tot nu toe apart werden uitgevoerd, zoals voor MOMO, ICES, OSPAR, WFD, MSFD.

2.1. Meetstrategie

Van maart 2018 tot September 2020 werden om het uur of om het anderhalf uur waterstalen genomen met 5l Niskin flessen op 2 m onder het oppervlak en ongeveer 2 m boven de bodem in drie stations (MOW1, W05 en W08) gedurende een getijcyclus (12.5 uren), zie Figuur 1.1. In 2018 werd vooral het station MOW1 bemonsterd, de uitgebreide monitoring in de drie stations begint vanaf januari 2019. De drie stations zijn gelegen langsheen de turbiditeitsgradiënt. MOW1 ligt in het kustnabije turbiditeitsmaximum, W05 aan de rand van het turbiditeitsmaximum en W08 nog meer offshore. In totaal werden 20 getijcycli (en of ½ cycli) bemonsterd te MOW1, 15 in het tussenliggende station W05, en 14 in het offshore station W08, zie tabel 2.1. De waterstalen werden aan boord gefiltreerd en geanalyseerd in het Ecochem labo te Oostende om de concentraties aan SPM, POC (particulate organic carbon), PON (particulate organic nitrogen), POM (particulate organic matter, enkel t.e.m. 2019), pigmenten (Chlorofyl-a en -b: Chl-a, Chl-b; Pheophytine-a, -b: Pheo-a, Pheo-b) en TEP (transparant exoplymeric particles). Het partikulair organisch materiaal (POM) werd door gloeiverlies bepaald. De turbiditeit (in FNU) wordt met een Hach TL2360 LED Turbidimeter gemeten en de saliniteit bepaald op de waterstalen. Stalen voor anorganische nutrienten (nitraat, nitriet, ammonium, fosfaat, silicaat), totaal opgelost stikstof (TDN), totaal opgelost fosfor (TDP) en opgelost organisch koolstof (DOC) worden bepaald op het filtraat. Met behulp van sensoren werd tijdens de metingen tevens de vlokgrootte gemeten met een LISST 100C en de SPM concentratie met een OBS.

2.2. Analyse van de stalen

Tijdens elke staalname werden drie substalen voor SPM concentratie genomen en gefiltreerd aan boord. Het watermonster wordt via een filtratiebank gefiltreerd over een gedroogde voorgewogen 47mm GF/C glasvezelfilter. Na filtratie wordt de filter gespoeld met MILLIQ water en onmiddellijk bewaard op -20°C. De filter worden dan gedurende minimum 24h gedroogd in een oven bij 50°C. Na afkoelen wordt het filter opnieuw gewogen om de SPM concentratie te bekomen (zie Ecochem protocol BMM LAB/AK006 'Materie in Suspensie'). De onzekerheid (uitgedrukt als de RMSE van de drie filters gedeeld door de gemiddelde waarde) neemt af met toenemende concentratie van 8.5% (SPM concentratie <5 mg/l) tot 6.7% (<10 mg/), 3.5% (10–50 mg/l) en 2.1% (>100 mg/l) en geeft de random fout weer ten gevolge van een gebrek aan precisie tijdens de filtratie. In vooral helder water, worden systematische fouten door de aanwezigheid van zout op de filter of andere fouten veel groter dan de random fouten (Neukermans et al. 2012; Fettweis et al. 2019). Deze systematisch fouten werden geschat op 1 mg/l gebaseerd op Stavn et al. (2009) en Röttgers et al. (2014).

Een van de SPM filters werd gebruikt om het POM gehalte te bepalen via gloeiverlies (loss on ignition: LoI). De filter wordt in een moffeloven op 500°C gedurende enkele uren geplaatst en opnieuw gewogen.

De stalen voor POC en PON werden aan boord gefiltreerd met 25mm glasvezelfilters en onmiddellijk bewaard op -20°C en nadien geanalyseerd in het labo met een FLASH EA 1112 – Element analyser. Verbindingen die koolstof en stikstof bevatten worden in een verbrandingsbuis met zuivere zuurstof (O_2) katalytisch verbrand. De koolstof wordt hierbij omgezet in koolstofdioxide (CO_2) en de stikstof in een mengsel van stikstofoxyden (NO_x). Vervolgens worden de reactiegassen m.b.v. helium door een reductiebuis met zuiver koper (Cu) gevoerd. Hier wordt de NO_x omgezet in stikstof (N_2) en de overmaat zuurstof uit de gasstroom verwijderd. Daarna wordt de gasstroom door een buis met magnesiumperchloraat gevoerd om het water te verwijderen. De reactiegassen worden gescheiden in een gaschromatograaf. Het gehalte aan N_2 en CO_2 wordt gemeten met een katarometer (zie Ecochem protocol BMM LAB/AK033 'Parameter POC/PON in zwevende stof na filtratie'). De analytische onzekerheden voor POC en PON bedragen 12% en 18% en de detectielimieten 0.018 mg/l en 0.009 mg/l respectievelijk. Hierbij werd de random error bijgeteld door de filtratie, deze werd verondersteld om gelijk te zijn als voor SPM concentratie.

De stalen voor de pigment concentraties (Chl-a, Chl-b, Pheo-a, Pheo-b) werden aan boord gefiltreerd op 47mm GF/C glasvezelfilters, gestockeerd in vloeibaar stikstof en in het labo geanalyseerd met ultra high-performance liquid chromatography. Extractie van de bevroren filter vindt plaats in een maalflesje, waarin zich een bepaalde volume extractievloeistof (= aceton/water (90/10 v/v)) en glasparels bevinden. Uit elk acetonextract wordt een bepaalde hoeveelheid op de scheidingskolom gebracht. Met behulp van een aceton/water mengsel als eluens worden de diverse componenten op de kolom gescheiden, en met een fluorescentie detector gedetecteerd. Kwantificering geschiedt aan de hand van meebepaalde standaard monsters (zie Ecochem protocols BMMLAB/AK063-CHLORa-WATER-UHPLC, BMMLAB/AK063-CHLORb-WATER-UHPLC, BMM LAB/AK063-FEOa-WATER-UHPLC). De analytische onzekerheden voor Chl-a en Chl-b is 23% en voor Pheo-a en Pheo-b 31%. Hierbij werd de random error bijgeteld door de filtratie, deze werd verondersteld om gelijk te zijn als voor SPM concentratie.

De methode voor de analyse van TEP is deze beschreven in Nosaka et al. (2017). Deze methode is, zoals andere semi-kwantitatieve methoden, gebaseerd op Aldredge et al. (1993) en Passow & Aldredge (1995). Drie substalen warden genomen voor bepaling van de TEP concentratie e naan boord gefiltreerd op 25mm 0.4 µm polycarbonaat filters met een

lage onderdruk. Na filtratie warden de filters onmiddellijk gekleurd met 1 ml of Alciaan blauw, gespoeld met 1 ml MilliQ water en op -20°C gestockeerd. De gekleurde deeltjes zijn gecorreleerd met een gewichtsequivalent van de anionendensiteit van TEP en gestandaardiseerd met xanthan gom (Passow & Alldredge 1995; Passow 2002). TEP wordt uitgedrukt in mg xanthan gom equivalenten per liter (mg XG eq./l).

De filtraten warden verzameld in plastiek buisjes voor de bepaling van DOC, anorganische nutriënten en geanalyseerd met behulp van standaard spectrophotometrische methoden met een Skalar autoanalyzer. De stalen worden rechtopstaand bij een temperatuur van -20°C bewaard. Voor de analyse wordt een hoeveelheid monster met behulp van een monsterwisselaar en een pomp slangensysteem in de keten gezogen. Voor DOC bepaling wordt in een bepaalde verhouding zwavelzuur toegevoegd om de anorganische koolstof te verwijderen en kaliumperoxodisulfaat/boraat buffer om het opgeloste organisch koolstof tijdens de UV-destructie om te zetten naar CO_2. Het hierbij ontstane chloor wordt door hydroxylammoniumchloride gebonden. Het CO_2 wordt door een gasmembraan gedialyseerd in een kleurreagens. De CO_2 geeft hier een verlaging van de pH waardoor de kleurintensiteit afneemt. De extinctie wordt gemeten bij 550 nm en is een maat voor de hoeveelheid organisch koolstof (zie Ecochem protocol BMM LAB/AK034). Nitraat wordt m.b.v. een koper/cadmium-kolom gereduceerd tot nitriet. Hieraan wordt een bepaalde hoeveelheid sulfanilamide en nafthyleen-diamine-dihydrochloride toegevoegd. In zuur milieu vormt het nitriet met deze chemicaliën een roodgekleurde diazo-verbinding. De extinctie wordt gemeten bij 540 nm. Deze absorbantie is een maat voor de aanwezige hoeveelheid nitriet, wat het gehalte aan $N\text{-}NO_{2+3}$ en $N\text{-}NO_2$ weergeeft (zie Ecochem protocol BMM LAB/AK011, BMM LAB/AK012). Fosfaat wordt op een analoge manier geanalyseerd. Hier wordt aan het monster een bepaalde hoeveelheid molybdaat reagens en ascorbinezuur toegevoegd. Na menging gaat het monster door een verwarmingsbad van 37°C. In zuur milieu vormt molybdaat met de orthofosfaat ionen door reductie met ascorbinezuur en in aanwezigheid van antimoon een blauwgekleurde verbinding. De extinctie wordt gemeten bij 880 nm. Deze absorbantie is een maat voor de aanwezige hoeveelheid orthofosfaat (zie Ecochem protocol BMM LAB/AK013). Ook de silicaat analyse is gelijkaardig. Aan het staal wordt een bepaalde hoeveelheid molybdaat reagens, ascorbinezuur en oxaalzuur toegevoegd. In zuur milieu vormt molybdaat met opgelost silicium een silicomolybdeen-zuurverbinding die door ascorbinezuur gereduceerd wordt tot een blauwgekleurde verbinding (molybdeenblauw). Om storingen door fosfaationen weg te werken, wordt oxaalzuur toegevoegd vooraleer ascorbinezuur wordt toegevoegd. De extinctie wordt gemeten bij 810 nm. Deze absorbantie is een maat voor de aanwezige hoeveelheid silicaat (zie Ecochem protocol BMM LAB/AK015). Voor de bepaling van TDN wordt in een bepaalde verhouding kaliumperoxodisulfaat en natriumhydroxide toegevoegd, waarna de oplossing door een verwarmingsbad van 90°C wordt geleid. Vervolgens wordt een hoeveelheid boraatbuffer toegevoegd, waarna de oplossing via een kwartsspiraal om een UV lamp wordt geleid. Hierna wordt een gedeelte van deze oplossing gedialyseerd met ammoniumchloride en vervolgens door een cadmiumkolom geleid waar het nitraat gereduceerd wordt tot nitriet. Na toevoeging van fosforzuur, sulfanilamide en α-nafthyleen-diamine-dihydrochloride vormt het nitriet met deze chemicaliën een roodgekleurde diazoverbinding. De extinctie wordt dan gemeten bij 540 nm (zie Ecochem protocol BMM/LAB/1K035). Voor de bepaling van TDP wordt in een bepaalde verhouding kaliumperoxodisulfaat en dinatriumtetraboraat toegevoegd, waarna de oplossing via een kwartsspiraal om een UV lamp wordt geleid. Vervolgens wordt zwavelzuur toegevoegd, waarna het door een verwarmingsbad van 97°C stroomt. Na toevoeging van een NaOH oplossing om te neutraliseren en ascorbinezuur om het eventuele ontstane chloor te binden. Hierna wordt een gedeelte van deze oplossing geresampled, waarna in een

Table 2.1: Overview of the biogeochemical monitoring at stations MOW1, W05 and W08 (March 2018 – September 2020). Standard parameters are SPM, POC, PON, POM (Loss on ignition: LoI), pigments, TEP, turbidity (HACH), DOC and nutrients.

No	cmp	data	station	Remarks
112	2018-08	27-28/03/2018	W05	no TEP, no nutrients, no DOC, no LoI, 1h sampling
113	2018-08	28/03/2018	MOW1	no TEP, no nutrients, no DOC, noLoI, 1h sampling
114	2018-13	15/05/2018	MOW1	no TEP, no DOC, no nutrients, 1h sampling
115	2018-18	20-21/08/2018	MOW1	no TEP, no DOC, no nutrients, 1h sampling
116	2018-29	18-19/12/2018	MOW1	no DOC, no nutrients, 1h sampling
117	2019-01	23-24/01/2019	MOW1	1h sampling
118	2019-01	24/01/2019	W05	1h sampling
119	2019-01	25/01/2019	W08	½ tidal cycle, 1h sampling
120	2019-03	12-13/02/2019	MOW1	only 6h of TEP, 1h sampling
121	2019-03	13/02/2019	W05	1h sampling
122	2019-03	14/02/2019	W08	no TEP, 1.5h sampling
123	2019-07	11-12/03/2019	MOW1	1h sampling
125	2019-11	08-09/04/2019	W05	1h sampling
126	2019-11	09/04/2019	MOW1	TEP only at surface, 1h sampling
127	2019-14	21-21/05/2019	MOW1	1h sampling
128	2019-14	21/05/2019	W05	1h sampling
129	2019-14	22/05/2019	W08	1.5h sampling
130	2019-17	24/06/2019	W08	no TEP, 1.5h sampling
131	2019-17	25/06/2019	W05	no TEP, 1h sampling
132	2019-17	26/06/2019	MOW1	no TEP, 1h sampling
133	2019-20	20-21/06/2019	W08	1.5h sampling
134	2019-20	22-23/08/2019	MOW1	1h sampling
135	2019-22	09-10/09/2019	W08	1.5h sampling
136	2019-22	11/09/2019	MOW1	1h sampling
137	2019-22	12/09/2019	W05	1h sampling
138	2019-25	15-16/10/2019	W05	1h sampling
139	2019-25	16/10/2019	MOW1	1h sampling
140	2019-25	17/10/2019	W08	1.5h sampling
141	2019-29	19/11/2019	W05	1h sampling
142	2019-29	20/11/2019	MOW1	1h sampling
143	2019-29	21/11/2019	W08	only 1 sample, no LoI
144	2019-32	16-17/12/2019	W05	1h sampling
145	2019-32	17/12/2019	MOW1	only a few POC/PON data
146	2019-32	18/12/2019	W08	no TEP, no LoI, 1.5h sampling
147	2020-01	21-22/01/2020	MOW1	no LoI, 1h sampling
148	2020-01	22-23/01/2020	W05	no LoI, 1.5h sampling
149	2020-01	23/01/2020	W08	no LoI, 1.5h sampling
150	2020-04	19/02/2020	MOW1	½ tidal cycle, no LoI, 1h sampling
151	2020-19a	22/06/2020	MOW1	½ tidal cycle, no LoI, 1h sampling
152	2020-19a	23/06/2020	W05	½ tidal cycle, no LoI, 1h sampling
153	2020-19a	24/06/2020	W08	½ tidal cycle, no LoI, 1.5h sampling
154	2019-19c	07/07/2020	W05	½ tidal cycle, no LoI, 1h sampling
155	2020-19c	08/07/2020	W08	½ tidal cycle, no LoI, 1.5h sampling
156	2020-20	19/08/2020	MOW1	no LoI, 1h sampling
157	2020-20	20/08/2020	W05	no LoI, 1h sampling
158	2020-20	21/08/2020	W08	½ tidal cycle, no LoI, 1.5h sampling
159	2020-22	07/09/2020	W05	no LoI, 1h sampling
160	2020-22	08/09/2020	W08	no LoI, 1.5h sampling
161	2020-22	09/09/2020	MOW1	no LoI, 1h sampling

bepaalde verhouding een mix-reagens van molybdaat en ascorbinezuur wordt toegevoegd. De oplossing wordt daarna verwarmd tot 40°C waarbij de kleurvorming de kleurvorming plaats vindt. De extinctie wordt dan gemeten m.b.v. een matrixfotometer bij 880 nm (zie Ecochem protocol BMM LAB/AK036). Detectie limiet voor DOC is 0.09 mgC/l en voor TDN, TDP, nitraat, nitriet, ammonium, fosfaat, silicaat 3.1, 0.5, 0.06, 0.06, 0.5 and 2 µmol, respectievelijk.

2.3. Overzicht metingen 2018-2020

Een overzicht van de beschikbare data wordt gegeven in Figuur 2.1 en Tabel 2.1. De gemiddelde data per station en per getij kunnen gevonden worden in Tabellen 2.3-2.8. In Figuur 2.2 en in Tabel 2.3 wordt de verhouding van de P90 over de P10 waarde van elke parameter weergegeven per getijcyclus. Dit, samen met de standaardafwijking in Tabellen 2.3-2.8, is een indicatie van de variabiliteit van een parameter. De ratio voor de particulaire parameters (SPM, turbiditeit, POC, PON, pigmenten en TEP) hebben een gelijkaardig patroon. Hoogste variabiliteit treedt op te MOW1 en de laagste te W08. De ratio P90/P10 is het meest uitgesproken voor SPM en bedraagt ongeveer 8 (MOW1), 2 (W05) en 1.5 (W08) met iets hogere waarden aan de bodem dan aan de oppervlakte. Voor de opgeloste parameters (saliniteit, nutriënten) is de variabiliteit geringer, maar is het verschil tussen de drie stations vrij gering. Met uitzondering van saliniteit, is de variabiliteit echter behoorlijk groot (gemiddeld 1.8) tijdens een getij. Beide resultaten onderstrepen het belang van een representatieve staalname in een getijde gedomineerd gebied en dus het belang van een meting gedurende een volledige getijcyclus.

Table 2.3: Mean ratio of the P90 over the P10 values during all tidal (1/2 tidal) cycles at MOW1, W05 and W08.

		MOW1	W05	W08
SPM (mg/l)	bot	8.7	2.1	1.6
	sur	7.0	2.2	1.7
Hach (FNU)	bot	9.6	3.3	2.6
	sur	7.7	4.3	2.8
POC (mg/l)	bot	6.3	2.3	1.9
	sur	5.1	2.1	2.0
PON (mg/l)	bot	4.8	2.2	1.8
	sur	3.8	1.8	2.1
Chl-a (µg/l)	bot	5.3	1.9	1.8
	sur	4.3	2.3	1.6
Chl-b (µg/l)	bot	3.9	1.8	1.6
	sur	3.2	2.3	1.5
Pheo-a (µg/l)	bot	10.6	2.3	1.8
	sur	5.9	2.6	1.6
Pheo-b (µg/l)	bot	3.2	-	-
	sur	2.2	-	-
TEP (mg xG eq/l)	bot	5.0	2.8	2.1
	sur	4.8	3.3	2.2
Salinity	sur	1.02	1.01	1.00
DOC (mg/l)	sur	1.5	1.6	1.5
TDN (µmol/l)	sur	1.6	1.5	2.0
NOx (µmol/l)	sur	1.8	2.0	3.1
NO_2 (µmol/l)	sur	1.8	1.6	1.5
NH_4 (µmol/l)	sur	2.1	2.3	2.1
TDP (µmol/l)	sur	1.5	1.4	1.4
PO_4 (µmol/l)	sur	1.7	1.8	1.3
Si (µmol/l)	sur	1.6	1.7	1.6

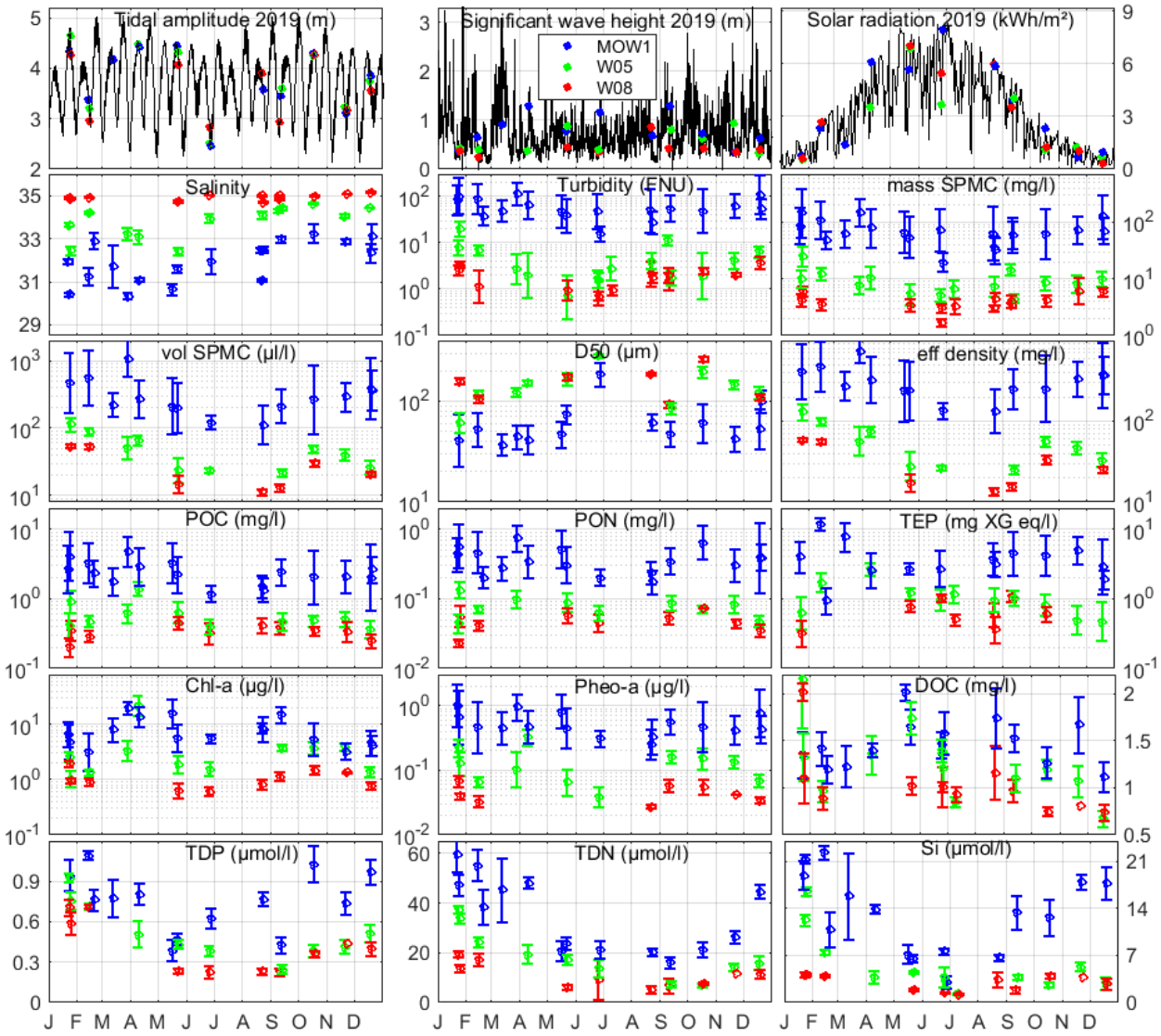

Figure 2.1: Physical (harmonic tidal amplitude, significant wave height, solar radiation in 2019), dissolved and particulate parameters from 2018-2020 (see Table 2.1). The error bars indicate the arithmetic (dissolved substances) or geometric (particulate substances) mean over the measuring period (usually 12 hours) and the standard deviation.

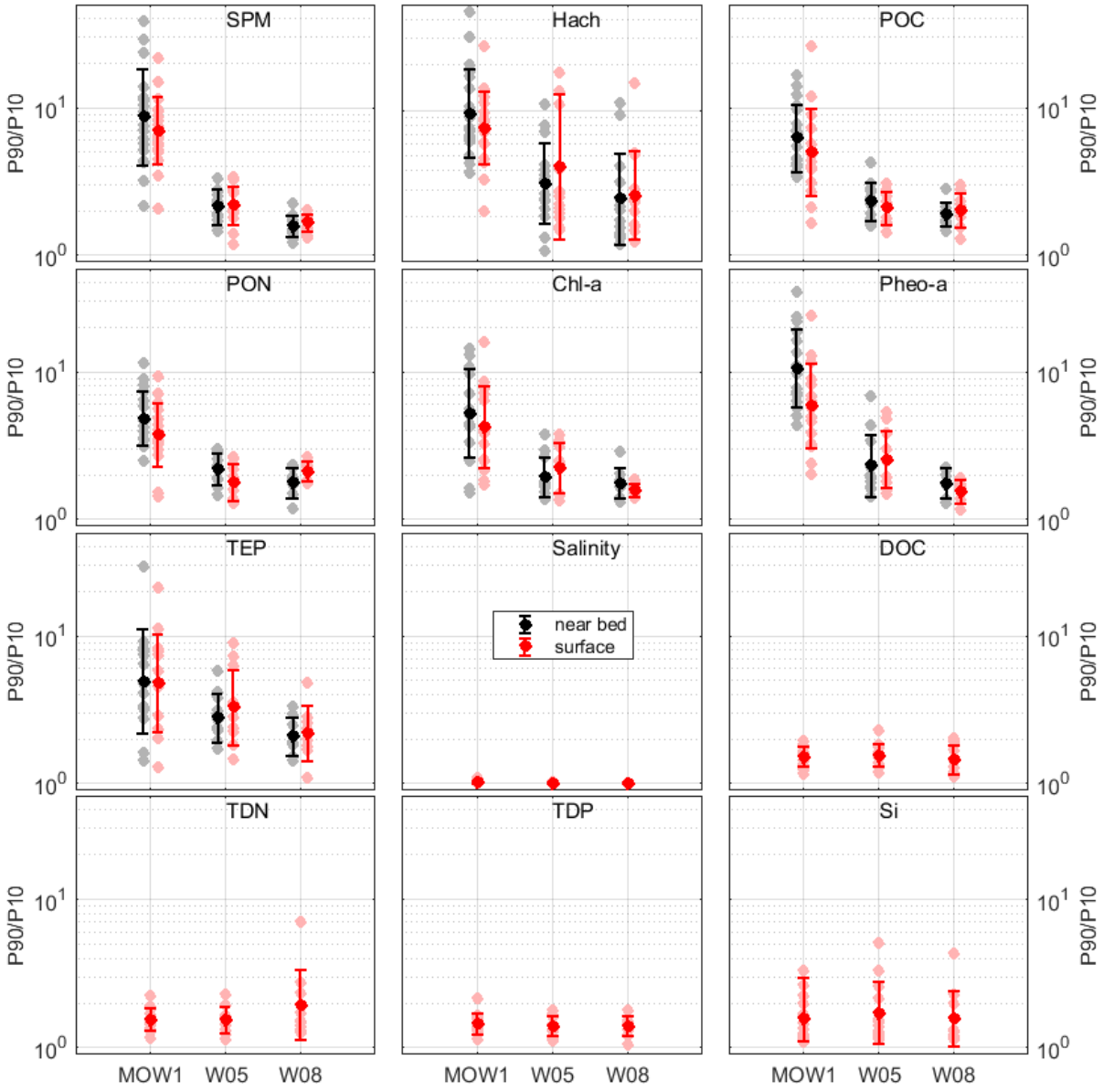

Figure 2.2: Ratio of the P90 over the P10 value during a tidal (1/2 tidal) cycle at MOW1, W05 and W08. The lighter points are the tidal cycle, the errorbar are the mean and standard deviation of all P90/P10 ration.

Table 2.3: MOW1 station. Geometric mean and multiplicative standard deviation of the particulate data over the measuring period and at the surface (sur) and the bottom (bot) and for all data (-: not measured, blanco: not yet available, <: below detection limit).

No	cmp	Date		SPM		Hach		POC		PON		TEP		ChlA		ChlB		FeoA		FeoB	
				mg/l		FNU		mg/l		mg/l		mgXG/l		µg/l		µg/l		µg/l		µg/l	
113	2018-08	28/03/2018	all	148.3	1.78	114.7	1.80	4.83	1.66	0.750	1.56	-	-	19.96	1.31	0.62	1.29	0.95	1.58	0.04	1.45
			bot	161.4	1.80	124.7	1.77	5.20	1.71	0.771	1.58	-	-	20.46	1.34	0.63	1.32	1.05	1.63	0.04	1.51
			sur	136.3	1.78	105.5	1.85	4.49	1.63	0.729	1.56	-	-	19.46	1.30	0.61	1.27	0.86	1.53	0.04	1.42
114	2018-13	15/05/2018	all	67.6	2.26	48.7	2.22	3.28	1.92	0.522	1.83	-	-	16.01	1.80	0.37	1.45	0.82	1.85	0.03	1.39
			bot	75.1	2.47	53.7	2.36	3.50	2.07	0.540	1.96	-	-	16.24	1.90	0.38	1.43	0.83	2.03	0.03	1.41
			sur	60.8	2.09	44.1	2.12	3.07	1.80	0.504	1.73	-	-	15.76	1.73	0.36	1.49	0.81	1.69	0.03	1.39
115	2018-18	20-21/08/2018	all	35.0	1.60	0.0	0.00	1.50	1.45	0.239	1.43	-	-	8.80	1.24	0.13	2.13	0.26	1.69	0.04	1.41
			bot	43.4	1.60	0.0	0.00	1.68	1.56	0.266	1.52	-	-	9.97	1.17	0.17	2.33	0.27	2.05	0.04	1.38
			sur	28.3	1.47	0.0	0.00	1.34	1.28	0.214	1.29	-	-	7.78	1.22	0.10	1.74	0.24	1.25	0.03	1.45
116	2018-29	18-19/12/2018	all	70.7	1.69	54.8	1.65	2.64	1.52	0.394	1.54	1.91	1.35	4.15	1.52	<	-	0.43	1.66	<	<
			bot	73.7	1.77	56.3	1.76	2.82	1.55	0.536	1.64	1.93	1.36	4.04	1.49	<	-	0.45	1.66	<	-
			sur	67.8	1.63	53.4	1.57	2.46	1.51	0.351	1.43	1.89	1.36	4.26	1.57	<	-	0.41	1.68	<	-
117	2019-01	23-24/01/2019	all	146.5	2.71	104.2	2.47	4.12	2.27	0.569	2.06	-	-	4.92	2.08	0.14	2.25	0.66	2.62	<	-
			bot	167.3	2.93	125.7	2.65	4.46	2.31	0.606	2.12	-	-	5.06	2.31	0.14	2.63	0.72	3.04	<	-
			sur	128.3	2.55	86.3	2.28	3.81	2.30	0.535	2.05	-	-	4.78	1.90	0.13	1.93	0.62	2.28	<	-
120	2019-03	12-13/02/2019	all	111.9	2.15	91.2	2.13	3.35	1.95	0.465	1.97	11.90	1.24	3.27	2.19	0.14	1.79	0.46	2.52	0.04	1.88
			bot	130.7	2.31	105.5	2.27	3.71	2.08	0.517	2.11	14.09	1.16	3.78	2.20	0.14	1.82	0.54	2.59	0.04	2.00
			sur	95.7	1.98	78.7	1.98	3.02	1.84	0.418	1.84	10.04	1.12	2.83	2.19	0.15	1.92	0.39	2.47	0.04	1.87
123	2019-07	11-12/03/2019	all	63.5	1.73	49.2	1.73	1.77	1.58	0.276	1.47	7.80	1.60	8.18	1.63	0.31	1.36	0.45	1.81	<	-
			bot	64.8	1.77	52.5	1.79	1.85	1.61	0.295	1.51	8.33	1.65	7.96	1.69	0.31	1.43	0.45	1.86	<	-
			sur	62.3	1.73	46.2	1.70	1.69	1.57	0.259	1.43	7.31	1.57	8.40	1.60	0.31	1.31	0.46	1.82	<	-
126	2019-11	09-04-2019	all	80.4	2.20	65.1	2.01	2.94	1.85	0.342	1.72	-	-	14.06	1.52	0.22	1.21	0.47	1.80	<	-
			bot	89.9	2.27	75.9	1.99	3.25	1.96	0.379	1.80	-	-	12.20	1.67	0.23	1.31	0.44	2.08	<	-
			sur	71.8	2.16	55.8	2.02	2.66	1.75	0.312	1.66	2.57	1.76	16.20	1.29	0.22	1.14	0.51	1.52	<	-
127	2019-14	20-21/05/2019	all	54.6	2.33	39.0	2.33	2.25	1.82	0.310	1.80	2.70	1.20	5.66	1.75	0.27	1.64	0.46	2.04	<	-
			bot	66.2	2.44	50.0	2.39	2.67	1.87	0.350	1.91	2.79	1.17	6.22	1.87	0.31	1.67	0.56	2.16	<	-
			sur	45.0	2.20	30.4	2.17	1.90	1.71	0.272	1.66	2.61	1.22	5.15	1.64	0.24	1.58	0.37	1.85	<	-
132	2019-17	26/06/2019	all	19.9	1.47	15.7	1.45	1.19	1.31	0.205	1.29	-	-	5.67	1.19	0.37	1.19	0.31	1.35	<	-
			bot	22.3	1.50	16.1	1.52	1.30	1.40	0.219	1.38	-	-	6.22	1.13	0.37	1.18	0.34	1.41	<	-
			sur	17.7	1.40	15.2	1.40	1.08	1.15	0.189	1.11	-	-	5.17	1.19	0.36	1.20	0.28	1.25	<	-

134	2019-20	22-23/08/2019	all	31.9	1.72	27.6	1.72	1.35	1.49	0.175	1.50	3.22	1.51	8.13	1.68	0.43	1.81	0.33	1.88	<	-
			bot	33.8	1.72	29.5	1.74	1.43	1.57	0.190	1.60	3.26	1.43	8.38	1.73	0.43	1.72	0.35	2.00	<	-
			sur	30.1	1.75	25.8	1.73	1.28	1.42	0.165	1.42	3.19	1.60	7.89	1.67	0.43	1.93	0.31	1.80	<	-
136	2019-22	11/09/2019	all	60.1	1.76	55.6	1.90	2.44	1.55	0.351	1.52	4.54	2.08	15.15	1.39	0.81	1.32	0.57	1.56	<	-
			bot	64.7	1.78	62.0	1.96	2.53	1.56	0.368	1.52	5.30	1.83	14.43	1.45	0.75	1.38	0.58	1.65	<	-
			sur	55.7	1.77	49.9	1.85	2.35	1.57	0.336	1.53	3.88	2.30	15.85	1.35	0.87	1.25	0.56	1.50	<	-
139	2019-25	16/10/2019	all	63.3	2.76	49.5	2.97	2.06	2.46	0.650	1.77	4.27	1.93	5.39	1.95	0.26	1.60	0.48	2.43	0.05	1.80
			bot	77.9	3.08	63.0	3.20	2.59	2.51	0.671	1.78	4.41	2.00	6.31	2.03	0.26	1.71	0.57	2.72	0.05	1.82
			sur	51.5	2.43	38.1	2.67	1.65	2.35	0.609	1.96	4.15	1.91	4.60	1.85	0.27	1.45	0.40	2.13	0.09	1.00
142	2019-29	20/11/2019	all	71.6	1.74	62.5	1.82	2.09	1.72	0.305	1.72	5.04	1.57	3.29	1.43	0.00	0.00	0.42	1.66	<	<
			bot	79.4	1.79	68.2	1.74	2.33	1.68	0.348	1.71	5.74	1.41	3.50	1.47	0.00	0.00	0.46	1.69	<	<
			sur	64.6	1.70	57.2	1.93	1.88	1.77	0.271	1.71	4.43	1.68	3.09	1.39	0.00	0.00	0.39	1.63	<	<
145	2019-32	17/12/2019	all	124.9	2.39	109.7	2.60	-	-	0.392	3.20	2.90	2.48	4.73	1.69	0.12	1.36	0.77	2.36	0.03	1.34
			bot	146.2	2.57	128.6	2.83	2.05	3.02	0.392	3.20	2.80	2.74	5.06	1.83	0.13	1.40	0.91	2.56	0.04	1.34
			sur	108.1	2.24	93.5	2.39	-	-	0.000	0.00	3.01	2.31	4.46	1.58	0.10	1.25	0.66	2.16	0.03	1.18
147	2020-01	21-22/01/2020	all	86.2	2.10	84.5	2.16	2.64	2.19	0.434	1.75	4.02	1.69	6.70	1.71	0.17	1.51	1.01	2.09	0.04	1.57
			bot	102.6	2.03	97.4	2.17	3.22	2.18	0.455	1.80	4.31	1.79	7.06	1.74	0.19	1.52	1.15	2.12	0.04	1.65
			sur	72.4	2.15	73.3	2.15	2.16	2.16	0.410	1.74	3.74	1.60	6.35	1.71	0.16	1.49	0.88	2.07	0.03	1.51
150	2020-04	19/02/2020	all	48.9	1.43	38.5	1.59	2.34	1.56	0.205	1.44	0.95	1.54								
			bot	60.5	1.38	46.7	1.74	2.96	1.63	0.242	1.50	0.90	1.60								
			sur	39.5	1.28	31.8	1.29	1.85	1.28	0.166	1.21	1.00	1.54								
151	2020-19a	22/06/2020	all	73.0	2.40	48.2	2.44					2.72	1.82								
			bot	129.3	1.63	84.9	1.76					2.64	2.23								
			sur	41.2	2.25	27.3	2.24					2.79	1.45								
156	2020-20	19/08/2020	all	63.5	2.96	49.7	2.94					3.77	1.70								
			bot	92.1	3.57	65.4	3.43					4.27	1.65								
			sur	43.8	2.09	37.8	2.36					3.36	1.72								
161	2020-22	09/09/2020	all	60.5	2.03	49.7	1.90														
			bot	87.4	1.91	64.7	1.92														
			sur	41.8	1.77	38.2	1.70														

Table 2.4: MOW1 station. Mean and standard deviation of the dissolved data at the surface over the measuring period (-: not measured, blanco: not yet available, <: below detection limit).

No	cmp	Date	Salinity		DOC		TDN		NOx		NO_2		NH_4		TDP		PO_4		Si	
					mg/l		µmol/l		µmol/l		µmol/l		µmol/l		µmol/l		µmol/l		µmol/l	
113	2018-08	28/03/2018	30.36	0.15	-	-	-	-	-	-	-	-	-	-	-	-	-	-	-	-
114	2018-13	15/05/2018	30.66	0.25	2.02	0.09	21.0	4.2	8.4	2.4	0.13	0.02	1.13	0.80	0.39	0.08	0.14	0.05	7.2	1.4
115	2018-18	20-21/08/2018	31.11	0.06	-	-	-	-	-	-	-	-	-	-	-	-	-	-	-	-
116	2018-29	18-19/12/2018	33.12	0.59	-	-	-	-	-	-	-	-	-	-	-	-	-	-	-	-
117	2019-01	23-24/01/2019	30.42	0.11	1.36	0.25	47.4	4.4	34.3	1.2	0.83	0.12	7.21	0.59	0.95	0.12	0.91	0.10	21.4	0.7
120	2019-03	12-13/02/2019	31.27	0.39	1.42	0.18	55.3	6.1	41.9	3.1	0.78	0.04	5.17	0.12	1.10	0.03	0.92	0.03	22.3	1.0
123	2019-07	11-12/03/2019	31.73	0.97	1.23	0.22	45.4	12.6	35.2	13.6	0.59	0.18	3.24	1.03	0.78	0.14	0.52	0.15	15.8	6.3
126	2019-11	09-04-2019	31.10	0.08	1.40	0.08	48.2	2.3	35.9	1.0	0.39	0.04	1.97	0.29	0.81	0.08	0.55	0.06	14.0	0.6
127	2019-14	20-21/05/2019	31.62	0.15	1.65	0.19	24.1	2.5	8.6	1.5	0.21	0.03	2.39	0.66	0.47	0.04	0.17	0.03	6.7	0.6
132	2019-17	26/06/2019	31.94	0.59	1.59	0.22	21.5	3.5	7.0	1.8	0.45	0.12	2.84	1.11	0.63	0.07	0.33	0.09	3.1	0.9
134	2019-20	22-23/08/2019	32.51	0.16	1.74	0.32	20.3	1.6	7.9	0.7	0.71	0.11	2.30	0.54	0.77	0.05	0.66	0.04	6.7	0.5
136	2019-22	11/09/2019	32.98	0.12	1.52	0.15	16.3	2.3	5.3	1.4	0.46	0.13	3.11	0.73	0.43	0.06	0.42	0.08	13.4	2.4
139	2019-25	16/10/2019	33.26	0.43	1.27	0.17	21.3	3.0	10.8	2.6	1.31	0.32	6.58	1.11	1.03	0.13	0.75	0.11	12.7	2.7
142	2019-29	20/11/2019	32.89	0.11	1.67	0.30	26.5	2.6	21.8	1.3	1.35	0.07	5.47	0.36	0.74	0.08	0.91	0.06	17.9	1.1
145	2019-32	17/12/2019	32.34	0.46	1.12	0.16	44.8	2.9	31.2	4.8	0.63	0.14	4.85	0.52	0.97	0.09	0.82	0.22	17.8	2.5
147	2020-01	21-22/01/2020	31.94	0.11	2.97	0.27	59.8	7.1	44.2	5.8	0.58	0.08	3.64	0.37	1.46	0.13	0.83	0.05	18.9	2.2
150	2020-04	19/02/2020	32.90	0.38	1.20	0.15	38.7	7.1	29.8	5.9	0.49	0.11	2.71	1.31	0.76	0.08	0.60	0.10	10.8	2.59
151	2020-19a	22/06/2020	30.65	0.06	1.46	0.14			15.8	1.74	0.70	0.04	6.51	1.08			0.57	0.05	7.7	0.45
156	2020-20	19/08/2020	32.47	0.11																
161	2020-22	09/09/2020	32.95	0.07																

Table 2.5: W05 station. Geometric mean and multiplicative standard deviation of the particulate data over the measuring period and at the surface (sur) and the bottom (bot) and for all data (-: not measured, blanco: not yet available, <: below detection limit).

No	cmp	Date		SPM		Hach		POC		PON		TEP		ChlA		ChlB		FeoA		FeoB	
				mg/l		FNU		mg/l		mg/l		mgXG/l		µg/l		µg/l		µg/l		µg/l	
112	2018-18	27-28/03/2018	all	7.83	1.41	-	-	0.63	1.36	0.099	1.33	-	-	3.37	1.50	0.24	1.49	0.10	1.86	-	-
			bot	8.72	1.39	-	-	0.66	1.35	0.103	1.33	-	-	3.71	1.35	0.25	1.49	0.13	1.8	<	-
			sur	7.03	1.41	-	-	0.6	1.38	0.095	1.34	-	-	3.09	1.61	0.23	1.55	0.08	1.77	<	-
118	2019-01	24/01/2019	all	25.36	1.52	20.24	1.47	0.91	1.46	0.135	1.33	-	-	1.04	1.41	0.03	1.93	0.13	1.54	<	-
			bot	34.12	1.30	25.83	1.33	1.16	1.31	0.152	1.29	-	-	1.34	1.22	0.03	1.74	0.18	1.29	<	-
			sur	18.85	1.39	15.86	1.37	0.71	1.36	0.113	1.29	-	-	0.80	1.28	0.03	2.1	0.09	1.36	<	-
121	2019-03	13/02/2019	all	12.23	1.29	7.04	1.3	0.48	1.18	0.072	1.13	1.72	1.37	1.38	1.15	<	-	0.07	1.19	<	-
			bot	14.43	1.24	8.38	1.26	0.51	1.17	0.073	1.15	1.78	1.45	1.47	1.16	<	-	0.07	1.17	<	-
			sur	10.36	1.20	5.91	1.16	0.46	1.18	0.071	1.10	1.67	1.31	1.30	1.12	<	-	0.06	1.11	<	-
125	2019-11	08-09/04/2019	all	10.7	1.57	2.02	2.97	1.41	1.24	-	-	2.70	1.22	22.29	1.49	0.28	1.24	0.33	1.35	<	-
			bot	14.46	1.46	4.70	1.65	1.55	1.14	-	-	3.22	1.31	27.62	1.21	0.29	1.24	0.39	1.19	<	-
			sur	7.92	1.33	0.87	2.28	1.28	1.27	-	-	2.60	1.19	16.75	1.54	0.27	1.25	0.27	1.35	<	-
128	2019-14	21/05/2019	all	5.44	1.53	0.69	3.01	0.64	1.40	0.089	1.35	1.22	1.2	1.92	1.42	-	-	0.07	1.61	<	-
			bot	7.37	1.32	1.44	1.98	0.81	1.38	0.105	1.39	1.23	1.26	2.15	1.44	0.12	1.06	0.08	1.56	<	-
			sur	4.01	1.36	0.31	2.45	0.51	1.13	0.076	1.15	1.20	1.14	1.72	1.36	<	-	0.05	1.49	<	-
131	2019-17	25/06/2019	all	3.11	1.23	1.59	1.45	0.40	1.30	0.062	1.29	-	-	1.57	1.33	0.17	1.16	0.04	1.43	<	-
			bot	3.69	1.12	1.63	1.37	0.38	1.23	0.058	1.23	-	-	1.89	1.12	0.18	1.11	0.05	1.11	<	-
			sur	2.61	1.11	1.55	1.55	0.42	1.36	0.066	1.33	-	-	1.29	1.33	0.16	1.18	0.03	1.28	<	-
137	2019-22	12/09/2019	all	4.54	1.21	1.82	1.47	0.48	1.33	0.086	1.28	1.04	1.27	3.85	1.16	0.44	1.09	0.16	1.25	<	-
			bot	5.12	1.12	2.29	1.37	0.59	1.27	0.093	1.34	1.08	1.22	3.88	1.20	0.42	1.08	0.18	1.22	<	-
			sur	4.03	1.2	1.45	1.35	0.40	1.21	0.079	1.12	1.00	1.32	3.82	1.12	0.46	1.08	0.15	1.25	<	-
138	2019-25	15-16/10/2019	all	8.52	1.31	1.93	3.17	0.48	1.20	0.072	1.14	0.82	1.43	3.79	1.31	0.21	1.27	0.15	1.44	0.03	1.21
			bot	10.14	1.24	3.87	1.61	0.53	1.17	0.074	1.13	0.82	1.42	4.2	1.25	0.22	1.25	0.19	1.35	0.03	1.00
			sur	7.25	1.25	0.96	3.41	0.44	1.19	0.068	1.13	0.83	1.47	3.42	1.32	0.19	1.26	0.12	1.37	0.03	1.00
141	2019-29	19/11/2019	all	8.03	1.43	4.22	1.49	0.52	1.28	0.083	1.33	0.50	1.61	4.00	1.18	0.18	1.19	0.14	1.24	<	-
			bot	10.35	1.19	5.38	1.47	0.52	1.34	0.084	1.40	0.58	1.53	4.28	1.18	0.19	1.19	0.16	1.15	<	-
			sur	6.23	1.36	3.31	1.26	0.51	1.23	0.082	1.26	0.43	1.64	3.75	1.16	0.17	1.16	0.12	1.17	<	-
144	2019-32	16-17/12/2019	all	10.07	1.37	6.41	1.35	0.37	1.32	0.048	1.21	0.48	1.88	1.42	1.23	0.08	1.14	0.07	1.27	<	-
			bot	12.31	1.27	7.34	1.20	0.4	1.35	0.052	1.17	0.54	1.88	1.54	1.20	0.08	1.12	0.08	1.19	<	-
			sur	8.25	1.28	5.60	1.40	0.34	1.28	0.045	1.20	0.43	1.90	1.30	1.23	0.07	1.11	0.06	1.24	<	-

148	2020-01	22-23/01/2020	all	10.07	1.44	7.91	1.47	0.42	1.50	0.045	1.36	0.63	1.70	-	-	0.15	1.17	0.22	1.38	<	-
			bot	13.15	1.35	10.52	1.35	0.55	1.49	0.056	1.31	0.70	1.40	-	-	0.17	1.14	0.28	1.26	<	-
			sur	7.72	1.21	5.95	1.23	0.32	1.18	0.036	1.11	0.56	1.97	2.27	1.03	0.14	1.11	0.18	1.19	<	-
152	2020-19a	23/06/2020	all	5.28	1.29	1.67	1.52					0.97	1.40								
			bot	6.48	1.23	2.15	1.57					1.08	1.43								
			sur	4.31	1.06	1.30	1.20					0.88	1.37								
154	2020-19c	07/07/2020	all	6.84	1.43	2.79	1.79					1.17	1.32								
			bot	8.92	1.24	4.63	1.10					1.32	1.29								
			sur	5.25	1.29	1.90	1.61					1.04	1.29								
157	2020-20	20/08/2020	all	7.45	1.48	4.02	1.50					0.97	1.45								
			bot	9.78	1.33	5.16	1.34					1.05	1.32								
			sur	5.67	1.31	3.13	1.41					0.90	1.57								
159	2020-22	07/09/2020	all	14.71	1.28	11.51	1.30														
			bot	17.45	1.13	13.54	1.12														
			sur	12.39	1.25	9.80	1.30														

Table 2.6: W05 station. Mean and standard deviation of the dissolved data at the surface over the measuring period (-: not measured, blanco: not yet available, <: below detection limit).

No	cmp	Date	Salinity		DOC		DON		NOx		NO_2		NH_4		TDP		PO_4		Si	
					mg/l		µmol/l		µmol/l		µmol/l		µmol/l		µmol/l		µmol/l		µmol/l	
112	2018-18	27-28/03/2018																		
118	2019-01	24/01/2019	32.46	0.18	1.33	0.25	34.2	1.9	23.9	1.3	0.39	0.02	5.36	0.14	0.76	0.07	0.70	0.07	16.6	0.07
121	2019-03	13/02/2019	34.24	0.06	0.97	0.11	24.4	2.1	17.3	1.8	0.73	0.01	1.21	0.16	0.72	0.03	0.57	0.01	7.5	0.3
125	2019-11	08-09/04/2019	33.10	0.30	1.35	0.20	19.5	3.9	10.2	4.5	0.23	0.03	0.26	0.10	0.51	0.09	0.10	0.05	3.8	0.9
128	2019-14	21/05/2019	32.41	0.16	1.74	0.17	17.4	2.1	1.7	0.6	0.10	0.02	2.80	0.68	0.44	0.03	0.13	0.02	4.6	0.2
131	2019-17	25/06/2019	33.95	0.19	1.22	0.16	13.8	3.6	3.3	1.3	0.25	0.06	1.44	0.62	0.39	0.04	0.16	0.03	3.1	0.8
137	2019-22	12/09/2019	34.43	0.10	1.10	0.14	7.5	1.1	0.3	0.1	<	-	0.48	0.23	0.25	0.03	0.20	0.02	3.8	0.4
138	2019-25	15-16/10/2019	34.66	0.03	1.20	0.11	7.1	0.9	1.8	0.5	0.20	0.05	1.00	0.26	0.39	0.05	0.21	0.03	2.7	0.3
141	2019-29	19/11/2019	34.08	0.07	1.07	0.17	14.3	1.4	10.5	0.9	0.62	0.06	2.17	0.37	0.41	0.05	0.43	0.04	5.3	0.6
144	2019-32	16-17/12/2019	34.46	0.02	0.68	0.09	16.0	2.8	7.8	2.1	0.50	0.14	0.74	0.16	0.52	0.07	0.53	0.11	2.9	0.9
148	2020-01	22-23/01/2020	33.67	0.08	2.15	0.51	37.6	1.6	24.0	1.3	0.69	0.05	3.05	0.18	0.93	0.03	0.75	0.02	12.3	0.8
152	2020-19a	23/06/2020	32.14	0.31	1.40	0.12			6.1	1.9	0.45	0.10	4.50	2.21			0.22	0.12	3.9	1.5
154	2020-19c	07/07/2020	34.77	0.02	0.86	0.05					0.19	-	0.36	0.11			0.07	0.01	1.3	0.1
157	2020-20	20/08/2020	34.11	0.17																
159	2020-22	07/09/2020	34.32	0.09																

Table 2.7: W08 station. Geometric mean and multiplicative standard deviation of the particulate data over the measuring period and at the surface (sur) and the bottom (bot) and for all data (-: not measured, blanco: not yet available, <: below detection limit).

No	cmp	Date		SPM		Hach		POC		PON		TEP		ChlA		ChlB		FeoA		FeoB	
				mg/l		FNU		mg/l		mg/l		mgXG/l		µg/l		µg/l		µg/l		µg/l	
119	2019-01	25/01/2019	all	6.05	1.22	3.43	1.18	0.36	1.39	0.057	1.40	-	-	0.95	1.11	0.10	1.11	0.04	1.11	<	-
			bot	6.62	1.23	3.84	1.15	0.40	1.30	0.060	1.36	-	-	0.97	1.10	0.10	1.12	0.04	1.09	<	-
			sur	5.52	1.17	3.06	1.12	0.32	1.44	0.053	1.49	-	-	0.92	1.12	0.09	1.11	0.04	1.13	<	-
122	2019-03	14/02/2019	all	3.58	1.24	1.19	2.25	0.29	1.21	0.042	1.18	-	-	0.93	1.17	<	-	0.03	1.24	<	-
			bot	3.84	1.21	1.55	2.00	0.30	1.15	0.042	1.15	-	-	0.97	1.18	<	-	0.03	1.26	<	-
			sur	3.35	1.26	0.92	2.38	0.28	1.25	0.041	1.23	-	-	0.9	1.16	<	-	0.03	1.22	<	-
129	2019-14	22/05/2019	all	3.48	1.30	0.97	1.64	0.45	1.24	0.057	1.28	0.79	1.21	0.63	1.37	<	-	<	-	<	-
			bot	3.84	1.29	1.29	1.56	0.48	1.16	0.058	1.21	0.81	1.2	0.74	1.4	<	-	<	-	<	-
			sur	3.16	1.26	0.74	1.46	0.43	1.29	0.056	1.35	0.76	1.23	0.53	1.22	<	-	<	-	<	-
130	2019-17	24/06/2019	all	1.69	1.16	0.71	1.53	0.32	1.43	0.045	1.35	-	-	0.61	1.19	<	-	<	-	<	-
			bot	1.71	1.09	0.71	1.61	0.27	1.43	0.043	1.38	-	-	0.67	1.18	<	-	<	-	<	-
			sur	1.67	1.21	0.70	1.50	0.38	1.35	0.047	1.34	-	-	0.56	1.15	<	-	<	-	<	-
133	2019-20	20/08/2019	all	3.13	1.13	2.14	1.86	0.41	1.27	-	-	0.59	1.46	0.81	1.23	0.14	1.07	0.03	1.07	<	-
			bot	3.34	1.14	1.95	2.05	0.38	1.24	-	-	0.54	1.54	0.88	1	<	-	0.03	1	<	-
			sur	2.94	1.09	2.34	1.70	0.45	1.29	-	-	0.66	1.36	0.81	1.24	0.14	1.07	0.03	1.06	<	-
135	2019-22	09/09/2019	all	3.47	1.12	1.48	1.56	0.39	1.23	0.053	1.25	1.1	1.22	1.15	1.22	0.19	1.31	0.06	1.24	<	-
			bot	3.61	1.07	1.44	1.38	0.41	1.23	0.056	1.24	1.14	1.25	1.11	1.25	0.18	1.36	0.06	1.26	<	-
			sur	3.34	1.15	1.52	1.75	0.38	1.23	0.051	1.25	1.07	1.2	1.2	1.19	0.2	1.26	0.06	1.23	<	-
140	2019-25	17/10/2019	all	4.22	1.27	2.52	1.18	0.35	1.16	-	-	0.61	1.27	1.51	1.23	0.15	1.13	0.06	1.31	<	-
			bot	4.81	1.20	2.70	1.15	0.35	1.20	-	-	0.58	1.24	1.58	1.26	0.16	1.15	0.06	1.34	<	-
			sur	3.70	1.24	2.35	1.19	0.34	1.10	-	-	0.63	1.30	1.44	1.19	0.15	1.11	0.05	1.18	<	-
143	2019-29	21/11/2019	all	-	-	-	-	-	-	-	-	-	-	-	-	-	-	-	-	-	-
			bot	9.03	-	2.28	-	0.27	-	0.040	-	-	-	1.33		<	-	0.04		<	-
			sur	4.23	-	1.92	-	0.43	-	0.050	-	-	-	1.41		<	-	0.04		<	-
146	2019-32	18/12/2019	all	5.94	1.21	3.75	1.38	0.25	1.26	0.035	1.22	-	-	0.78	1.18	0.07	1.18	0.03	1.12	<	-
			bot	6.45	1.18	4.22	1.38	0.30	1.23	0.035	1.23	-	-	0.81	1.21	0.07	1.20	0.04	1.11	<	-
			sur	5.47	1.19	3.34	1.35	0.22	1.14	0.039	1.00	-	-	0.76	1.17	0.06	1.17	0.03	1.00	<	-
149	2020-01	23/01/2020	all	4.25	1.26	2.58	1.30	0.20	1.37	0.024	1.15	0.32	1.54	1.97	1.14	0.21	1.15	0.07	1.22	<	-
			bot	5.04	1.12	2.91	1.23	0.23	1.27	0.023	1.07	0.36	1.49	2.1	1.12	0.22	1.06	0.08	1.17	<	-
			sur	3.59	1.22	2.28	1.30	0.18	1.43	0.024	1.24	0.29	1.59	1.85	1.13	0.2	1.19	0.06	1.19	<	-

153	2020-19a	24/06/2020	all	3.08	1.20	0.72	1.24					1.04	1.14								
			bot	3.25	1.27	0.77	1.23					1.09	1.20								
			sur	2.92	1.14	0.68	1.26					0.99	1.05								
155	2020-19c	08/07/2020	all	3.26	1.37	0.97	1.27					0.51	1.21								
			bot	4.05	1.22	1.15	1.12					0.51	1.16								
			sur	2.62	1.29	0.82	1.23					0.50	1.28								
158	2020-20	21/08/2020	all	4.47	1.26	1.83	1.28					0.36	1.55								
			bot	4.68	1.30	1.96	1.25					0.31	1.54								
			sur	4.26	1.26	1.67	1.33					0.43	1.53								
160	2020-22	08/09/2020	all	4.03	1.30	2.03	1.42														
			bot	4.99	1.14	2.48	1.33														
			sur	3.26	1.17	1.65	1.34														

Table 2.8: W08 station. Mean and standard deviation of the dissolved data at the surface over the measuring period (-: not measured, blanco: not yet available, <: below detection limit).

No	cmp	Date	Salinity		DOC		TDN		NOx		NO_2		NH_4		TDP		PO_4		Si	
					mg/l		µmol/l		µmol/l		µmol/l		µmol/l		µmol/l		µmol/l		µmol/l	
119	2019-01	25/01/2019	34.89	0.03	1.11	0.27	13.9	1.6	9.7	0.4	0.29	0.10	0.25	-	0.59	0.08	0.58	0.14	4.16	0.23
122	2019-03	14/02/2019	34.93	0.02	0.89	0.12	17.3	2.5	11.3	1.6	0.37	0.01	0.27	0.12	0.72	0.01	0.53	0.02	3.98	0.17
129	2019-14	22/05/2019	34.76	0.06	1.02	0.09	6.2	1.0	<	-	<	-	0.63	-	0.24	0.02	0.07	0.01	2.00	0.22
130	2019-17	24/06/2019	35.04	0.02	1.01	0.21	9.3	7.9	2.30	3.18	<	-	0.96	-	0.23	0.05	0.09	0.02	1.50	0.13
133	2019-20	20/08/2019	35.02	0.02	1.16	0.29	5.2	1.7	1.31	1.19	<	-	0.19	0.03	0.23	0.02	0.10	0.01	3.46	1.05
135	2019-22	09/09/2019	35.01	0.02	0.97	0.12	7.0	3.0	1.25	1.89	<	-	0.40	0.26	0.23	0.03	0.14	0.02	1.89	0.45
140	2019-25	17/10/2019	35.00	0.02	0.75	0.05	7.7	0.6	1.75	0.26	0.16	0.03	0.69	0.26	0.37	0.02	0.20	0.01	3.98	0.35
143	2019-29	21/11/2019	35.09	-	0.81	-	11.9	-	6.3	-	0.60	-	0.46	-	0.44	-	0.44	-	3.87	-
146	2019-32	17/12/2019	34.95	0.44	0.74	0.09	11.6	1.9	5.6	1.4	1.24	0.14	0.17		0.40	0.05	0.49	0.03	2.80	0.78
149	2020-01	23/01/2020	34.91	0.05	2.02	0.09	19.5	1.24	10.7	0.92	0.62	0.06	0.23	0.11	0.71	0.06	0.56	0.04	4.18	0.41
153	2020-19a	24/06/2020	34.43	0.09	1.01	0.05							0.19	0.06						
155	2020/19c	08/07/2020	35.03	0.02	0.94	0.08											0.08	0.01	1.26	0.11
158	2020/20	21/08/2020	34.72	0.03																
160	2020/22	08/09/2020	34.84	0.01																

3. Chemische en sedimentologische karakterisatie van suspensiemateriaal verzameld met sedimenttraps(*)

Persistent organic pollutants, such as polychlorinated biphenyls (PCBs), transferred to the environment from different anthropogenic activities are of worldwide concern. PCBs are organic pollutants of aquatic environments (Mearns et al. 1988). They are highly hydrophobic, bio-accumulating in the fatty tissues, resistanting to biodegradation, and have various effects on health (Connell et al. 1998) and ecosystems (Long et al. 1995). Their behaviour in different environmental matrices (water, sediments, suspended particulate matter (SPM), and biota) is being increasingly investigated to evaluate their fate and potential risks. Sediments and SPM are composite materials, which contain inorganic substances, mineral particulates, and organic matter in various stages of decomposition, and constitute the fingerprint of natural and anthropogenic activities of the environment they are encountered in. A diversity of methods and equipment are routinely used to collect SPM in the water column, such as Niskin bottles, Go-Flo bottles, and stand-alone or onboard sea water pumps or suction systems. The water samples are filtered to capture the particulate matter for further analysis of organic and inorganic matter, or chemical analysis of pollutants (Neukermans et al. 2012; Tsompanoglou et al. 2017; Schartau et al. 2019). The amount of SPM that can be collected depends on the concentration of SPM in the water, however, sampling capacity is limited as filters typically clog during loading. As a result, the above-mentioned sampling devices typically fail to collect sufficient material. This limits the analysis of certain organic, inorganic or chemical substances in the SPM, due to insufficient sample size collected on a filter. For example, the minimum sample size in grams per dry weight is 20 g for grain size analysis and 1 g for total organic carbon (TOC), while several grams are required for priority pollutants, pesticides, PCB, and clay mineral analysis (Środoń et al. 2001). In tidal dominated areas, the time series that can be collected with in situ water sampling rarely exceeds the duration of a tidal cycle (e.g. Fettweis & Lee 2017; Chapalain et al. 2019; Deng et al. 2019). The use of a water centrifuge on board facilitates the collection of more matter, but the number of samples remains limited. Further, the water samples reflect the composition only at the moment of sampling and do not allow further investigation of the natural variability during longer periods or storm events. In addition, the occurrence of specific phenomena caused by episodic or isolated contamination events are often overlookedusing such methods. The use of automatic water samplers is suitable in protected environments, such as on a vessel or along a river, but remains impractical in marine areas. In oceanography, it is common to sample the SPM using vertical sediment traps that consist of a broad funnel and a collecting jar at the bottom (Fowler et al. 2007; Honjo et al. 1980; Madrid & Zayas 2007; McDonnell et al. 2015). As the currents in oceans are generally low, the particles move quasi vertical and can be collected in these traps. This method is less suited for dynamic coastal environments where the horizontal currents are about 3 orders of magnitude larger than the vertical ones. Cartwright et al. (2015) use a horizontal sediment trap to collect SPM in tidal dominated areas with strong horizontal currents. This type of trap has not yet been used in pollution research and there is currently no examination of its trapping efficiency. This study therefore aims to evaluate the efficiency of horizontal and vertical traps in a dynamic nearshore area by comparing the characteristics of the trapped SPM with the concentration and particle size distributions derived from optical sensors, and to reconstruct TOC and PCB time series from the trapped material.

(*) Adamopoulou A, Baeye M, Belháčová-Minaříková M, Parmentier K, Fettweis M. Chemical and sedimentological characterization of suspended particulate matter in coastal marine ecosystems using sediment traps. submitted to Marine Polltion Bulletin

3.1. Methodology

3.1.1. Sediment trap

Three types of particle interceptor traps (PIT) trapping SPM horizontally and a Technicap PPS4/3 trapping SPM vertically have been examined (Figure 3.1). The Technicap PPS4/3 (1310 cm x 490 cm) equipped with a 12-bottle carousel, is commonly deployed in oceans or less-dynamic shelf seas. Its vertical alignment is designed to trap particles from vertical transport (Prouty et al. 2017; Mienis et al. 2012). The custom-made horizontal sediment trap PIT is based on the design of Cartwright et al. (2015). It consists of a 60 cm high PVC tube with 7.6 cm inner diameter, lidded at the bottom with a PVC lid and vertically attached to a frame. This study investigates three different PIT designs: one with three holes of 1 cm and one with five holes of 2 cm diameter, respectively, which are placed 4 cm below the top of the tube, and which do not have a top lid during the first half of the sampling; and one PIT design with three holes of 1 cm and both ends of the tube lidded with a PVC lid during the second half of the sampling (this design is hereafter termed the CPIT).

Figure 3.1: Tripod ready to be deployed at MOW1. Attached are left (white cylinder) the Technicap PPS4/3 and at the cage a CPIT (2mab). Right photo shows a 0.6mab PIT.

3.1.2. Sampling and in situ measurements

The measurements were carried out between 14th March and 20th May 2016 (Julian day 74 to 141), at the MOW1 station (51°N 21.50', 3°E 8.08') situated about 5 km offshore and in the port of Zeebrugge (51°N 19.85', 3°E 11.98'), see Figure 3.2. At MOW1 a tripod was deployed at MOW1 that was equipped with, amongst others, a Laser in-situ Scattering and Transmissometry 100X (LISST), which measures the volume concentration in 32 logarithmically spaced size groups over the range of 2.5-500 µm and thus the particle size distribution (PSD) (Agrawal & Pottsmith 2000). The Technicap PPS4/3 was attached to the tripod during the first half of the sampling period (14th March to 14th April 2016). Each bottle sampled during five tidal cycles (62 h). The PIT with three holes of 1 cm, the Technicap PPS4/3, and the LISST were all mounted at 2 m above the seabed (mab). The PIT with five holes of 2 cm was attached at about 0.6 mab. The open PITs will be referred as 2mab PIT and 0.6mab PIT, on the basis of their distance above the seabed, respectively. The CPIT was sampling during the second half of the sampling period from 14th April to 20th May 2016 and was placed at 2 m above the seabed and is termed as the 2mab CPIT. Further a 2mab PIT and 0.6 mab PIT were placed in the port of Zeebrugge. At the beginning and at the end of the measuring period, sediment was sampled with a Van Veen grab at both locations.

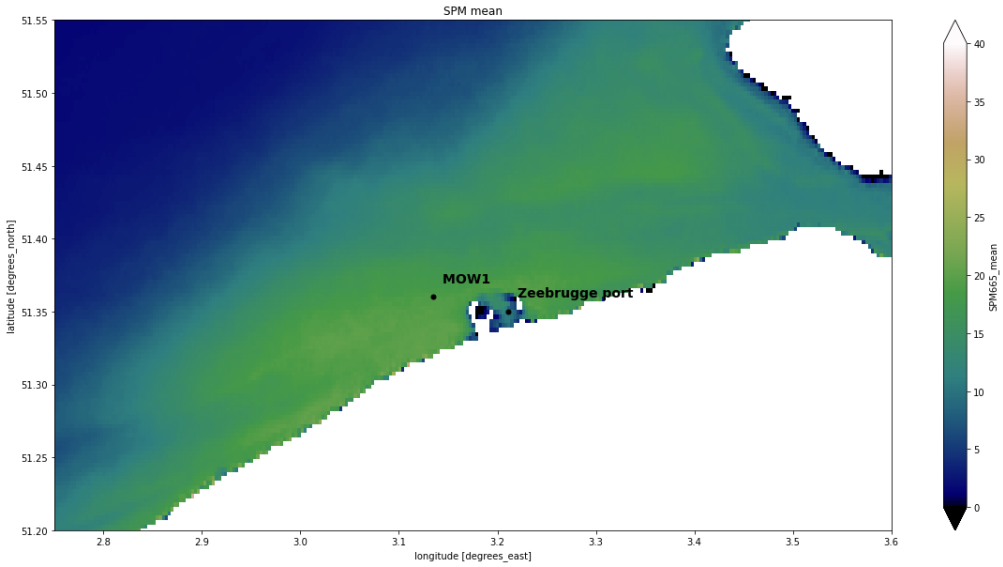

Figure 3.2: Averaged near surface SPM concentrations in the Belgian coastal zone (southern North Sea) computed from satellite images during the period 2017–2019. The sampling stations at MOW1 and in the port of Zeebrugge are indicated.

3.1.3. Sample processing

3.1.3.1. Technicap PPS4/3 samples

The samples obtained from the Technicap PPS4/3 are shown in Figure 3.3. The amount of collected material is low.

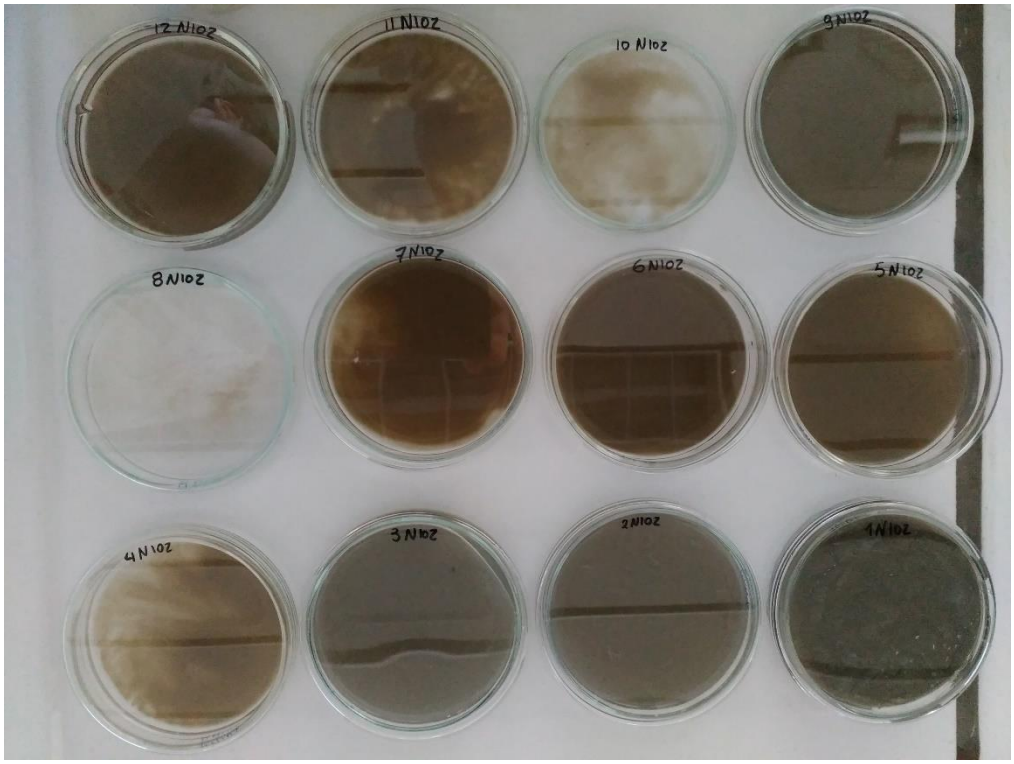

Figure 3.3: Samples obtained from the Technicap PPS4/3 during the period 14 March 14 April 2016. Each sample represents 5 tidal cycles.

3.1.3.2. PITs and CPIT samples

The PITs and the CPIT were scanned with a Siemens Somatom Definition Flash X-ray computed tomography (CT) scanner in order to visualise the density structure of the sampled SPM. The scanner was operated at 120 kV, with an effective mAs of 200 and a pitch of 0.45.A 'soft tissue' and 'bone' reconstruction scan was applied in each sediment trap. Volume 1 Graphic's VG Studio 2.2 software was used to visualize the central scan of the trap (Cnudde & Boone 2013). The PITs and the CPIT were split lengthwise and photos were taken with a Geotek Multi – Sensor Core Logger (MSCL-S), see Figure 3.4.

The layers observed in the CT images (Figure 3.4) were counted and sampled. The latter was done with the Volume Graphics'sVGStudio 2.2 software that places a ruler next to the real size photo allowing sampling of every layer of interest. A low-density polyethylene (LDPE) plastic circle (0.76 m diameter) and a metal spatula were used for the subsampling of the layers. The SPM samples from the harbour PITs were extracted as a whole without further subsampling.

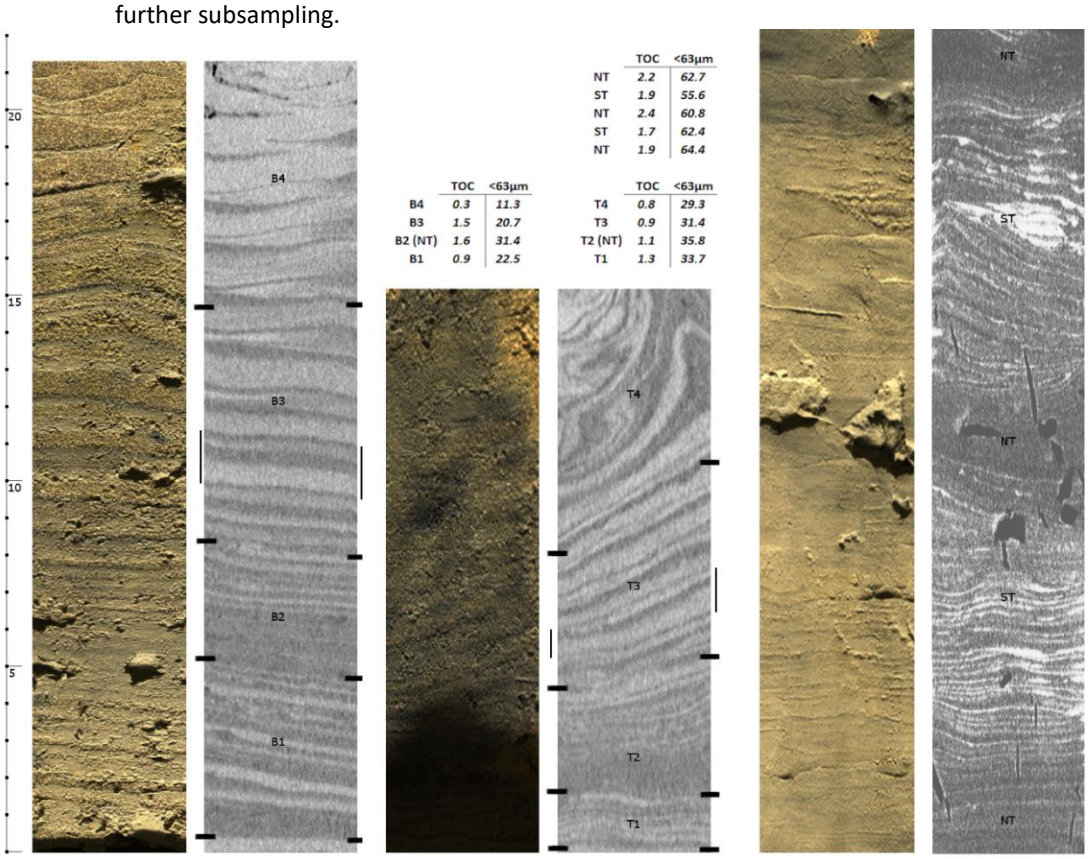

	TOC	<63µm
NT	2.2	62.7
ST	1.9	55.6
NT	2.4	60.8
ST	1.7	62.4
NT	1.9	64.4

	TOC	<63µm
B4	0.3	11.3
B3	1.5	20.7
B2 (NT)	1.6	31.4
B1	0.9	22.5

	TOC	<63µm
T4	0.8	29.3
T3	0.9	31.4
T2 (NT)	1.1	35.8
T1	1.3	33.7

Figure 3.4: Geotek photos and medical X-ray CT scans, revealing a rhythmic sequence of greyish layers. The SPM layers with a lower X-ray attenuation appear darker, whereas SPM layers with a higher X-ray attenuation appear lighter. The included table is TOC percentages and mud percentages of the sub-samples (see sections T, B, NT, and ST).

3.1.3.3. Grain size and organic matter analysis of samples from traps and Van Veen grab

Grain size analysis of the SPM from the traps and the seabed samples was conducted with a Malvern Mastersizer 3000 laser grain size analyser equipped with a Hydro MV dispersion unit. Organic carbon, calcium carbonate ($CaCO_3$) and biogenic silica were removed prior to grain size analysis using H_2O_2 and HCL. NaOH was used to achieve total disaggregation of the clay particles. The carbon content of the samples was determined using Flash TCD 2000. Prior to TOC analysis, the inorganic carbon was removed with hydrochloric acid.

3.1.3.4. Chemical extraction of samples from traps and Van Veen grab

After addition of recovery internal standards (RIS), i.e. PCB 4, 29, and 185 (50 ng), the freeze-dried SPM subsamples with a range of 10 - 30g, depending on their TOC content (TOC%), were Soxhlet extracted for 8 hours using 100 ml of dichloromethane (Smedes & De Boer 1997). After Kuderna-Danish solvent reduction to 2 ml, sulphur was removed by addition of ca. 100 mg activated copper powder and ultrasonic treatment for 30 min. Thereafter, the extracts were reduced to less than ca. 2 ml by evaporation in a water bath using a Kuderna-Danish apparatus. After the addition of 20 ml hexane, the extracts were azeotropically transferred to hexane and evaporated to ca.1 ml. Aliquots of sampler extracts were divided into vials for different types of GC/MS analysis. A 70% portion of extract (for analysis of PCBs) was purified by clean-up using a glass column containing 8 g of silica gel, modified with concentrated sulfuric acid (44%, w:w), and eluted with 30 ml of hexane-dichloromethane, 1:1 (v:v) mixture. After addition of 10 ng PCB 121, the eluates were Kuderna-Danish concentrated down to ca. 1 ml, quantitatively transferred to cone-shaped mini vials, and the volume was further reduced to 0.1 ml under a gentle nitrogen flow. The same procedure was performed for the sediment samples.

3.1.3.5. PCB analysis

PCBs were analysed using a 7890B gas chromatograph (GC; Agilent, USA) equipped with a 60m×0.25mm×0.25µm HT-8 capillary column (SGE Analytical, UK) coupled to an Agilent 7000B Mass Spectrometer (MS) triple quadrupole operated in EI+ mode. At least 2 MRM transitions were recorded for each analysed compound. Three µl of extract were injected in pulsed splitless mode at 280 °C. Helium was used as carrier gas at the flow of 1.5 ml per minute. The GC temperature program started at 80 °C (1.5 min hold), ramped 40 °C min^{-1} to 200 °C (18 min hold), and finally ramped 5 °C min^{-1} to 305 °C.

3.2. Results

3.2.1. Sediment traps

The environmental conditions (wind direction and velocity and wave height) and the hydrodynamic ones measured by the tripod (temperature and salinity; ADV current velocity, altimetry and acoustic backscatter) during the sampling periods are shown in Figures 3.5 and 3.6. The three PITs (2mab PIT, and 2mab CPIT) trapped sediments in suspension with total volumes of 0.975 (height of 21.5 cm), 0.703 (height of 15.5 cm), and 1.029 (height of 22.5 cm) litres, respectively. The layering visible in the CT scans (Figure 3.4) corresponds to tidal variations, which become more disturbed towards the top of the traps. Every four layers correspond to one tidal cycle allowing identification of the exact date of the tide. The two thinner layers represent low current conditions (when less and finer material is trapped) and the two thicker layers represent high current conditions (when more and coarser SPM is trapped). Long term variations such as spring and neap tide have also been captured. The rhythmic sequence of greyish layers highlighted in the X-ray CT scans (Figure 3.4) is caused by differences in X-ray attenuation of the particles trapped and indicates changes in composition of the material. The latter is confirmed by particle size analysis of different subsamples from the (B1, B2, B3, B4), 2mab PIT (T1, T2, T3, T4) and 2mab CPIT (ST and NT referring to spring tide and neap tide, see labels Bx, Tx, ST, and NT in Figure 3.4). The alternation of sandier and muddier layers corresponds with the lunar tidal cycle with weaker current magnitudes, lower SPM concentrations, and less sand grains in suspension during neap tide compared to spring tide.

The layers in the PITs correspond with the SPM trapped during the ebb, flood, and slack water periods and thus represent a time series of about 10 days that reflects the recurring increasing and decreasing current magnitudes associated with the semi-diurnal tidal regime

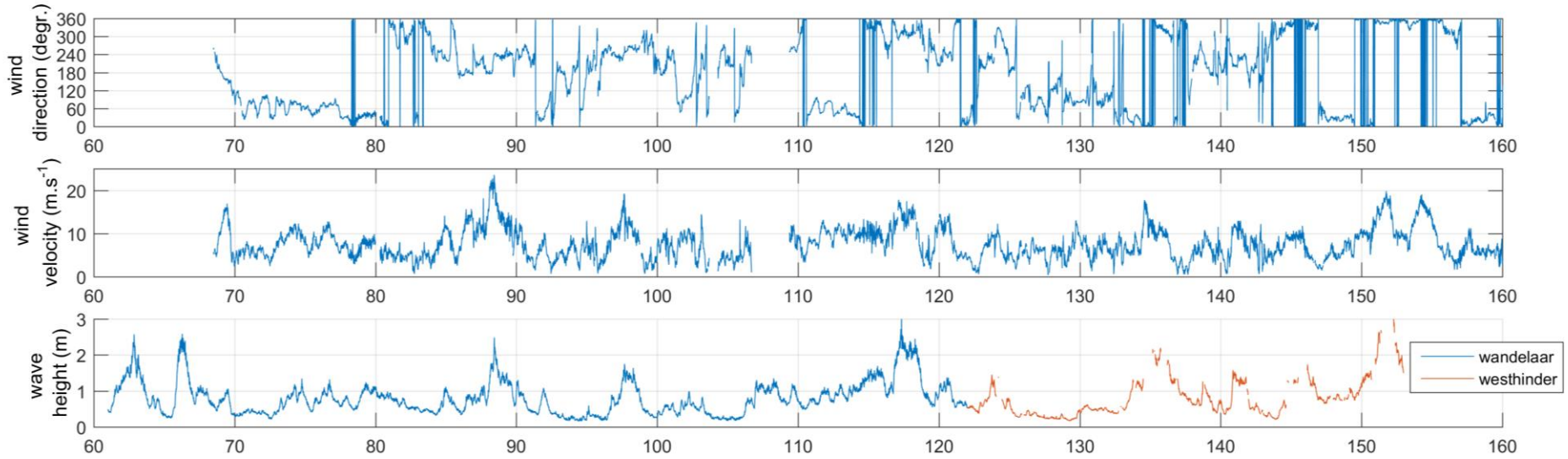

Figure 3.5: Wind direction and velocity (Wandelaar) and significant wave height from February till June 2016.

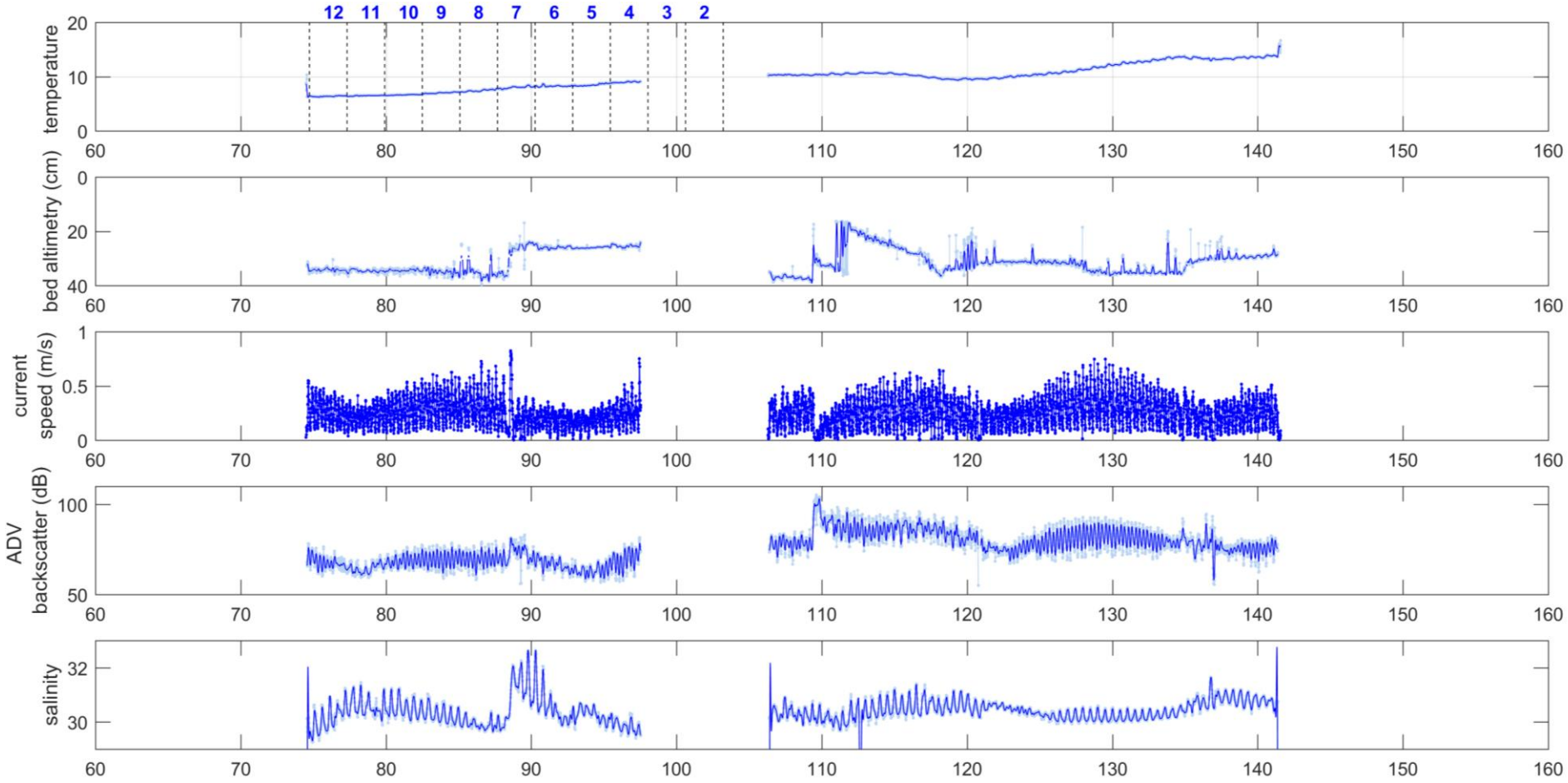

Figure 3.6: Hydrodynamic conditions measured by the tripod (temperature and salinity: CTD; Current velocity, altimetry and acoustic backscatter at 0.2 mab: ADV) during the period 20 March – 20 May.

of the study area. For example, each vertical black line in the 0.6mab and 2mab PIT (Figure 3.4) corresponds with a tidal cycle. Towards the top, we distinguish between (1) a light grey layer enriched in sand grains that was trapped during flood, followed by (2) a thinner darker layer with higher mud content trapped during slack water, followed by (3) a light grey layer, somewhat less bright than during flood, corresponding with ebb, and finally, (4) a darker layer containing more mud particles trapped during the subsequent slack tide. The flood layer at the beginning of the cycle that is highlighted in Figure 3.4 and described above is thicker than the flood layer before and after as the associated flood currents were stronger. This is mainly due to wind effects rather than variations in tidal amplitude, allowing us to allocate an exact time-date to this event (Julian day 81.5 or 22nd March). In Figure 3.4, the different sections indicated with T1 to T4 and B1 to B4, for the 2mab PIT and respectively, correspond to the sampling periods of the Technicap trap and each cover five tidal cycles (Figure 3.7). The 0.6mab and the 2mab PIT cover a period of 10 days, whereas the 2mab CPIT corresponds to a time-series of 35 days with 3 neap tides and 2 spring tides. The mud content in the four sections varies between 11.3% and 31.4% in the and between 29.3% and 35.8% in the 2mab PIT. The mud percentages in the sediments trapped during neap tide (i.e. the B2 and T2 sections) are highest in both open-end PITs, but remain relatively low compared to the 2mab CPIT. The neap tide sections in this trap have mud contents between 60% and 65%, which are almost double the values recorded in the open-end PITs. Spring tides in the CPIT have slightly lower mud contents of 62.4% and 55.6%. Table 3.1 presents the PPS4/3 sand and mud percentages during the four sampling periods, indicating that the percentages are 3 times higher compared to the 2mab PIT.

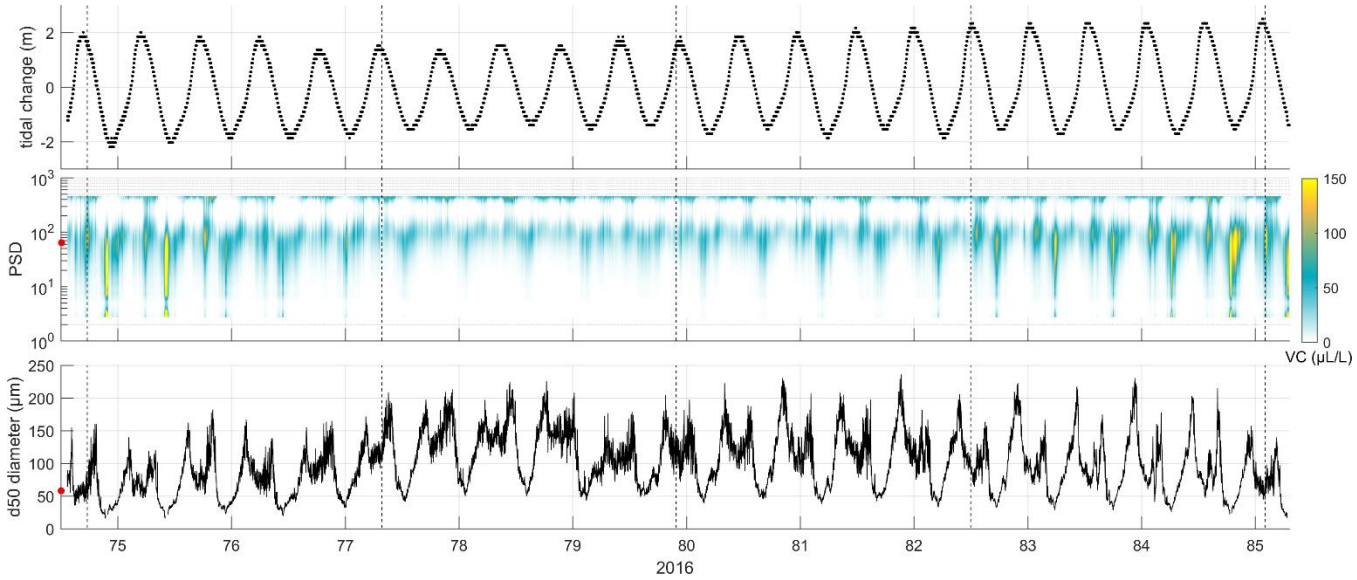

Figure 3.7: Upper graph shows the tidal sea level change in meters; the middle graph shows the volume concentrations (VC) in the 32size classes. The lowest graph represents the median particle diameter in µm. The red dot is at 63 µm. The vertical dashed lines separate each sampling window of five tides (cfr. PPS 4/3 sampling scheme).

Table 3.1: The mud percentages of trapped particles by the PPS 4/3 in each sampling window.

start Julian day	end Julian day	>63µm fraction
74.73	77.32	91.1
77.32	79.91	95.3
79.91	82.50	71.0
82.50	85.09	92.1

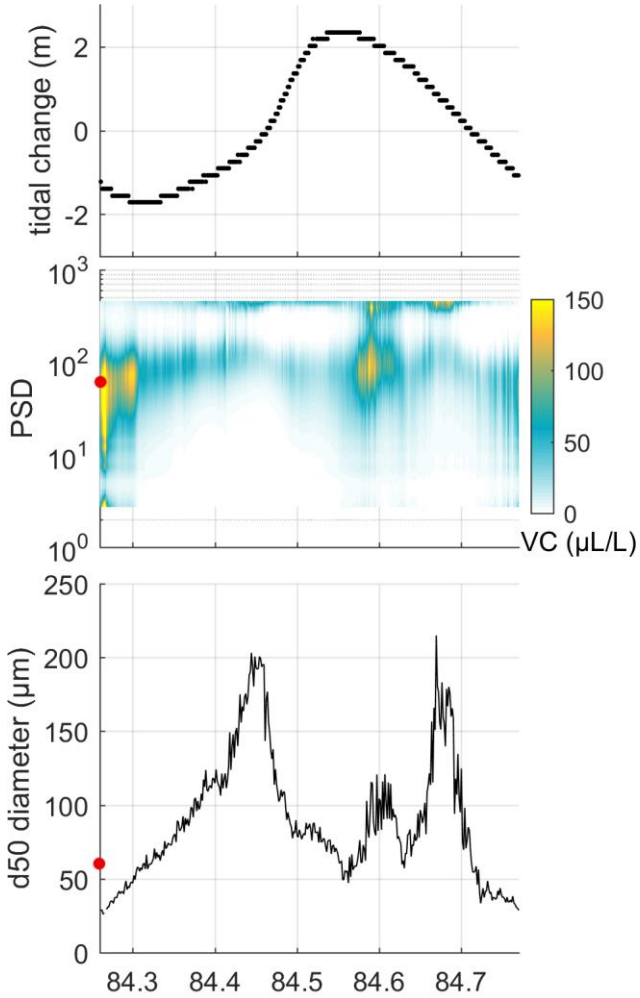

Figure 3.8: Detail from Figure 3.7 (day 84). Upper graph shows the tidal sea level change in meters; the middle graph shows the volume concentrations (VC) in the 32size classes. The lowest graph represents the median particle diameter in µm. The red dots are at 63 µm.

3.2.2. LISST data (2mab)

The SPM volume concentration (VC) and particle size distribution measured by the LISST at the 2mab PIT during the PPS4/3 deployment are shown in Figure 3.7. The vertical dashed lines separate each sampling window (i.e. 5 tides) of the PPS 4/3. The tidal variations in water level are shown in the upper graph, with neap tide occurring around day 78 and spring tide around day 85. The middle graph shows the VC in the 32 size classes of the LISST and the lower graph the median particle diameter (d50). The d50 varies between 20 and 230 µm (T2 section in Figure 3.4). The variations in d50 are typically associated with the tidal current variations, with the largest sizes occurring around slack water (around low and high-water level) and the smallest ones during maximum currents (at about half tidal level), see Figure 3.7. This indicates that the SPM consist of mainly flocs rather than sand grains. However, since the measurements have been carried out in a sand-mud mixed-sediment environment, the LISST has also detected fine sand grains in suspension (as shown in Figure 3.8), where the small peak in the d50 that occurred at maximum flood currents (around day 84.6) is caused by fine sand grains in suspension. This result is in line with similar observations by Baeye et al. (2011).

3.2.3. PCB concentrations

All the subsamples from the sections T, B, NT, and ST from both PITs and from the CPIT were extracted for PCB analysis (PCB 28, PCB 52, PCB 101, PCB 138, PCB 153, and PCB 180). The

total PCB concentration in µg/kg normalized to TOC% are presented in Figure 3.9. The 0.6mab and the 2mab PIT exhibit a PCB concentration range from 4.71 to 8.54 µg/kg. The 2mab CPIT has a PCB concentration range from 3.5 to 5.0 9 µg/kg. Interestingly, the PCB concentration range was higher for the open PITs. The highest PCB value for all PITs was found at the T4 section and the lowest at NT_5. There was no correlation between PCBs - TOC% and PCBs - mud fraction found. However, the samples allowed the creation of PCB time-series of 45 days with average value of 5.81 µg/kg.

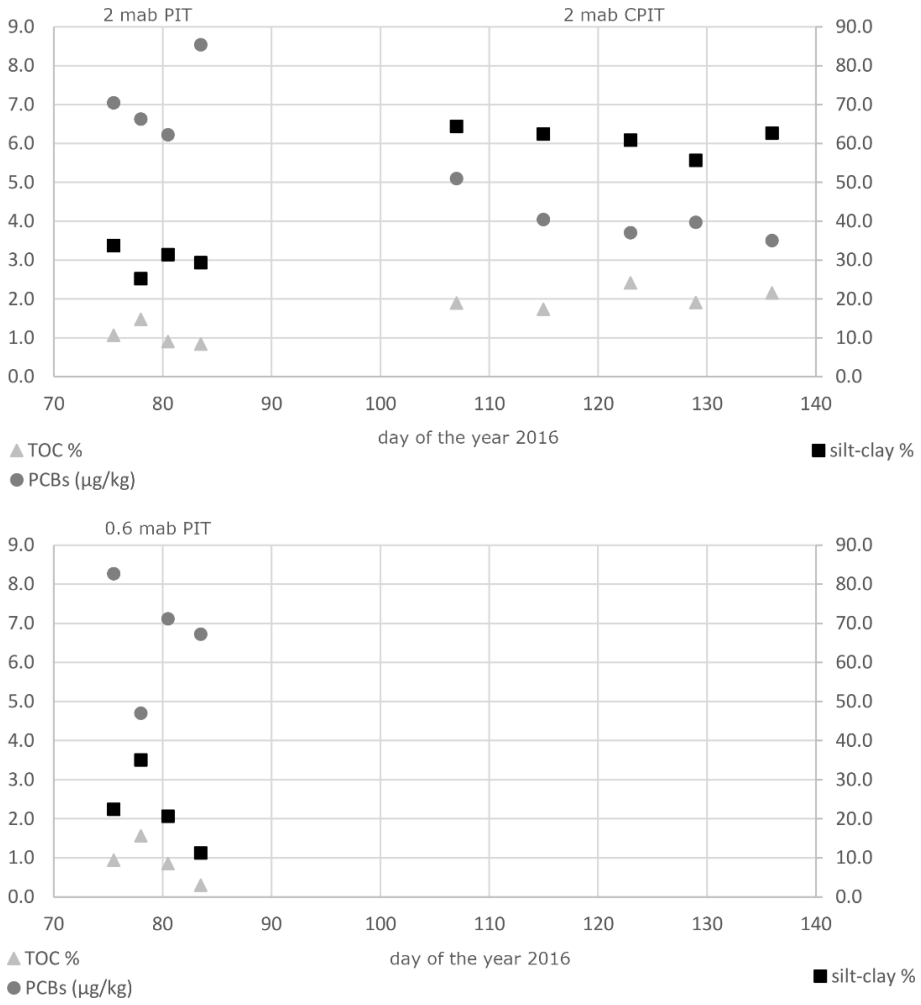

Figure 3.9: PCB, TOC and silt- clay series of 45 days, where cycle points represent the total PCB concentration in µg/kg normalized to TOC content, triangle points represent TOC% and square points represent the silt-clay % from both PITs and the CPIT.

3.2.4. TOC and mud content

The average TOC and mud content were highest during neap tides, when overall currents are weaker and relatively less sandy material is in suspension. The 0.6mab and the 2mab PIT exhibited TOC contents ranging between 0.31% and 1.49% and presented the highest TOC values at B2 and T2 (where the NT was also observed) with mud fractions of 31.41% and 35.75%, respectively. The 2mab CPIT had a TOC content ranging between 1.73% and 2.41%, with a NT average of 2.2% and ST average of 1.8%, respectively. TOC content in the CPIT ranged between 0.3% and 2.4%, and is positively correlated with corresponding mud content (Pearson r = 0.85). The TOC and mud content in the CPIT were double (approximately 2%) that observed in the PITs (approximately 1%). This is probably due to the presence of a top lid that resulted in improved settlement of the fine material and a reduction

of the flow of fine material out of the trap. The TOC% variation in the PIT samples was 3.4 times greater than in CPIT samples; however, it is important to remember that this represents a sampling period of 10 days for the PIT samples compared to 35 days for the CPIT (Figure 3.9).

3.2.5. PCB concentrations, TOC and mud content of the seabed and the harbour samples

The total PCB concentration, TOC, and mud content in both SPM and sediment samples was higher in the samples from the port of Zeebrugge than from the 5 km offshore MOW1 station (Table 3.2). The average TOC content in the sediment samples from the port was 2.4% while at MOW1 it was 0.3%. The average PCBs concentration in the sediment samples was 2.4 times higher than at MOW1. PCB levels were 2-3 times higher in samples with a higher TOC content. The total PCB concentration in the SPM from the port of Zeebrugge was 7.66 ng/kg compared to5.82 ng/kg (2mab PIT).

Table 3.2: Total PCB concentrations, TOC and mud content in the SPM and sediment from Zeebrugge harbour and sediment from MOW1 station.

Area	sampling depth	Sediment	Total PCB (µg/kg)	TOC%	Mud %
Harbour		-	7.66	2.65	85
Harbour	2mab PIT	-	5.82	2.7	66
Harbour	-	start	8.76	2.41	93.69
Harbour	-	end	5.73	2.34	95.07
MOW1	-	start	3.30	0.41	22.89
MOW1	-	end	2.87	0.19	2.59

3.3. Discussion

3.3.1. Representativeness of SPM from sediment traps

The PSD analysed with the Malvern in each sample of the PPS4/3 and the 2mab PIT are significantly different from the corresponding in situ measurements by the LISST (Figure 3.10). This figure shows that the main Malvern-PSD mode is around 15 µm for the PPS4/3 and 160 µm for the 2mab PIT, while the LISST main mode was about 80 µm. The differences between Malvern and LISST derived PSD are caused by the grain size measurements and the trapping method. The LISST measures the SPM in situ and encompasses formation and break up of flocs by flocculation processes. When analysing with the Malvern3000 (PPS4/3 and 2mab PIT) on the other hand, the pre-treatment results in a deflocculation of the particles. Nevertheless, the mismatch between the PSD of the PPS4/3 and the 2mab PIT is remarkable (about 145 µm). It appears that the PPS4/3 has trapped mostly the SPM that occurs as flocs, whereas the 2mab PIT has trapped flocs and fine to medium sands. The 2mab PIT further demonstrates a bimodal PSD, with a first mode around 30 µm and a second main mode around 160 µm. Figure 3.11 illustrates the deflocculated PSD analysed with the Malvern for the three PITs. The first set of PSDs (left column), which correspond with the 0.6mab and 2mab PIT, are very similar regarding the main grain size modes. The small changes in PSD can be explained by the different sampling height. The Malvern PSDs from the 2mab CPIT contain finer particles; however, the peak in the fine sand size class remains prominent. Each type of trap clearly represents only a specific part of the PSD. The PPS4/3 is biased towards flocs (the material that quickly settles during slack water) while the PITs and the CPIT are biased towards the coarser granular particles (which are suspended during maximum currents). In the (C)PIT traps, sand-sized particles are present during all phases of the tide. This is probably due to the settlement of the sand grains in the fresh and fluffy layers.

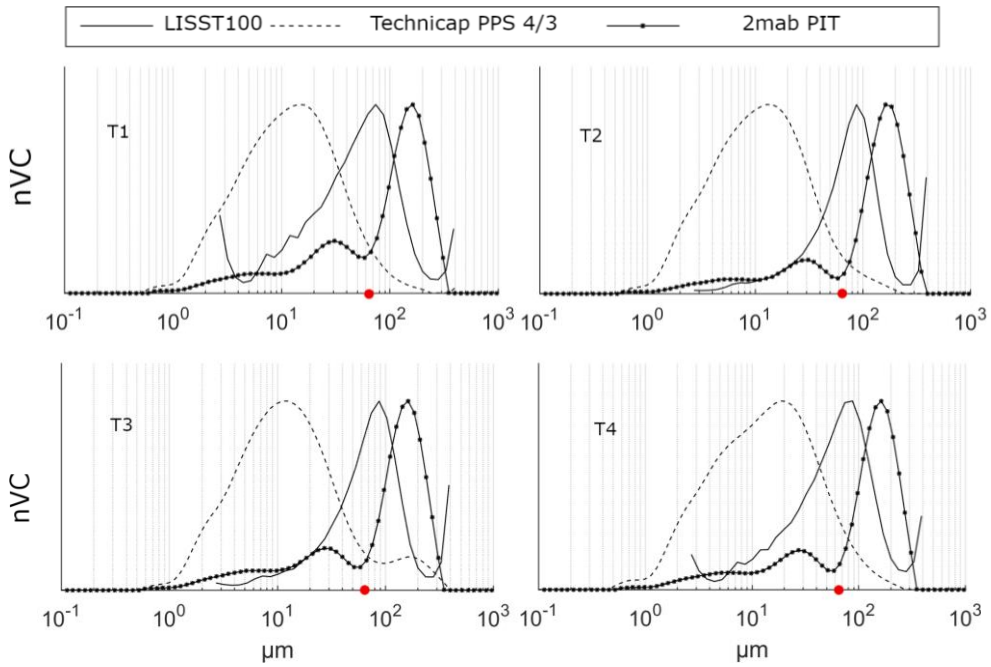

Figure 3.10: Normalized PSD comparison at 2 mab between LISST measurements (solid line), PPS 4/3 (dashed line) and 2mab PIT (point-to-point line). The latter two were PSD-analysed with Malvern3000). The red dot is the 63 µm border.

Notwithstanding the occurrence of sand-sized particles in suspension at MOW1 during maximum flood currents, the main volume fraction of the SPM behaves as flocs (Baeye et al. 2011). It is therefore surprising that the amount of sand grains in the (C)PITs is high and in contrast with other results and with the PPS4/3 analysis. For example, SPM sampled using a centrifuge on board a vessel in the same area contained almost no sand sized fractions (<2%) and had a deflocculated median particle size (Malvern) of 1-7µm (Fettweis 2008) and a not-deflocculated particle size (Malvern) of 8-30µm (Adriaens et al. 2018). The SPM from other high turbid environments is generally described as flocs without significant sand content (Manning et al. 2010; Verney et al. 2009). However, the majority of samples have not been collected in the near bed layer, where sand may occur in suspension when a critical shear stress is exceeded (Soulsby 1997). Major beach nourishment works have been carried out along the Belgian coast in recent years (Van den Eynde et al. 2019) and beach erosion during storms could partly explain the sand content in the traps. However, given the contrasting results between the PPS3/4 trap and the 2mab (C)PIT, it is most probable that the sand fraction is over-represented in the latter traps and that the SPM present in the PPS4/3 trap corresponds better with the SPM measured by the LISST. Based on these results, we argue that sediment traps for quantitative studies of SPM dynamics should be tested further in tidal environments such as the Belgian nearshore area, as the material in the traps does not necessarily correspond that found in situ. Sediment traps should therefore be installed together with sensors that allow examination of the in-situ composition of the SPM in order to obtain integrated results. PITs remain a useful tool to collect a sufficient amount of material for pollution and sediment dynamics monitoring.

3.3.2. PCBs in the traps

Numerous spot sampling studies have examined the fluxes of SPM and their associated contaminants such as heavy metals (Helali et al. 2016; Suja et al. 2017), PAHs (Zhang et al. 2017), and PCBs (Jartun et al. 2008; He et al. 2006). Our study focuses on the PCB contaminants and the creation of a PCB time-series sampling scheme. It appears that PCB concentrations obtained during the present study are of the same order of magnitude as

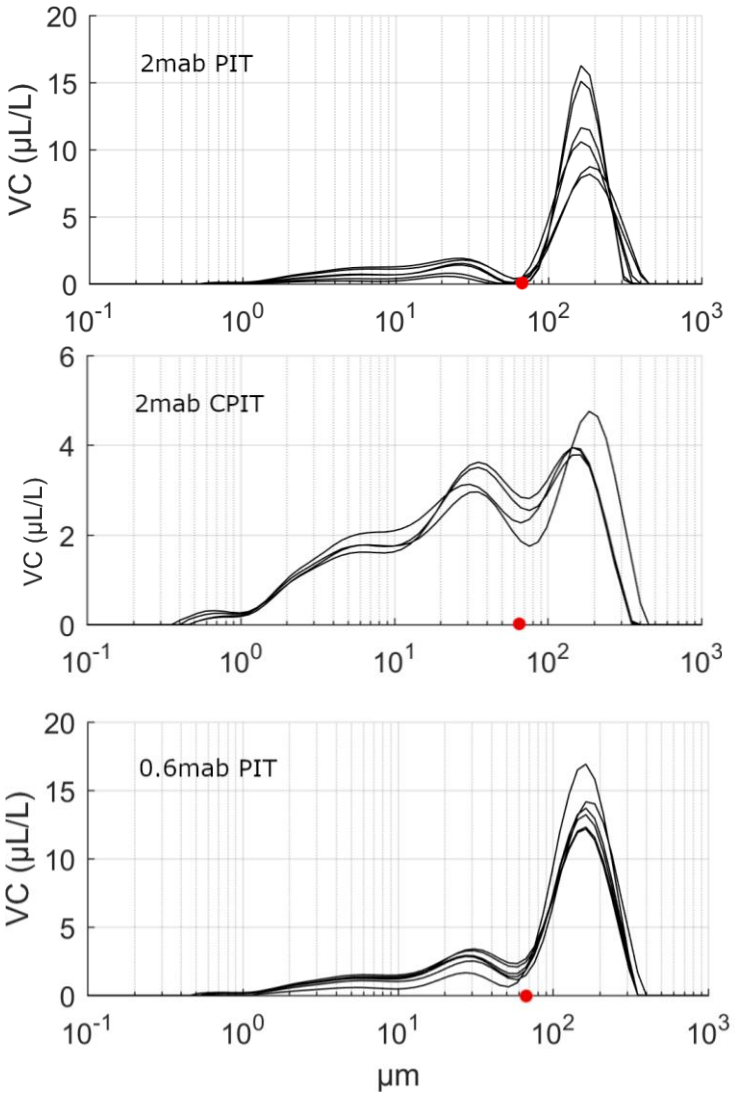

Figure 3.11: PSD comparison between all samples from each PIT (PSD analysis with Malvern3000). The red dot is at 63 µm.

those previously reported for the Belgian part of the North Sea (Dewitte et al. 2016). The PCB concentration in the SPM at MOW1 was higher during the first half of the sampling compared to the second half, although the TOC content increased. It is likely that the presence of fresh and therefore uncontaminated organic matter (OM)explains the negative relation of PCB concentration to TOC in the SPM during the second sampling period. Indeed, results from water sampling and from remote sensing observations at MOW1 indicate that the particulate organic carbon (POC) content of the SPM is higher in spring and summer than in winter and that the peak in chlorophyll concentration occurs in the beginning of May (Shen et al. 2018), see Figure 3.12. This increase in the fresh OM content in spring and summer is caused by the seasonal biological cycle (Schartau et al. 2019). The first sampling period is thus largely situated before the algae bloom peak, while the second sampling period occurs during the algae bloom and thus contains more non-contaminated fresh OM.

The higher mud content observed during the second sampling period is likely due to a change in trap design (from PIT to CPIT). On average there was higher TOC and mud percentage observed at the CPIT compared to the PITs. No correlation was observed between the PCB concentrations and the neap or spring tide. Nevertheless, a larger number of samples would help us gain a more precise understanding of the relation between PCBs and the tides.

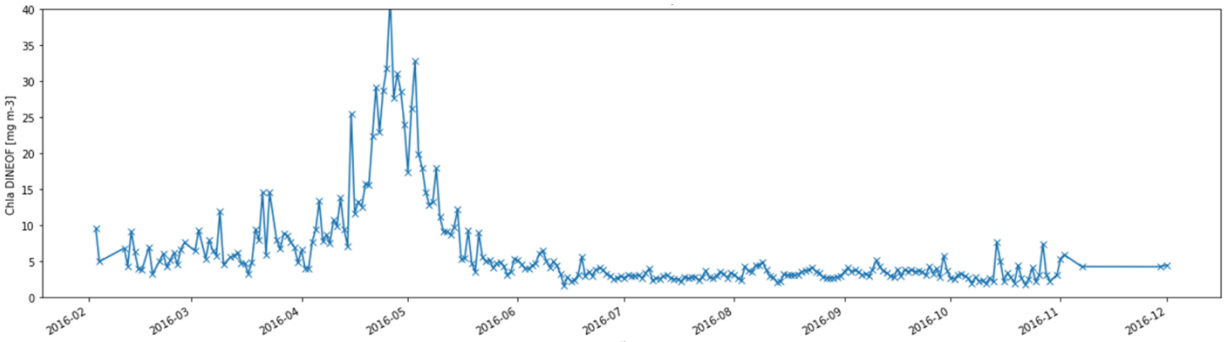

Figure 3.12: Chl-a concentration at MOW1 derived from satellites during 2016. The 1st period (14/03-14/04) is before the peak concentration, the 2nd is (14/04-20/05) is during the algae bloom peak.

The TOC content and the PCB concentrations in the seabed sediments from the port of Zeebrugge were higher than at MOW1. This is in line with our expectations, with a TOC content of above 2% at the port of Zeebrugge and below 0.5% in the sediments at MOW1. In accordance, the PCB concentrations are 2-3 times higher in the TOC enriched samples, which is in line with Heemken et al. (2000), who observed higher pollutant levels (including PCBs) at locations with higher TOC content. On average, the sediments at MOW1 exhibit lower TOC and PCB concentrations compared to the SPM from the same location. This indicates that the samples contained old material that had not yet been involved in the resuspension/deposition cycle. Previous studies have shown that freshly deposited muds generally occur as thin fluffy layers. Below these Holocene deposits consisting of semi-consolidated mud, more sandy layers occur (Fettweis et al. 2009). Sampling with a Van Veen grab or a box core may capture these older sediments. The sediment samples from both MOW1 and the port of Zeebrugge at the start of the sampling period had higher TOC and PCB values compared to the end of the sampling period. This is similar to the SPM and probably also related to the fresh and refractory OM content in the sediment. The occurrence of fresh OM increases not only the floc size of the SPM, but also the settling velocity and thus the thickness of the fluffy layer (Fettweis et al. 2014). A Van Veen grab sample will thus contain less contaminated sediments. The data collected from the (C)PIT traps represent the first PCB time-series covering several tidal cycles for the Belgian part of the North Sea. Such an approach can serve as a spot sampling of contaminants by tracing back the date of the tidal layer extracted but also as a time averaged approach when estimating the average PCB value of the subsamples taken over the sampling period.

3.4. Conclusions

This study examines different sediment traps deployed in the coastal turbidity maximum near Zeebrugge in order to evaluate their applicability for SPM dynamics and pollutant monitoring. Two trap styles are utilized, namely a vertical trap (PPS4/3) and horizontal trap (with 0.6 mab PIT, 2mabPIT, and CPIT variants). The key findings are as follows. Firstly, the horizontal traps have a bias towards trapping coarser particles, while the vertical trap corresponds better with in situ measurements from a LISST optical sensor.

Secondly, the major advantage of the horizontal sediment traps is that they enable collection of sufficient material for further analysis of water quality and other parameters over longer periods. Due to the pervasive strong horizontal currents, vertical traps primarily collect particles (flocs) during slack water and thus are not representative of the whole tidal cycle. The amount of SPM collected is also much lower than with a horizontal trap.

Thirdly, the horizontal traps allow continuous collection of material in suspension, thus providing insight into short-term and long-term variations in SPM composition through the

rhythmic sequence of the tidal layers. Using a horizontal trap, a tidal cycle can be separated into four layers, corresponding with flood and ebb currents and the consecutive slack waters. Further, variations due to lunar cycles can also be depicted (for example, spring tide periods exhibit higher sand content than neap tide periods).

This sampling method could serve as an easy and cheap chemical monitoring technique for pollutants attached to the SPM.

4. Referenties

Agrawal YC. Pottsmith HC. 2000. Instruments for particle size and settling velocity observations in sediment transport. Marine Geology 168, 89–114.

Alldredge AL, Passow U, Logan BE. 1993. The abundance and significance of a class of large, transparent organic particles in the ocean. Deep-Sea Research 40,1131–1140.

Baeye M, Fettweis M, Voulgaris G, Van Lancker V. 2011. Sediment mobility in response to tidal and wind-driven flows along the Belgian inner shelf, southern North Sea. Ocean Dynamics 61, 611–622.

Cartwright GM, Fall KA, Friedrichs CT. 2015. Identification of suspended resilient pellets in particles tracked by a Particle Image Camera System (PICS) in a muddy estuary. Book of abstracts 13th International Conference on Cohesive Sediment Transport Processes, Leuven, Belgium (eds. Toorman E, Mertens T, Fettweis M, Vanlede J), 11-12.

Chapalain M, Verney R, Fettweis M, Jacquet M, Le Berre D, Le Hir P. 2019. Investigating suspended particulate matter in coastal waters using fractal theory. Ocean Dynamics, 69, 59-81.

Cnudde V, Boone MN. 2013. High-resolution X-ray computed tomography in geosciences: A review of the current technology and applications. Earth-Science Review 123, 1-17.

Connell BJ, Singh A, Chu I. 1998. Interaction of PCB congeners and 2,3,7,8-TCDD in the rat liver: An electron microscope study. Journal of Submicroscopic Cytology Pathology, 30, 157-163.

Deng Z, He Q, Safar Z, Chassagne C. 2019. The role of algae in fine sediment flocculation: In-situ and laboratory measurements. Marine Geology 413, 71-84.

Dewitte B, Ruttens A, Ampe B, Waegeneers N, Gauquie J, Devriese L, Cooreman K, Parmentier K. 2016. Chemical analyses of dredged spoil disposal sites at the Belgian part of the NorthSea. Chemosphere 156, 172-180.

Fettweis M. 2008. Uncertainty of excess density and settling velocity of mudflocs derived from in situ measurements. Estuarine Coastal and Shelf Science 78,428-436.

Fettweis M, Houziaux JS, DuFour I, Van Lancker V, Baeteman C, Mathys M, Van den Eynde D, Francken F, Wartel S. 2009. Long term influence of maritime accessworks on the distribution of cohesive sediments: Analysis of historical and recent data from the Belgian nearshore area (southern North Sea). Geo-Marine Letters 29, 321-330.

Fettweis M, Baeye M, Van Der Zande D, Van Den Eynde D, Lee JB. 2014. Seasonality of floc strength in the southern North Sea. Journal of Geophysical Research Ocean 119, 1911–1926.

Fettweis M, Lee BJ. 2017. Spatial and seasonal variation of biomineral suspended particulate matter properties in high-turbid nearshore and low-turbid offshore zones. Water 9, 694.

Fettweis M, Riethmüller R, Verney R, Becker M, Backers J, Baeye M, Chapalain M, Claeys S, Claus J, Cox T, Deloffre J, Depreiter D, Druine F, Flöser G, Grünler S, Jourdin F, Lafite R, Nauw J, Nechad B, Röttgers R, Sotollichio A, Vanhaverbeke W, Vereecken H. 2019. Uncertainties associated with in situ long-term observations of suspended particulate matter concentration using optical and acoustic sensors. Progress in Oceanography, 178, 102162.

Fowler SW, Buesseler KO, Antia AN, Chen M, Fowler SW. 2007. An assessment of the use of sediment traps for estimating upper ocean particle fluxes. Journal of Marine Research 65, 345-416.

He M-C, Sun Y, Li X, Yang Z. 2006. Distribution patterns of nitrobenzenes and polychlorinated biphenyls in water, suspended particulate matter and sediment from mid- and down-stream of the Yellow River (China). Chemosphere 65, 365-374.

Heemken OP, Stachel B, Theobald N, Wenclawiak BW. 2000. Temporal variability of organic micropollutants in suspended particulate matter of the River Elbe at Hamburg and the River Mulde at Dessau, Germany. Archives of Environmental Contamination and Toxicology 38, 11-31.

Helali MA, Oueslati W, Zaaboub N, Added A, Aleya L. 2016. Chemical speciation of Fe, Mn, Pb, Zn, Cd, Cu, Co, Ni and Cr in the suspended particulate matter off the Mejerda River Delta (Gulf of Tunis, Tunisia). Journal of African Earth Science 118, 35–44.

Honjo S, Connell JF, Sachs PL. 1980. Deep-ocean sediment trap; design and function of PARFLUX Mark II. Deep Sea Research 27, 745–753.

Jartun M, Ottesen RT, Steinnes E, Volden T. 2008. Runoff of particle bound pollutants from urban impervious surfaces studied by analysis of sediments from stormwater traps. Chemosphere 396, 147–163.

Lauwaert B, Fettweis M, De Witte B, Van Hoei G, Timmermans S, Hermans L. 2019. Vooruitgangsrapport (juni 2019) over de effecten op het mariene milieu van baggerspeciestortingen (Vergunningsperiode 01/01/2017 – 31/12/2021). RBINS-ILVO-AMT-CD rapport. BL/2019/01, 28pp.

Long ER, Macdonald DD, Smith SL, Calder FD. 1995. Incidence of adverse biological effects within ranges of chemical concentrations in marine and estuarine sediments. Environmental Management 19, 81-97.

Manning AJ, Langston WJ, Jonas PJC. 2010. A review of sediment dynamics in the Severn Estuary: Influence of flocculation. Marine Pollution Bulletin 61, 37–51.

Madrid Y, Zayas ZP. 2007. Water sampling: Traditional methods and new approaches in water sampling strategy. Trends in Analytical Chemistry 26, 293–299.

McDonnell AMP, Lam PJ, Lamborg CH, Buesseler KO, Sanders R, Riley JS, Marsay C, Smith HEK, Sargent EC, Lampitt RS, Bishop JKB. 2015. The oceanographic toolbox for the collection of sinking and suspended marine particles. Progress in Oceanography 133, 17–31.

Mearns AJ, Matta MB, Simecek-Beatty D, Buchman MF, Shigenaka G, Wert W. 1988. PCB and chlorinated pesticide contamination in US fish and shellfish: A historical assessment report. NOAA Tech Memo NOS OMA 39. US Department of Commerce, 140 pp, Seattle WA.

Mienis F, De Stigter HC, De Hass H, Van der Land C, Van Weering TCE. 2012. Hydrodynamic conditions in a cold-water coral mound area on the Renard Ridge, southern Gulf of Cadiz. Journal of Marine Systems 96-97, 61-71.

Neukermans G, Ruddick K, Loisel H, Roose P. 2012. Optimization and quality control of suspended particulate matter concentration measurement using turbidity measurements. Limnology and Oceanography Methods 10, 1011–1023.

Nosaka Y, Yamashita Y, Suzuki K. 2017. Dynamics and origin of Transparent Exopolymer Particles in the Oyashio region of the Western Subarctic Pacific during the spring diatom bloom. Frontiers in Marine Science 4, 79.

Passow U, Alldredge AL. 1995. A dye-binding assay for the spectrophotometric measurement of transparent exopolymer particles. Limnology and Oceanography 40, 1326–1335.

Passow U. 2002. Transparent exopolymer particles (TEP) in aquatic environments. Progress in Oceanography 55, 287–333.

Prouty NG, Mienis F, Campbell-Swarzenski P, Roark EB, Davies AJ, Robertson CM, Duineveld G, Ross SW, Rhode M, Demopoulos AWJ. 2017. Seasonal variability in the source and composition of particulate matter in the depositional zone of Baltimore Canyon, U.S. Mid-Atlantic Bight. Deep Sea Research I 127, 77-89.

Röttgers R, Heymann K, Krasemann H. 2014. Suspended matter concentrations in coastal waters: methodological improvements to quantify individual measurement uncertainty. Estuarine, Coastal and Shelf Science 151, 148–155

Schartau M, Riethmüller R, Flöser G, van Beusekom JEE, Krasemann H, Hofmeister R, Wirtz K. 2019. On the separation between inorganic and organic fractions of suspended matter in a marine coastal environment. Progress in Oceanography 171, 231–250.

Shen X, Toorman EA, Lee BJ, Fettweis M. 2018. Biophysical flocculation of suspended particulate matters in Belgian coastal zones. Journal of Hydrology 567, 238-252.

Smedes F, De Boer J. 1997. Determination of chlorobiphenyls in sediments – Analytical methods. Trends in Analytical Chemistry 16, 503-517.

Soulsby R. 1997. Dynamics of marine sands: A manual for practical applications. Thomas Telford, London.

Środoń J, Drits VA, McCarty DK, Hsieh JCC, Eberl DD. 2001. Quantitative X-ray diffraction analysis of clay-bearing rocks from random preparations. Clays and Clay Minerals 49, 514–528.

Stavn RH, Rick HJ, Falster AV. 2009. Correcting the errors from variable sea salt retention and water of hydration in loss on ignition analysis: Implications for studies of estuarine and coastal waters. Estuarine, Coastal and Shelf Science 81, 575-582

Suja S, Kessarkar PM, Fernandes LL, Kurian S, Tomer A. 2017. Spatial and temporal distribution of metals in suspended particulate matter of the Kali estuary, India. Estuarine Coastal and Shelf Science 196, 10–21.

Tsompanoglou K, Anagnostou C, Krasakopoulou E, Pagou K, Karageorgis AP, Pavlidou A, Albanakis K, Tsirambides A. 2017. Distribution and geochemical composition of suspended particulate material in the shallow embayment of northern Thermaikos Gulf, Greece. Continental Shelf Research 143, 295–310.

Van den Eynde D, Baeye M, Francken F, Montereale Gavazzi G, Terseleer N, Van Lancker V. 2019. Monitoring of the impact of the extraction of marine aggregates, in casu sand, in the zone of the Hinder Banks. Period 1/1 – 31/12 2018. Brussels, RBINS-OD Nature. Report MOZ4-ZAGRI/X/DVDE/2019/EN/SR05, 23 pp. + 4 Annexes

Verney R, Lafite R, Brun-Cottan J-C. 2009. Flocculation potential of estuarine particles: The importance of environmental factors and of the spatial and seasonal variability of Suspended Particulate Matter. Estuaries and Coasts 32, 6798-693.

Zhang J, Liu G, Wang R, Huang H. 2017. Polycyclic aromatic hydrocarbons in the water-SPM-sediment system from the middle reaches of Huai River, China: Distribution, partitioning, origin tracing and ecological risk assessment. Environmental Pollution 230, 61–71.

COLOPHON

Dit rapport werd voorbereid door de BMM in oktober 2020
Zijn referentiecode is .MOMO/9/MF/202010/NL/AR/3

De scheepstijd met de RV Belgica werd voorzien door BELSPO en KBIN-OD Natuur

Indien u vragen hebt of bijkomende copies van dit document wenst te verkrijgen, gelieve een e-mail te zenden naar mfettweis@naturalsciences.be, met vermelding van de referentie, of te schrijven naar:

Koninklijk Belgisch Instituut voor Natuurwetenschappen
OD Natuur – BMM
t.a.v. Michael Fettweis
Vautierstraat 10
B–1000 Brussel
België
Tel: +32 2 627 41 83

BEHEERSEENHEID VAN HET
MATHEMATISCH MODEL VAN DE NOORDZEE

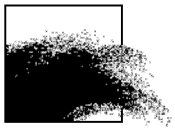

APPENDIX 1

van Maren DS, Vroom J, Fettweis M, Vanlede J. 2020. Formation of the Zeebrugge coastal turbidity maximum: The role of uncertainty in near-bed exchange processes. Marine Geology

Marine Geology 425 (2020) 106186

Contents lists available at ScienceDirect

Marine Geology

journal homepage: www.elsevier.com/locate/margo

Formation of the Zeebrugge coastal turbidity maximum: The role of uncertainty in near-bed exchange processes

D.S. van Maren[a,b,*], J. Vroom[a], M. Fettweis[c], J. Vanlede[d,b]

[a] Deltares, Dept. of Coastal and Marine Systems, P.O. Box 177, 2600, MH, Delft, the Netherlands
[b] Delft University of Technology, Faculty of Civil Engineering and Geosciences, the Netherlands
[c] Royal Belgian Institute of Natural Sciences, Operational Directorate Natural Environment, Vautierstraat 29, 1000 Brussels, Belgium
[d] Department of Mobility and Public Works, Flanders Hydraulics Research, Berchemlei 115, 2140 Antwerp, Belgium

ARTICLE INFO

Keywords:
Uncertainty
Sand-mud interaction
Turbidity Maximum
Fine sediments
Zeebrugge

ABSTRACT

Despite availability of a large amount of observational data and modelling studies, the mechanisms maintaining the Turbidity Maximum in the Belgian-Dutch coastal zone around the port of Zeebrugge (Belgium) are insufficiently understood. In order to better understand the dynamics of this turbidity maximum we examine the role of baroclinic (salinity and sediment-induced) processes and local sediment sources on the formation and persistence of the turbidity maximum through two different numerical model approaches. One model approach allows erosion of the highly compacted muddy seabed, serving as a sediment source, in line with observations of bed level change over several decades. The other approach reduces the exchange between the bed and the water column, to mimic the formation of highly concentrated near-bed suspensions with concentrations of several g/l observed around the port of Zeebrugge. Both model approaches are calibrated to various sources of available data (in situ sediment concentration observations, satellite image, bed level changes, mud content and dredging data), which they reproduce comparably well. However, reducing the water-bed exchange strengthens sediment convergence in the turbidity maximum, whereas the sediment source leads to sediment export. With the available data, it is difficult to determine which of the approaches is more realistic. Apparently, the lack of knowledge on near-bed exchange processes introduces an important source of uncertainty which cannot be adequately addressed with currently available observations. This work therefore shows that more quantitative knowledge on water-bed exchange processes in turbid marine environments is needed. It is further hypothesized that the large-scale erosion of the muddy seabed following the extension the port of Zeebrugge in the early 1980's brought such a large amount of sediment in suspension (50–100 million ton) that sediment convergence was strengthened. This increasing sediment convergence introduces a positive feedback mechanism that maintains sediment in the Turbidity Maximum, or even strengthens it. The high sediment concentrations observed today may therefore be a long-term effect of port construction carried out decades earlier.

1. Introduction

Estuarine Turbidity Maxima (ETM's) are regions of elevated suspended sediment concentration within an estuary, see e.g. de Nijs and Pietrzak (2012), Ralston et al. (2012), McSweeney et al. (2016), Grasso et al. (2018), Burchard et al. (2018), and Hesse et al. (2019) for recent examples and detailed references. ETM's are the result of converging sediment pathways generated by estuarine circulation and lag effects (Dyer, 1994). Estuarine circulation is the combined effect of gravitational circulation (Postma, 1967), internal tidal asymmetry (Jay and Musiak, 1994) due to tidal straining (Simpson et al., 1990), lateral tidal residual flows (Lerczak and Geyer, 2004) and river flow; the relative importance of each component is highly variable. Residual transport by time lag effects, such as settling lag and scour lag, are the result of the sediment properties (settling velocity, critical shear stress for erosion) in combination with asymmetries in the hydrodynamics (Allen et al., 1980) and topographical effects, such as divergence or convergence of channel cross sections (Friedrichs et al., 1998). Most ETM's are set within their estuary, although some are pushed into the coastal zone by high river discharge, such as the Turbidity Maxima (TM's)s of the Amazon (Kineke et al., 1996) and Yangtze river (Beardsley et al., 1985).

Coastal areas with elevated suspended sediment concentration such as the Wadden Sea have been explained by the occurrence of estuarine circulation (Burchard et al., 2008). However, not all coastal TM's show

* Corresponding author at: Deltares, Dept. of Coastal and Marine Systems, P.O. Box 177, 2600, MH, Delft, the Netherlands.
E-mail address: bas.vanmaren@deltares.nl (D.S. van Maren).

https://doi.org/10.1016/j.margeo.2020.106186
Received 17 December 2019; Received in revised form 13 March 2020; Accepted 20 March 2020
Available online 08 April 2020

a clear correlation with estuarine trapping processes, one of them being the Zeebrugge turbidity maximum. The Zeebrugge TM is located on the Belgian-Dutch continental shelf, with the Scheldt estuary as the primary fresh water source. The river discharge is low (20–600 m^3/s with an average of 100 m^3/s) compared to the tidal discharge (~50.000 m^3/s), and therefore insufficient to create a seaward-located ETM (as in the above examples). We therefore refer to a Coastal Turbidity Maximum (TM) rather than an ETM. However, despite generally well mixed conditions, the proximity of a fresh water source may generate salinity-driven residual currents which may play a role in the formation of the Zeebrugge TM, similar as for ETM's.

First studies on the Zeebrugge TM date back to the end of the 19th century when the planning works for the port of Zeebrugge started; they indicated a trend to deposition of muddy sediment in the near-shore area south of Zeebrugge (Van Mierlo, 1899). Later, Nihoul (1975) postulated that the Zeebrugge TM was generated by a large-scale gyre trapping fine-grained sediments transported north-eastward by the residual currents. Fettweis and van den Eynde (2003) argued that the northward decrease in fine sediment transport capacity was the main mechanism, resulting in sediment deposition and subsequent strengthening of the bed through consolidation processes during neap tides. They also hypothesize that sediment not only originates from the Strait of Dover (Irion and Zollmer, 1999) but also from local marine clay deposits deposited during the Holocene transgression. The erosion of these clay deposits (hereafter referred to as consolidated Holocene mud) accelerated in recent times as a result of maritime access works of the port of Zeebrugge (Fettweis et al., 2009a), providing a source for the TM. Bathymetric changes derived from charts indeed indicate yearly erosion up to 2.4 million tonnes of the consolidated Holocene mud bed (Bastin, 1974). Quantitative clay mineral composition of potential source areas showed that the paleo-estuary was the main provenance of the clay deposits and of the fine-grained sediments in the TM, rather than the present-day Scheldt river and estuary (Adriaens et al., 2018). Additionally, high SSC gradients (> 3 g/l difference between observations 0.2 and 2.2 m above the bed) observed near-bed around Zeebrugge (Fettweis et al., 2010) may lead to sediment-induced suppression of turbulence (Winterwerp, 2001) which may generate and enhance high concentration near-bed suspensions and fluid mud layers and may also contribute to siltation in the port of Zeebrugge (Winterwerp, 2006). Clear evidence for turbulence suppression of such near-bed suspensions is provided in Fettweis's data by the observations that the concentration in the upper sensor (2.2 m above the bed (mab)) is minimal during a storm, when concentrations in the lowest sensor (0.2 mab) reach peak values. Fluid mud exists in the approach channel to the port and in the port itself, but outside these deeper channels high near-bed concentrations occur irregularly and depend on hydrodynamic conditions. The location of the high concentration near-bed suspensions therefore also varies. And finally, disposal of fine-grained sediment from maintenance dredging works in the port of Zeebrugge and the navigation channels may strengthen the Zeebrugge TM and act as a semi-permanent source (Fettweis et al., 2011, 2016).

Mechanisms that have been demonstrated to contribute to the formation of Estuarine Turbidity Maxima (density-driven effects of both salinity and sediments) have to our knowledge not yet been investigated for the Zeebrugge TM. Important research questions are therefore to what extent the Zeebrugge TM is formed and maintained by (1) erosion of the consolidated Holocene mud bed, (2) salinity-induced density effects, and (3) sediment-induced density effects. In order to answer these questions a process-based numerical 3D model is set up in which sediment- and salinity-induced density effects as well as a consolidated Holocene mud source are implemented to study the effect of individual processes. Since sediment transport mechanisms in this area (tide- and wave induced resuspension and salinity-driven flows in combination with highly concentrated near-bed suspensions, in combination with anthropogenic dredging and dumping operations) are extremely complex, reproducing the observed sediment concentration observations in detail is beyond the present state-of-the-art of numerical modelling. Yet, our model reproduces the most essential transport mechanisms and can therefore be applied to execute numerical experiments to better understand the dynamics of the TM. Of particular importance in the numerical model setup are the exchange processes between the water and the bed. Near the bed, the suspension increases in concentration from a dilute suspension to a highly concentrated benthic suspension, and within the bed from a poorly consolidated mud at the surface to -over time - a well consolidated soil at greater depth. The resulting strong variability in sediment concentration and associated transport processes requires a vertical resolution that cannot yet be resolved in numerical 3D models due to computational limitation (especially when modelling dynamic morphologic equilibrium, which requires simulation periods of several years). In order to advance our knowledge on the formation mechanisms of the TM, despite the low vertical model resolution and simple parameterizations, we apply two alternative concepts of water-bed exchange with the numerical model: (1) sediment may be supplied by erosion of consolidated Holocene mud deposits, and (2) the high near-bed sediment concentration may influence sediment dynamics of the TM. Despite inevitable shortcomings in the model set-up, the results provide valuable insight into the role of model assumptions on the dynamics of turbidity maxima, and on the mechanisms responsible for the formation and maintenance of the turbidity maximum near Zeebrugge in particular.

2. Study area

The port of Zeebrugge is situated on the Belgian coastline (Fig. 1), just south of the Dutch-Belgian border and the Western Scheldt estuary (the downstream part of the Scheldt estuary). The Scheldt River is a fresh water source with an average discharge around 100 m^3/s, ranging from 20 to 600 m^3/s (Fettweis et al., 1998). The salinity in the Belgian coastal zone are also influenced by the larger Rhine and Meuse rivers entering the North Sea some 100 km northeast of Zeebrugge (Lacroix et al., 2004). The Zeebrugge TM is located on the Belgian-Dutch continental shelf in a long band of elevated sediment concentration originating from the English Channel on the French coast and extending onto the Dutch continental shelf. Residual currents along the French, Belgian, and Dutch coastlines transport sediment from the Straits of Dover northward resulting in an alongshore north-east-directed sediment flux of about 30 million tonnes/year (Fettweis et al., 2007). The yearly averaged sea surface sediment concentration in the TM is around 50 mg/l (Fig. 1). Near the bed, the sediment concentration becomes several 100 mg/l during peak tidal flow conditions, and may even be several g/l during storm conditions (Fettweis et al., 2010). The highest observed suspended sediment concentrations occur near Zeebrugge (regularly exceeding 3 g/l; Fettweis et al., 2010), although high near-bed sediment concentrations (up to 2 g/l) have been episodically observed along the Dutch coast as well (van der Hout et al., 2017) during and after storm conditions. Trapping of sediments close to the Dutch coastline under the influence of density effects and cross-shore currents has been studied in greater detail (de Boer et al., 2009; Van der Hout et al., 2015). The Dutch coastline more towards the north is strongly influenced by the fresh water discharge from the Rhine and Meuse Rivers, generating strong salinity-induced currents. However, the Zeebrugge TM occurs in a zone where the salinity is higher (28 to 34 psu) and vertical and horizontal salinity gradients are smaller. Salinity-driven currents will therefore be less important than in the coastal area along the Dutch coast where salinity-induced trapping of sediment was extensively investigated.

The seabed of the Belgian-Dutch nearshore is composed of fine sands with variable mud content. The recent sediments in the seabed around Zeebrugge predominantly consists of sand-dominated cohesive sediment (following the classification of van Ledden et al., 2004), with pockets of clay-dominated cohesive sediments (Fettweis et al., 2009b). The cohesive sediments occur mainly in the Zeebrugge TM area and are

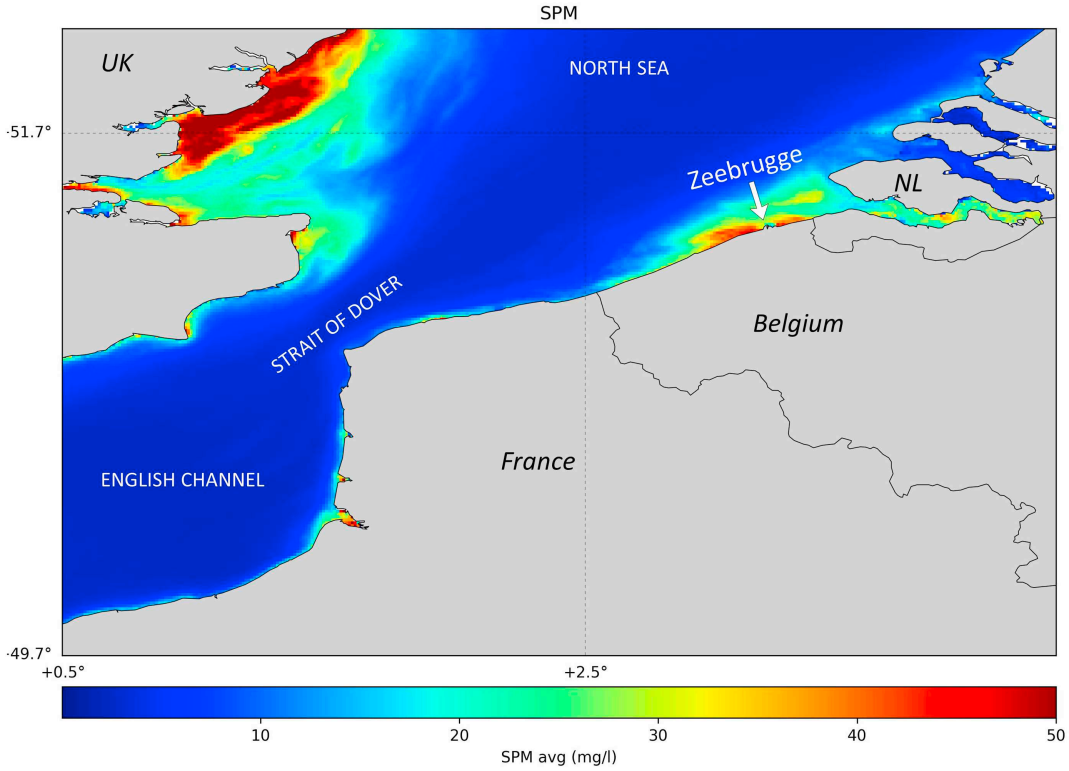

Fig. 1. Near surface sediment concentrations in the English Channel and southern North Sea, revealing elevated SSC near Zeebrugge computed from satellite images covering the period 2003–2011 and using the algorithms of Nechad et al. (2010).

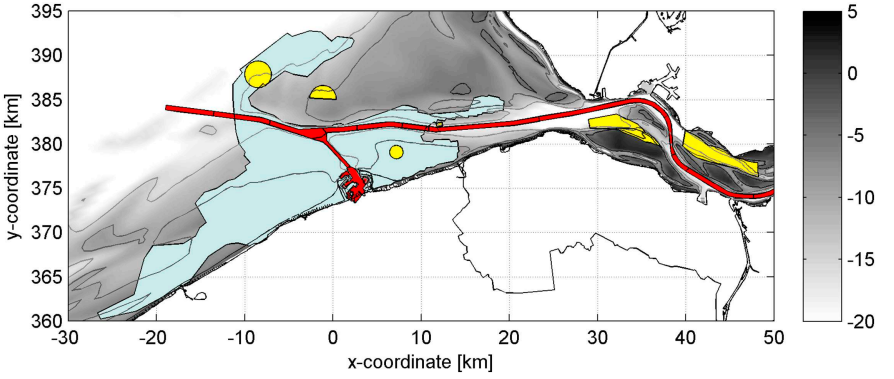

Fig. 2. Dredging locations (red), disposal locations (yellow), and the area with consolidated Holocene mud in the bed (blue; based on Fettweis et al., 2006). The main navigation channels connecting the North Sea with the Port of Zeebrugge and the Western Scheldt estuary cross the consolidated Holocene mud deposits. (For interpretation of the references to colour in this figure legend, the reader is referred to the web version of this article.)

characterised by consolidated to more recently deposited layers from various ages (Fettweis et al., 2009a; Adriaens et al., 2018). Note that the stiff Holocene clays underneath the recent deposits have a much higher clay content. This consolidated mud is outcropping in-between the main navigation channel and the port of Zeebrugge (Fig. 2) and covered with recently deposited mud with critical erosion strengths of 0.5 (top layer) to 2.5 Pa (Fettweis et al., 2010). These recent deposits become several dm to > 1–2 m thick in the channels and the port, requiring regular maintenance dredging works. Approximately 10 million tonnes of dry sediments are annually dredged from the port of Zeebrugge and its approach channels (De Maerschalck and Vanlede, 2013) and disposed northwest and northeast of Zeebrugge (see Fig. 2).

The location of the mud deposits is very comparable to the location of the TM, suggesting that sediments in the TM may have been eroded from the subsoil. This relation is also suggested by the clay mineralogy of the consolidated Holocene mud layers and in the suspended matter in the TM (Adriaens et al., 2018). An analysis of frequent bathymetrical soundings data from the period 1975–2011 suggests that on average 2.8 million m^3 is eroded annually outside the maintained fairways (Fig. 3a), in the area with outcropping consolidated Holocene mud (compare Fig. 2 with Fig. 3b). Note that the spatial extent of the consolidated Holocene mud is much larger than the area for which frequent bathymetric surveys are available and therefore the total amount of eroded sediment may be larger. A major enlargement of the port took place between 1979 and 1986, with the construction of two breakwaters extending 4 km into the North Sea. Flow contraction led to erosion of on average 3–6 million m^3/y throughout the 1980's (Fig. 3a) and approximately 50 million m^3 over the period 1975–2011. The bulk density of the consolidated Holocene mud is 1500–1800 kg/m^3 (Fettweis et al., 2006), equivalent to 800–1300 kg/m^3 dry weight density. Assuming a dry weight density of 1000 kg/m^3 implies that the eroded dry mass directly resulting from the port expansion is approximately 50 million tonnes over 37 years. Erosion in front of the jetties gradually declined significantly and reached an equilibrium depth by 2005.

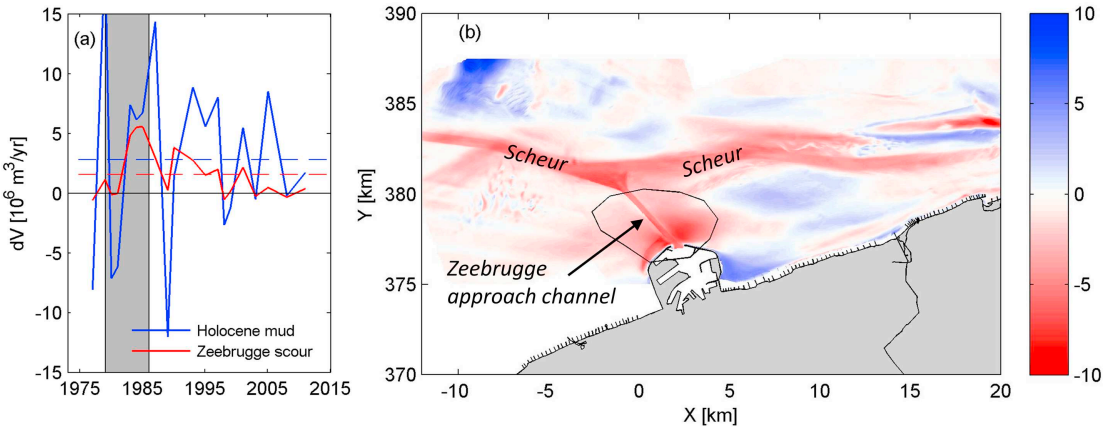

Fig. 3. Annual volume change *dV* (panel (a), positive values indicate erosion) based on bed level observations over the Belgian shoreface covering the consolidated Holocene mud patch (Fig. 2) but excluding the fairways. The blue line provides volumetric changes in the area of the consolidated Holocene mud patch, the red line the volumetric changes in front of the port of Zeebrugge (black polygon in panel b). Harbour extension works were carried out during the period indicated with the grey box (1979–1986). The dashed lines indicate the average volumetric changes in the period from 1975 to 2011 (2.8 and 1.6 million m^3/y for the Holocene mud area and the Zeebrugge area, respectively). The right panel (b) depicts the bathymetric change (in m, red is erosion) between 1976 and 2014, with names of the two main fairways (Scheur and Zeebrugge approach channel). (For interpretation of the references to colour in this figure legend, the reader is referred to the web version of this article.)

3. Model setup

3.1. General model layout

The model is setup in Delft3D, solving the unsteady shallow water equations in three dimensions under the hydrostatic pressure assumption. Sediment transport and morphological updates are computed simultaneously with the flow (see Lesser et al. (2004) for a description and validation). The generation, transport, and dissipation of turbulence are resolved with a k-ε model, in which turbulent mixing is modified by sediment-induced buoyancy effects through the equation of state (see Winterwerp and van Kessel, 2003).

The model domain covers an 80 km long stretch along the Belgian-Dutch coast (extending 30 km in the offshore direction) and a part of the Scheldt estuary, see Fig. 4. The mesh resolution is approximately 150 × 150 m near the port of Zeebrugge and increases to 1500 × 1500 m in the North Sea. The model domain consists of 19,000 horizontal cells and has 10 vertical σ-layers with a thickness logarithmically increasing from the bed (2% of the water depth) to the surface (20% of the water depth). The bathymetry of the model domain has been derived from bathymetric data collected by the Dutch Ministry of Public Works and completed with lower resolution EMODnet data in the North Sea. The bed roughness is defined with a Chézy formulation using a Manning roughness which value has been obtained by calibration of the hydrodynamics. The model has been set up for 2014 because of availability of observations. The hydrodynamic model is coupled online with a SWAN wave model (Booij et al., 1999), using the same computational grid and bathymetry. Timeseries of wave height, period and direction measured at a wave buoy close to the model boundary are prescribed as boundary conditions, whereas wind-generated waves are computed with wind observed at a coastal meteorological station. All boundary conditions and initial conditions are summarized in Table 1, and for conciseness not repeated in the text.

A multi-fraction morphodynamic sediment transport model has been setup with 1 sand fraction and 3 mud fractions, in which the bed level is updated at each hydrodynamic time step. Multiple mud fractions are needed to represent the vertical variation of the sediment concentration typically observed in nature, with the faster settling particles leading to large intratidal variability near the bed, and the slower settling particles to more constant sediment concentrations near-

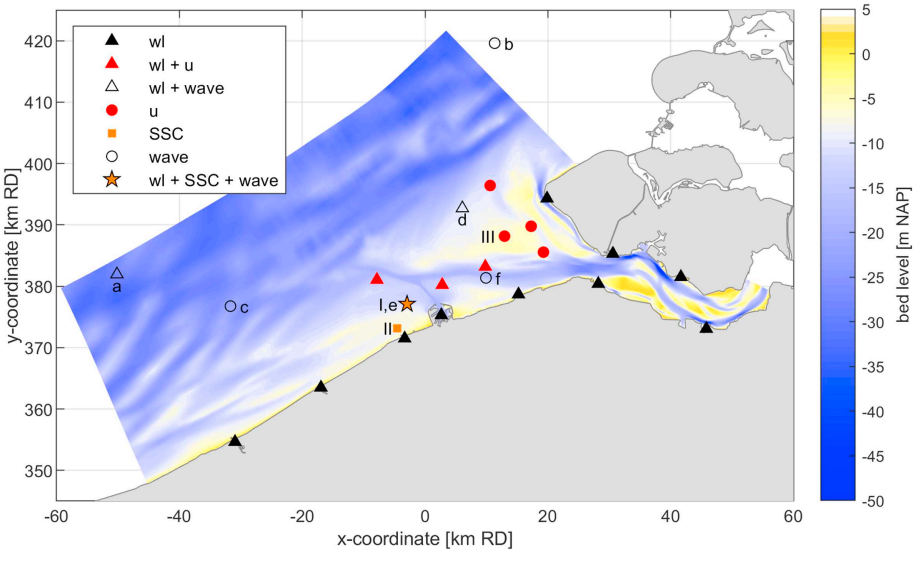

Fig. 4. Bathymetry in the numerical domain, and location of observation stations. Black triangles are water level observations (red when combined with flow velocity observations; blank when combined with wave observations). Red circles are stations with only flow velocity observations; blank circles only wave observations; orange squares only SSC observations; the orange star refers to a station where water levels, waves, and SSC is collected. The water level and flow velocity station names are used for the aggregate bias and RMSE values and are not discussed individually. Station I is MOW1, II is Blankenberge, and III is VvdR. The wave station letters correspond to panels in Fig. S1. (For interpretation of the references to colour in this figure legend, the reader is referred to the web version of this article.)

Table 1
Initial and boundary conditions.

	Boundaries	Initial conditions
Hydrodynamics	Water levels and Riemann invariants (a combination of water level and currents allowing waves to propagate out of the model domain) at sea; tidal discharge in the Scheldt estuary; derived from a numerical model (Zijl et al., 2015)	–
Salinity	Offshore: measurements at various observations stations operated by the Dutch Ministry of Public Works, close to the model boundaries. Salinity in the Scheldt boundary is from an existing Scheldt model.	30 ppt with 3 year spin-up
Waves	Observed significant wave heights and peak periods at a station close to the offshore model boundary, assuming a JONSWAP spectrum (Hasselman et al., 1985). The prescribed wind field is based on observations at station Vlissingen (coastal station 30 km NE of Zeebrugge)	–
Sand	Local equilibrium	30 cm with 3 year spin-up
Mud	5 mg/l offshore to 30 mg/l (summer) to-60 mg/l (winter near the coast, based on satellite images (Fettweis et al., 2007). In the Scheldt estuary 45 mg/l is prescribed. All concentrations are equally distributed over the three fractions.	0 mg/l in suspension and on the bed (both the fluff and buffer layer); 3 year spin-up

surface. Sand is transported following the van Rijn (2007a, 2007b) formulations, prescribed as particles with a diameter of 200 μm and an initial layer thickness of 30 cm. Sand transport is reduced with a factor (1-p_2), where p_2 is the fractional mass of mud in the buffer layer (see hereafter). Transport of fine sediments (mud) is modelled with the algorithms developed by Van Kessel et al. (2011a), which have also been applied previously to the North Sea (van Kessel et al., 2011a), the Western Scheldt estuary (Van Kessel et al., 2011b), and the Ems Estuary (van Maren et al., 2015a). The model distinguishes two bed layers: a typically thin, fluffy upper layer of mud only (S_1) which rapidly accumulates and erodes, and a deeper layer (S_2), which typically represents a sandy bed in which fine sediments accumulate during calm conditions and supplies sediment during high energy events. The consolidated Holocene mud deposits (when used) and recent mud deposits are also part of this buffer layer – this is explained in the following section. The computed thickness of the fluff layer depends on erosion parameter settings and local hydrodynamics (also see hereafter).

Dredging and disposal is implemented following actual dredging strategies: sediment that deposits in navigation channels and the port of Zeebrugge is dredged when the bed level exceeds a certain intervention level and disposed on the allocated disposal areas (see Fig. 2 for dredging and disposal locations). The amount of dredged sediment can therefore be used as a validation parameter.

3.2. Erosion of mud

The erosion rate E_1 of layer S_1 linearly depends on the amount of sediment in this layer below a user-defined threshold M_0/ M_1 and is independent of the amount of sediment above this threshold:

$$E_1 = mM_1\left(\frac{\tau}{\tau_{cr,1}} - 1\right) \quad m < \frac{M_0}{M_1} \tag{1a}$$

$$E_1 = M_0\left(\frac{\tau}{\tau_{cr,1}} - 1\right) \quad m > \frac{M_0}{M_1} \tag{1b}$$

Here m (kg/m^2) is the mass of sediment per unit surface in layer S_1, M_0 is the standard zero-order erosion parameter (kg/m^2/s) and M_1 (1/s) is the erosion parameter for limited sediment availability. Reducing the erosion rate of fine sediment when the availability is limited, has the benefit of a smoother and more realistic model behaviour in mixed sand-mud environments ($m < M_0/M_1$). For completely muddy areas ($m > M_0/M_1$), the buffer model switches to the standard Krone-Partheniades formulations for erosion of bed layer S_1.

The erosion E_2 of S_2 scales linearly with the excess shear stress:

$$E_2 = p_2 M_2\left(\frac{\tau}{\tau_{cr,2}} - 1\right) \tag{2}$$

Here, p_2 is the fraction of mud in S_2 as computed by the model and M_2 is the erosion parameter for S_2 (kg/m^2/s). The erosion of sand and mud is scaled proportionally with the available mass of sand and mud in S_2. E_2 becomes zero if the mass of mud in layer S_2 becomes zero (i.e. layer S_2 consists of pure sand).

Physically, when the mud fraction in layer S_2 is larger than the sand fraction, layer S_2 represents recently deposited mud with critical erosion strengths of 0.5–2.5 Pa (Fettweis et al., 2010). When sand is dominant, layer S_2 represents a sandy layer in which mud fills the pores. Even though the initiation of motion for sand with D50 = 200 μm is slightly below 0.2 Pa (e.g. van Rijn, 2007a), mud within a sandy matrix is only released when large amounts of sand are brought in suspension. For such conditions, earlier model work suggests a value for $\tau_{cr,\ 2}$ around 1 Pa (Van Kessel et al., 2011a). This conveniently corresponds to the critical shear strength of the recent mud deposits (see above). Sediment which does not or only marginally consolidates (represented by the fluff layer) typically has a critical shear stress for erosion, τ_{cr}, of several 0.01 to several 0.1 Pa (e.g. Widdows

Table 2
Parameter settings of the sediment transport model.

Parameter	Description	Fraction		
		1	2	3
$w_{s,x}$	Settling velocity sediment fraction x [mm/s]	0.5	2	4
$\tau_{cr,\ 1}$	Critical bed shear stress layer S_1 [Pa]	0.2	0.2	0.2
$\tau_{cr,\ 2}$	Critical bed shear stress layer S_2 [Pa]	1	1	1
$M_{0,x}$	Zero-order erosion rate layer S_1 for fraction x [kg/m^2/s]	10^{-3}	10^{-3}	10^{-3}
$M_{1,x}$	First-order erosion rate layer S_1 for fraction x [/s]	10^{-4}	10^{-4}	10^{-4}
$M_{2,x}$	Erosion rate layer S_2 for fraction x [kg/m^2/s]	10^{-3}	$2*10^{-3}$	$4*10^{-3}$
$M_{2,x,source}$	Erosion rate layer S_2 for fraction x kg/m^2/s] for marine sediment source	$5*10^{-5}$	$5*10^{-4}$	$1*10^{-3}$
		General		
D_{50}	Median grain size sand []	200 μm (w_s = 22 mm/s)		
n	Manning's roughness (m/s$^{1/3}$)	0.022 (0.018 for marine sediment source)		

et al., 2007). Therefore the critical shear stress for the fluffy layer was set low ($\tau_{cr,\ 1} = 0.2$ Pa for all fractions – see Table 2). Except for the model with a consolidated Holocene mud source, all erosion parameters are prescribed as uniform values. The erosion parameters M0, M1, and M2 (Table 2) are obtained through calibration.

3.3. Settling and deposition

The deposition flux D is the product of the near-bed settling velocity $w_{s,\ b}$ and the near-bed sediment concentration C_b and is divided between layers S_1 and S_2 with a burial parameter α:

$$D_1 = (1 - \alpha)\beta w_{s,b} C_b \tag{3b}$$

$$D_2 = \alpha\beta w_{s,b} C_b \tag{3c}$$

The value for α is based on calibration, and is typically between 0.05 and 0.2 (Van Kessel and van Maren, 2013). A low value for α implies a slow exchange with buffer layer S_2. In combination with settings for M_2 and $\tau_{cr,\ 2}$ it determines the residence time of fines in the buffer layer.

The dimensionless β is the 'reduced deposition' factor, introduced by Van Kessel and Vanlede (2009) to approximate physical processes that occur near the bed, but are not part of the model setup or formulations. Without reduced deposition (i.e. $\beta = 1$) the deposition rate into the bed may be overestimated because of 4 mechanisms:

1. The vertical discretization with 10 logarithmic layers is insufficient to properly reproduce high near-bed SSC. This has two implications. First, turbulent mixing is modified by sediment-induced buoyancy effects through the equation of state. An underestimation of concentration gradients (due to low vertical resolution) leads to overestimation of mixing (thereby further reducing near-bed concentrations). Secondly, the settling velocity scales non-linearly with the sediment concentration. Hindered settling is modelled through an adaptation of the Richardson and Zaki (1954) formula using $w_{s,\ b} = w_{s,\ 0}(1 - c/c_g)^n$. Herein is $w_{s,\ 0}$ the clear water settling velocity, c_g a reference concentration (for cohesive sediments equal to the gelling concentration, in our case set to 100 g/l) and n a power depending on the particle Reynolds number (for low particle Reynolds numbers $n = 5$). Underestimation of near-bed SSC due to the vertical discretization will therefore lead to overestimated settling velocities.
2. The critical shear stress for erosion τ_{cr} is not attained instantaneously, but after deposition a particle only gradually gains strength through consolidation. A large amount of the particles that deposit on the bed, are therefore immediately re-entrained (even by fairly weak currents). A model with $\beta = 1$ will therefore always overestimate deposition rates during a phase of net deposition, especially since values for τ_{cr} are often based on the erosion phase and therefore fairly high. As far as we know, there is no field observational data on deposition / erosion processes on such small time and spatial scales.
3. Flocs may be broken up in the near-bed boundary layer, resulting in lower settling velocities (e.g. Hill et al., 2001).
4. Irregularities such as bed forms on a spatial scale smaller than the grid cell size may result in areas with low deposition rates (e.g. top of ripples) further reducing deposition. On the other hand, mud may at the same time more easily deposit on the lee side of ripples – the net effect is therefore not known.

With the current state of knowledge, it is not clear how especially mechanism 2 and 3 operate under dynamic field conditions, and consequently which of the 4 mechanisms is more important. However, their combined effect is a reduced sediment flux into the bed, leading to higher near-bed sediment concentrations. In this study we primarily focus on the effect of the resulting high near-bed sediment concentrations on ETM dynamics, but do not quantify the individual contribution of the various mechanisms to β. We therefore evaluate the effect of highly concentrated near bed layers and TM dynamics by comparing model results without reduced deposition ($\beta = 1$, default value) to simulations with pronounced reduced deposition ($\beta = 0.1$). A more elaborate discussion on β follows in the discussion.

The sediment settling velocity w_s is computed from current velocity and SSC observations, measured from 2005 to 2009 at stations Blankenberge and MOW1 (see Fig. 4 for location) at two positions in the water column (0.2 and 2.2 m above the bed). Under the assumption that the sediment concentration profile is in equilibrium during peak flow conditions and that the current velocity profile is logarithmic, the settling velocity $w_s$can be computed from observations of SSC and current velocities using the Rouse profile:

$$\frac{c}{c_a} = \left(\frac{a}{h-a}\frac{h-z}{z}\right)^P \tag{4}$$

In which c is the sediment concentration (g/l), c_a is the sediment concentration at $z = a$, h is the local water depth (m), z is the vertical position in the water column (M), $P = \frac{\sigma_T w_s}{\kappa u_*}$ is the Rouse number with σ_T being the Prandtl-Schmidt number (equal to 0.7), κ the von Karman constant (equal to 0.41), and u_* the bed shear velocity (m/s). Under the assumption that $a = 0.2$ m (and therefore c_a is equal to the near-bed measurements), P can be fitted to the data by rewriting Eq. 4 to

$$\log\left(\frac{c}{c_a}\right) = \log\left(\frac{a}{h-a}\frac{h-z}{z}\right)P \tag{5}$$

Both u_* and z_0 are calculated by fitting a logarithmic profile through the current velocity observations using

$$u = \frac{u^*}{\kappa}\ln(z) - \frac{u^*}{\kappa}\ln(z_0) \tag{6}$$

For every pair of SSC observations at two depths during peak flow velocity conditions, one value for w_s can be computed. Note that P does not include the effect of turbulence damping, because turbulence damping is negligible during peak flow conditions. The computed settling velocities are converted into a frequency distribution of settling velocity (Fig. 5). The median settling velocity is slightly > 2 mm/s.

We realise that fitting a Rouse profile to two observation points introduces inaccuracies, that the profile might not be in equilibrium at peak flow velocities, and as a consequence the higher and lower range of the computed settling velocity have high uncertainties. Also the settling velocities seem rather large compared to quite a few modelling

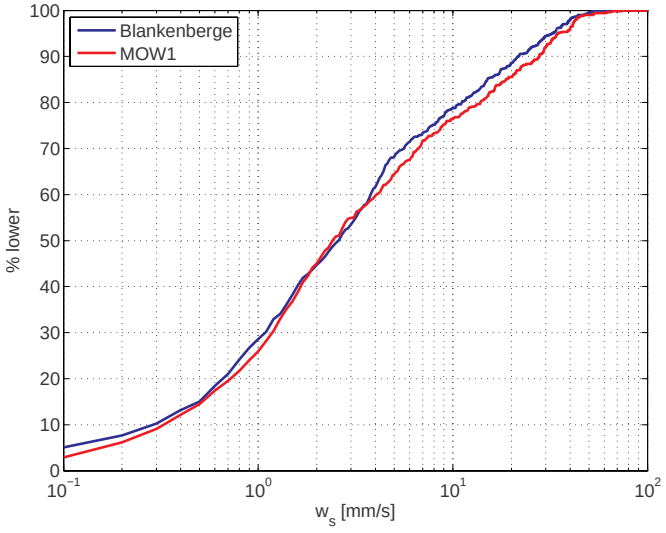

Fig. 5. Cumulative frequency distribution (over time) of the settling velocity, computed from a Rouse profile fit during peak flow conditions to continuous SSC measurements at stations Blankenberge and MOW1.

studies carried out in the past (e.g. Van Kessel et al., 2011a, 2011b; van Maren et al., 2015a, 2015b; Grasso et al., 2018; Toublanc et al., 2016). However, we believe that such large settling velocities are realistic for several reasons. First, such large settling velocities are not unusual in areas with concentrations up to several g/l (resulting in fast-settling flocs, see e.g. observational data by Manning and Dyer, 2007) and proved necessary for modelling the ETM of the Weser (Hesse et al., 2019). Secondly, the settling velocity of particles of sand-mud mixtures (as is the Zeebrugge area) increases relative to pure muds (Manning et al., 2011). In their experiments (with a typical range of the settling velocity of the flocs of 0.5–4 mm/s), microflocs settle much faster than macroflocs whereas in pure muds the fragile macroflocs settle faster. This may be the result of increased bonding potential between clay particles when sand is added to a muddy matrix (Mitchener et al., 1996; Manning et al., 2010). Thirdly, the good agreement in the settling velocity distribution between the two stations suggests that methodology (despite its shortcomings) has predictive value. And fourthly, settling velocities of several mm/s were needed to reproduce the observed SSC in the Zeebrugge TM (see hereafter).

Based on Fig. 5 and model calibration results, the settling velocities of the three fine sediment classes implemented in the model have been chosen as w_s = 0.5, 2 and 4 mm/s (Table 2), corresponding to ~15%, 45%, and 60% of exceedance, respectively. The slowest settling fraction represents poorly flocculated mud, fraction 2 moderately flocculated mud, and fraction 3 strongly flocculated mud.

The parameter values in Table 2 are based on an extensive calibration procedure which involved variation of the erosion parameters, bed roughness and settling velocity. Results of this calibration procedure are not presented here. The model results described hereafter as the standard model results are based on the best results obtained by varying the parameters in Table 2.

4. Model results

4.1. Hydrodynamics

The hydrodynamic model has been calibrated for the year 2014 by varying the Manning's roughness parameter *n*. Best agreement with model and observations was obtained using a Manning's value (throughout the model domain) of 0.022 s/m$^{1/3}$ (equivalent to a Chézy value of 67 and a Nikuradse roughness height of 2.4 cm at a typical water depth of 10 m). Such a value represents a moderately smooth bed, indicating that bed roughness is dominated by sand particles and small-scale bedforms (the majority of the model domain is not dominated by mud, this is only around Zeebrugge). A detailed evaluation of the hydrodynamic model is beyond the scope of the present paper, and therefore we only present a concise summary of model performance. We compute the model bias *B* and the root-mean-square-error (*RMSE*) for 16 water levels and 9 flow velocity observation stations, using the following definitions:

$$\mathrm{B} = \overline{M} - \overline{D} \tag{6}$$

$$RMSE = sign(\sigma_M - \sigma_D)\sqrt{\frac{\sum_{n=1}^{N}[(M_n - \overline{M}) - (D_n - \overline{D})]^2}{N}} \tag{7}$$

with $\overline{M}$ and $\overline{D}$ as the time-averaged modelled and observed variable respectively, σ_M and σ_D the standard deviation of the modelled and observed variable, and *N* the number of observations. The model bias *B* is a measure for the *mean* reproduction of a particular variable whereas the *RMSE* quantifies the difference between model and data *variability*. The bias *B* of the astronomical water levels is close to 0 whereas the *B* for water levels including meteorological effects is up to 11 cm (generally positive, implying that the model slightly overestimates surges). The modelled bias for flow velocity is typically 1–2 cm/s, implying hydrodynamic residuals are well reproduced. The *RMSE* of flow velocities is typically 5–10 cm/s, meaning that the model overestimates peak flow velocities.

The modelled wave height decreases in the shoreward direction, corresponding to the observational data (Fig. S1). With a correlation coefficient typically between 0.85 and 0.9 the agreement between observed and modelled wave height can be considered good. The salinity typically varies between 30 and 34 ppt, with a tidal variation in the same order of magnitude as low frequency salinity variations (Fig. S2). Both the low-frequency variation in salinity (in response to wind-driven flows and river discharge – see panel a) and tidal variability (panels b and c) are largely represented by the model. The offshore salinity (imposed on the model boundaries) is 33–34 ppt whereas the salinity ranges between 14 and 25 ppt at the Scheldt boundary location. The modelled tidal variability, with values well below those imposed on the offshore boundaries, therefore demonstrates the importance of the Scheldt River discharge on the salinity distribution around Zeebrugge.

4.2. Sediment transport

The sediment transport model has been setup and calibrated in two steps. The first step is the generation of the seabed composition, which is initially only composed of sand. Tidal currents, and the superimposed northeast-directed residual flow, bring fine-grained sediments into the model domain at concentrations determined by the boundary concentrations (5 to 60 mg/l, three fine sediment fractions, see Table 1). As a result, the sandy seabed fills in with fine sediments until the model achieves a dynamic equilibrium between hydrodynamic forcing, offshore boundary conditions, sediment availability and parameter settings. Dynamic equilibrium is defined as a state where the long-term variation (timescale of years) in the amount of sediment in the bed and in suspension is small compared to short-term variations (intratidal and spring-neap variation), and sediment fluxes into the model are equal to sediment fluxes out of the model.

Initially, the sediment flux into the model (mostly the southern boundary) is much larger than the sediment flux out of the model (the northern boundary) as sediment deposits within the model domain. Additionally, the sediment influx at the southern boundary is larger during initialisation than in equilibrium, as outflowing tidal currents (which are an order of magnitude larger than residual currents) are low in mud content during outflow. After 2 years the flux into the model is equal to the flux out of the model (around 30 million ton/year) and the influx no longer decreases. These values are close to earlier estimates by Eisma and Irion (1988) and Fettweis et al. (2007), between 1.4 and 1.7 times higher than values reported by Van Alphen (1990), Lafite et al. (1993) and Velegrakis et al. (1997), and about 1.5 times lower than those given by McManus and Prandle (1997). After 2 years, the mud content in the bed is up to 30 kg/m^3 near the harbour, and decreasing in offshore direction. After three years, this amount has become quasi-stationary, and this equilibrium bed provides the initial bed sediment composition for the various model runs executed as part of this paper (see Fig. 10 below, computed after 4 years).

The second step is the calibration against observations of the suspended sediment concentration and the mass of dredged sediments. Note that for each set of model parameters, step 1 (generation of the initial condition) is done anew. Available data are (1) satellite-based maps with distribution of near-surface SSC, (2) time series of in situ observed SSC, (3) dredged masses of both mud and sand; and (4) the amount of mud in the bed. The best agreement between data and model (using realistic model settings and boundary conditions) is referred to as the standard simulation (see Fig. 6 and Fig. 7), using the settings of Table 2. The model-data comparison reveals that although the computed spring-neap variation is in line with observations, the general level of SSC is too low. Traditional calibration methods for the sediment transport module are insufficient to raise concentration levels. Increasing erosion rates through the parameter settings leads to higher sediment concentration over short timescales, but also depletes the bed of sediment, resulting in lower SSC over longer timescales. Reducing

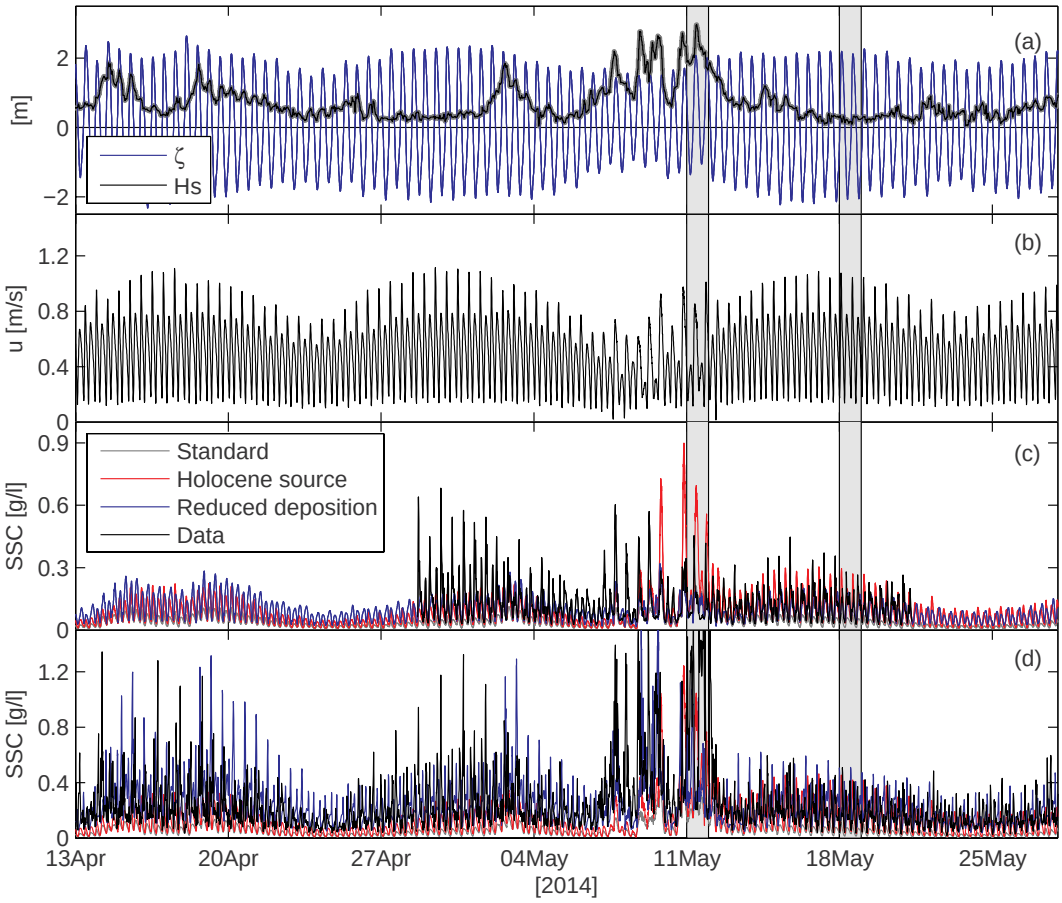

Fig. 6. Computed water level ζ and significant wave height Hs (a), Depth-averaged flow velocity u (b), observed (black) and computed (coloured) SSC at 2.2 mab (c) and 0.2 mab (d) for the standard simulation (grey), model alternative 1 (consolidated Holocene mud source, in red) and model alternative 2 (reduced deposition, in blue) during summer conditions at station MOW1 in 2014. The grey shaded areas indicate two distinct periods (storm-dominated and tide-dominated) for which more detailed results are provided in Fig. 7. (For interpretation of the references to colour in this figure legend, the reader is referred to the web version of this article.)

the erosion rate simply leads to a reduction in SSC (over short but also longer timescales). The standard simulation is an optimum setting obtained through a calibration procedure not shown here: apparently essential processes are missing.

Important processes cited in literature (see Section 2) that potentially influence the sediment dynamics around the study area are (1) sediment is eroded from the bed, and (2) high near-bed sediment concentrations influence turbulence damping and thereby residual transport and deposition. Both these aspects are therefore further evaluated with the model.

Highly concentrated near-bed suspensions (observed during field surveys after storm conditions, see e.g. Fettweis et al. (2010) and also Fig. 6 and Fig. 7) profoundly influence hydrodynamics and sediment dynamics. The resulting high vertical concentration gradients reduce vertical mixing of sediment, further strengthening the near-bed sediment concentration. Also a local sediment source (not implemented in the standard model settings) leads to higher near-bed concentrations and therefore better agreement with data. High near-bed sediment concentrations are not properly represented in the reference model because of vertical resolution limitations and poor understanding of near-bed exchange processes related to flocculation and consolidation (as explained in detail in Section 3.3); both are represented by the bulk parameter β. Using β, the near-bed concentrations are higher in areas where sediment converges, which better corresponds to observations but also influence mixing properties within the water column.

To test the effect of a local source and the reduction of near-bed exchange of sediment, two alternative model configurations were setup and compared against the standard simulation: one with a local sediment source and one with reduced bed exchange. For model alternative 1, mud is prescribed as a net sediment source on the location indicated in Fig. 2. This mud replaces the sand-mud mixture and is thicker (3 m) than can be eroded within the timeframe of this model study. As this mud is consolidated, the erodibility is lower compared to more recently deposited mud. The erodibility parameters M0, M1, and M2 of the mud patch were therefore varied (see Table 2) until the net loss from the consolidated Holocene mud area in the model (2.6 million m^3/y) was comparable to the observed loss of 2.79 million m^3/year (Fig. 3). Note that better agreement between observed and modelled sediment concentrations can be achieved by either increasing erosion rates from the consolidated Holocene mud area (by decreasing $\tau_{cr,\,2}$, or increasing the erodibility parameters M0, M1 and M2) or increasing the local roughness. This has not been done, however, since it would result in unrealistically large erosion rates of the consolidated Holocene mud. For model alternative 2, the near-bed sediment concentration is enlarged through reduced deposition (as explained above), parameterized by the parameter β. We have not used combinations of both approaches in order to be able to differentiate between their individual impact.

Both adaptations to the standard simulation lead to higher suspended sediment concentrations throughout the water column. At 2.2 m above the bed (mab) the computed sediment concentration is comparable with observations, especially the spring-neap variation (see Fig. 6c). The intra-tidal SSC variability is reasonably reproduced for

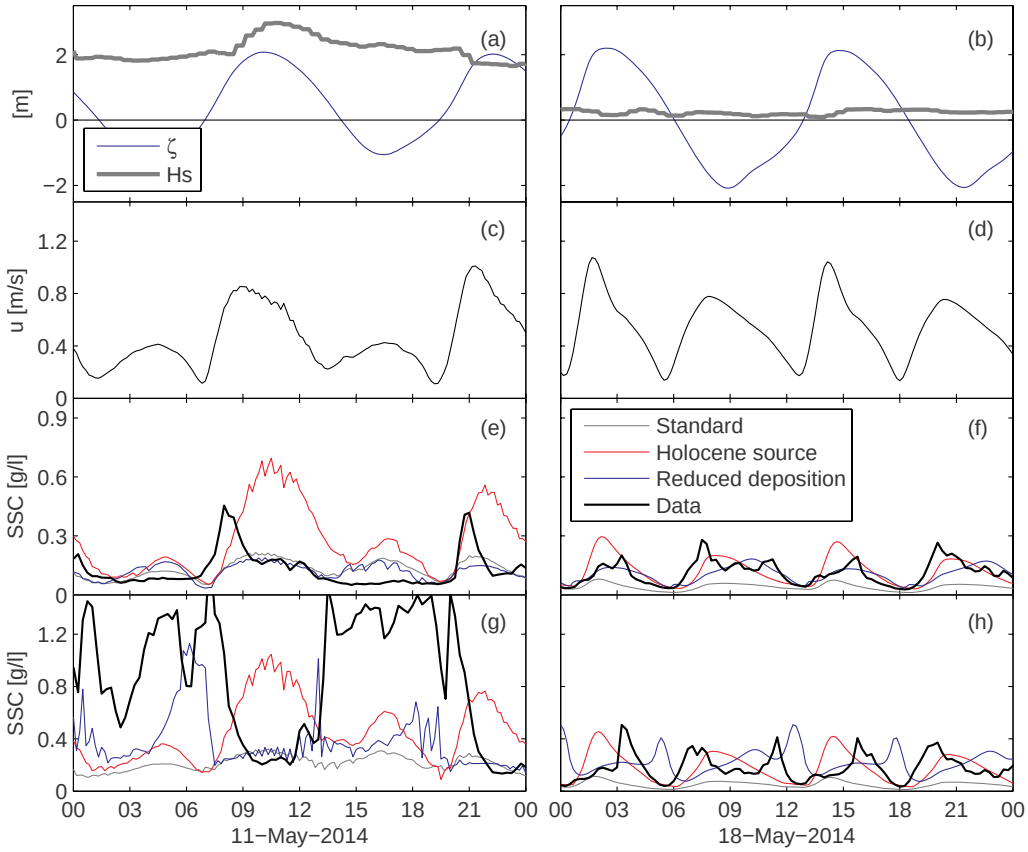

Fig. 7. Details of water levels and wave height (a-b), depth-averaged flow velocity (c-d) and sediment concentrations at station MOW1 2.2 m.a.b. (e-f) and 0.2 m.a.b. (g-h) for the grey shaded periods in Fig. 7. The left panels represent a period with wave-dominated conditions (high waves, neap tide), the right panels a period with tide-dominated conditions (low waves, spring tide).

both model adaptations during tide-dominated conditions (Fig. 7f): the concentrations are typically around 0.2 g/l during peak flow conditions and reduce to several 10's of mg/l during flow reversal. During storm conditions (Fig. 7e), the model with a consolidated Holocene mud source overestimates SSC levels, but the standard model and reduced deposition approach show reasonable agreement. Again, the concentrations are typically highest during periods with high flow velocity. The data-model comparison suggests that the additional shear generated by the wave model leads to an overestimation of the sediment erosion rates.

Closer to the bed the general levels of SSC are reasonably reproduced for both model adaptations during tide-dominated conditions, but the intra-tidal phasing is poorly represented. The observations suggest that the concentrations are highest in-between peak flow and slack water, whereas the modelled concentrations are highest during peak flow (standard approach and consolidated Holocene mud source approach) or during slack tide (reduced deposition). During storm conditions, the level of near bed sediment concentration is reasonably reproduced with the consolidated Holocene mud source, but the phasing is completely wrong (Fig. 7g). The data suggests that sediment concentration variations result from vertical mixing, with a vertical uniform concentration around 0.2 g/l during high shear. During slack tide conditions, the sediment settles, leading to highly concentrated suspensions of 1.5 g/l near the bed. This vertical mixing behaviour is conceptually best represented with reduced deposition. Using this approach, the near-bed concentration is indeed lowest during periods with maximum hydrodynamic energy, in agreement with observations. This is the result of vertical mixing, which will be elaborated in more detail hereafter.

The vertical structure of the computed suspended sediment concentration (Fig. 8) reveals that during periods of high flow velocities (shortly before high and low waters) the sediment concentration follows a Rouse profile. The sediment concentration is higher for the simulation with a consolidated Holocene mud source and lower for the standard simulation. However, the concentration profiles differ most during flow reversal. With reduced deposition, suspended sediment settles towards the lower computational layers, but remains suspended in the water column. This leads to strong near bed gradients in the concentration profiles, influencing the water density and hence turbulence damping. These high-concentration near-bed layers are regularly observed at the observation stations in the Zeebrugge TM, supporting the reduced deposition approach.

On a larger spatial scale, the computed spatial distribution of surface sediment concentration in the TM is compared to satellite images (Fig. 9) and computed bed sediment distribution to observations (Fig. 10). The general pattern of elevated SSC is in line with the satellite observations, although the peak in computed SSC is slightly north of Zeebrugge whereas the data suggests SSC is highest just south of Zeebrugge (Fig. 9g,h). The spatial distribution of surface sediment is better reproduced with the additional consolidated Holocene mud source (Fig. 9 c, d), especially over the triangle-shape sand bar situated at the mouth of the Scheldt estuary. The fact that the consolidated Holocene mud source is located south of estuary mouth implies that sediment eroded from the consolidated Holocene mud is transported towards this sand bar. Reduced deposition only marginally influenced the magnitude of the surface sediment concentrations but interestingly leads to a southward shift of the TM (compare Fig. 9a, b with Fig. 9e, f) which is more in line with the observations. Apparently, reducing the exchange of sediment between the water and the bed generates a southwestward directed transport component and/or reduces the northeastward transport compared to standard water bed exchange simulations.

The seasonal variability in sediment concentration is underestimated by the model for all scenarios. Seasonal variations in SSC are typical for mid-latitude shelf seas such as the North Sea and are related to the seasonal patterns in wind forcing and wave heights (Howarth

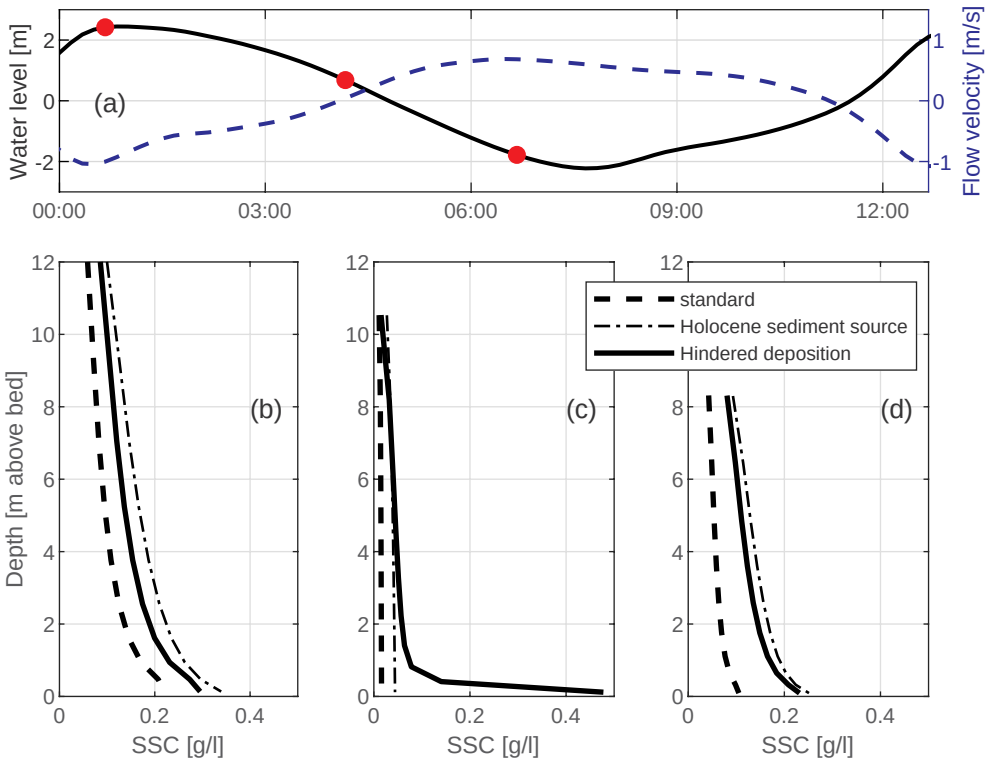

Fig. 8. Computed suspended sediment concentration at station MOW1 at peak flood flow (high water, b); slack tide (halfway ebb; c) and peak flood flow (high water; d) – see top panel (a) for corresponding water level (with red dots indicating the timing of computed SSC profiles) and depth-averaged flow velocity (positive is south-westward ebb flow). (For interpretation of the references to colour in this figure legend, the reader is referred to the web version of this article.)

et al., 1993; van der Hout et al., 2017), density effects caused by higher fresh water discharges in winter, and biological effects (e.g. Jago et al., 2007). The model accounted for the seasonal variability in wind forcing (and its effect on wave height) and discharge, but not for biological effects on the settling velocity or bed erosion. This introduces three potential reasons why the observed sediment concentration in summer deviates more from that in winter, compared to the model. First, particles settle faster in summer due to the greater availability of organic material strengthening flocculation (Mietta et al., 2009), especially during the spring and summer phytoplankton blooms (Jago et al., 2007; Fettweis and Baeye, 2015). Secondly, in muddy areas affected by organic exopolymers the erosion rates are lower in summer due to strengthening of the bed (Kornman and De Deckere, 1998; Paterson and Hagerthey, 2001), leading to lower summer sediment concentrations. And thirdly, biological cohesion reduces bedform size and therefore bed roughness (Malarkey et al., 2015; Parsons et al., 2016); a lower bed roughness leads to lower erosion rates.

The computed amount of sediment in the bed differs strongly among the different model simulations. Obviously, the simulation with prescribed bed sediment shows close agreement with observed bed sediment. Without sediment prescribed to the bed, the highest mud content is observed in the channels. These deposits best agree with the recent, unconsolidated muds described by Fettweis et al. (2006). The model alternative with reduced deposition predicts the lowest amount of mud in the bed, which is an obvious consequence of reducing the sediment flux to the bed. Apparently, despite a fairly good agreement of surface concentrations (as in Fig. 12, for all model realisations), the predicted amount of sediment in the bed may strongly vary.

Computed dredging volumes serve as a last model validation parameter. The dredging quantities (Table 3) correspond most to simulations with a consolidated Holocene mud source. This model alternative overestimates the siltation in the navigation channels, but underestimates siltation in the Port of Zeebrugge with a factor 2. This suggests that mechanisms transporting sediment through the channels into the port itself are underestimated. This may be the result of vertical processes (as indicated by the low computed near-bed sediment concentrations at MOW1 in winter) but also by the underestimated SSC west of the port of Zeebrugge (Fig. 9 - bringing relatively low SSC water into the port during flood). Furthermore, the entrance of the port is represented by 5 horizontal grid cells, which is insufficient to accurately resolve horizontal circulation cells (eddies), while horizontal exchange accounts for 43% of net sediment transport into the port (Vanlede and Dujardin, 2014). The computed siltation rates are overall slightly lower using reduced deposition; lowest siltation rates are computed for the standard simulation.

Data-model comparison reveals that the large-scale sediment concentration levels are reasonably eproduced by reducing the exchange between the water column and the bed (reduced deposition approach), or by prescribing a local sediment source (consolidated Holocene mud source approach). Both approaches also resemble the intratidal variation of SSC observed several meters above the bed, but fail at capturing the intratidal variation near the bed. But even though the variability is wrong, the levels of suspended sediment concentration are captured by applying reduced deposition, supporting the reduced deposition approach. The bathymetric changes and the dredging quantities are more in line with the modelling approach prescribing a consolidated Holocene mud source.

Apparently, sediments in the water column resemble observational data best using reduced deposition, whereas sediments in the bed correspond better with data using a prescribed mud source. Which of the two approaches better describes sediment transport processes in the Zeebrugge TM cannot be established with the presently available data and process understanding – a combination of both approaches is most likely. The model does therefore not conclusively reveal which of the two investigated mechanisms is responsible for the formation of the TM (and if both are – which one is more important). In order to further understand the role of sediment supply and bed exchange, we explore the sensitivity of both model approaches to salinity and sediment-induced density effects.

4.3. Model scenarios

Both salinity and sediments influence the density of water through the equation of state, generating density currents and damping

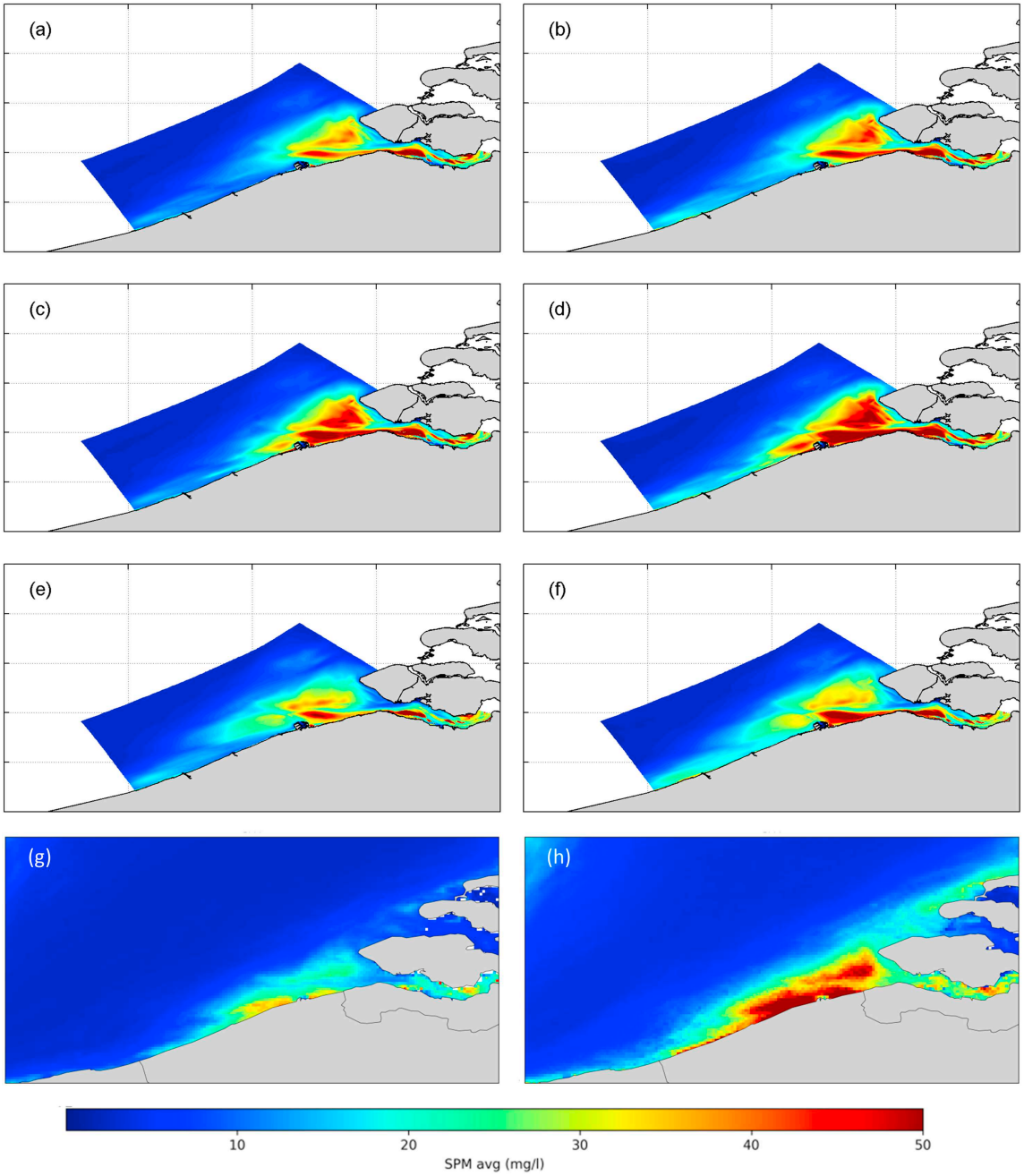

Fig. 9. Modelled and observed spatial distribution of surface SSC in summer (from 1 April to 1 October; a, c, e, and g) and in winter (from 1 October to 1 April; b, d, f, and h) computed from the standard simulation (a, b); with a consolidated Holocene sediment source (c, d); with reduced deposition (e,f); and from satellite images (g, h). The model has been run for the year 2014, the sediment concentration is based on observations covering the period 2003–2011 (using the algorithms by Nechad et al., 2010).

turbulence mixing (Winterwerp, 2001, 2006). The effect of the two model alternatives on transport mechanisms are further explored by individually switching off the effect of salinity (by assuming all water is saline) and sediment (by switching of the contribution of the sediment concentration on the density in the equation of state) on the hydrodynamics. Both salinity and SSC influence the hydrodynamics in two ways: (1) horizontal gradients in the salinity or SSC generate a horizontal pressure gradient that drives a near-bed flow towards the area of lower pressure, and (2) vertical gradients in SSC or salinity dampen vertical mixing (as computed by the k-ε turbulence model).

The difference in the computed SSC for the various model alternatives increases towards the bed (Fig. 8), and therefore the impact on SSC is evaluated here for the near-bed layer. The impact of salinity and sediment-induced density-effects on SSC differs substantially for both model alternatives. For both model approaches, including salinity-driven currents leads to an increase of turbidity in the nearshore northeast of Zeebrugge and a decrease in turbidity in the estuary mouth: the TM is pushed towards the coast. The effects are much more pronounced and stretch further in westward direction, however, for simulations with reduced deposition. The sediment-induced density coupling results in both cases in a lower turbidity in the estuary mouth.

With a reduced deposition flux, both sediment-induced suppression of turbulence and salinity effects lead to > 100 mg/l increase in SSC (right panels in Fig. 11). The average near-bed sediment concentration is many 100 mg/l, and therefore the relative near-bed increase in SSC is only several 10's %. However, sediment introduces a positive feedback

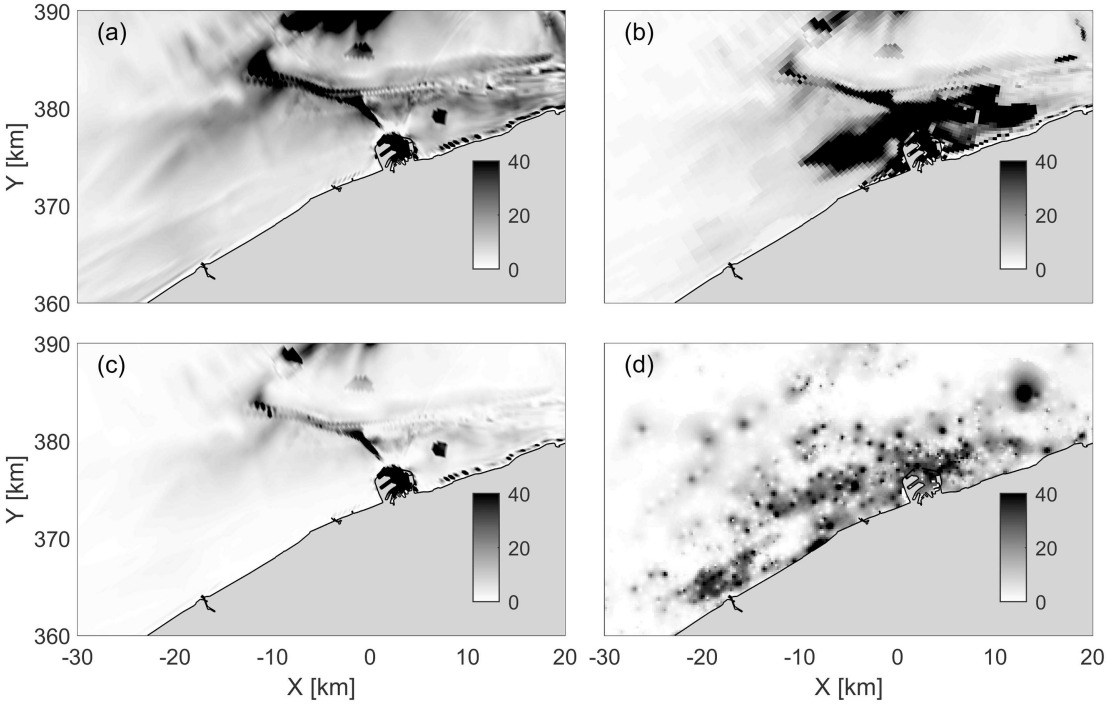

Fig. 10. Amount of mud in the bed computed by the model for the reference model (a), model alternative 1 (mud source, b) and model alternative 2 (reduced deposition, c), in kg/m^2 (sum of layer 1 and 2, and all mud fractions). Panel d provides the measured clay fraction (from Fettweis et al., 2009b) in %.

mechanism, where an increase in the sediment concentration may reduce vertical mixing, further strengthening vertical concentration gradients. The computed near surface sediment concentrations (not shown) are indeed lower, meaning the vertical sediment concentration gradients become larger.

The impact of salinity and sediments on hydrodynamics is illustrated with yearly average flow velocity profiles in the Zeebrugge access channel and in the approach channel to the Western Scheldt (Scheur) (Fig. 12). Horizontal salinity gradients generate salinity-driven currents which are directed towards the freshwater source near the bed and in opposite direction near the surface. As sediment concentrations increase towards the bed, salinity gradients generate a transport component directed towards the freshwater source (the Scheldt River, but also the port of Zeebrugge where local drainage water is discharged (up to 10 m^3/s during peak discharge conditions). The overall effect is that sediment remains closer attached to the coast, as illustrated in Fig. 11c and d.

Sediment-induced density effects only have a limited impact on the residual current (Fig. 12). The impact of sediment-induced density effects is therefore primarily a vertical redistribution of sediments, with more sediments close to the bed and less up in the water column. However, when combined with salinity-driven currents (generally directed landward closer to the bed), sediment-induced density effects lead to enhanced landward transport of suspended sediment. As the vertical gradients in SSC are stronger when using reduced deposition, salinity-driven currents have a more pronounced impact on the sediment redistribution.

When SSC is sufficiently high, self-organizing mechanisms apparently exist which maintain or strengthen the TM: the higher the sediment concentration, the stronger the sediment-induced stratification, leading to larger salinity-induced landward sediment transport. The impact hereof on the formation of the Zeebrugge TM will be discussed in more detail in Section 5.3.

5. Discussion

Both model approaches presented here (reduced deposition and a local sediment source) reproduce the basic sediment dynamics in the Zeebrugge TM: the spring-neap variation and spatial distribution of SSC as well as typical dredging volumes. A number of shortcomings remain, however, such as the underestimation of thick, high concentration suspensions near the bed and the north-eastward shift of the TM. Despite these shortcomings, our model underlines that (1) our knowledge on near-bed sediment dynamics has significant deficiencies, limiting predictive modelling of fine sediments in turbid environments, (2) multiple model approaches exist which can reproduce the dynamics of

Table 3
Observed and modelled dredged sediment mass (in million tonnes/year) and the mud fraction (by mass, in %) for the three main dredging areas in the TM: the port of Zeebrugge, the approach channel to Zeebrugge, and Scheur (see Fig. 3 for locations). Observed dredging numbers are based on personal communications with the Flemish ministry of Public Works, compiled in Vroom and Schrijvershof (2015). The model scenarios with the closest agreement are in bold.

Simulation	Zeebrugge			Approach channel Zeebrugge			Scheur		
	Total (10^6 t/year)	Obs./comp. (%)	Mud fraction (%)	Total (10^6 t/year)	Obs./comp. (%)	Mud fraction (−)	Total (10^6 t/year)	Obs./comp. (%)	Mud fraction (−)
Observed	5.96	/	77	1.06	/	66	0.68	/	43
Standard	1.17	19	64	0.68	64	16	1.32	194	6
Consolidated Holocene mud source	**2.99**	**50**	98	**1.13**	**107**	91	1.45	213	85
Reduced deposition	2.18	37	80	0.74	70	17	**1.12**	**165**	7

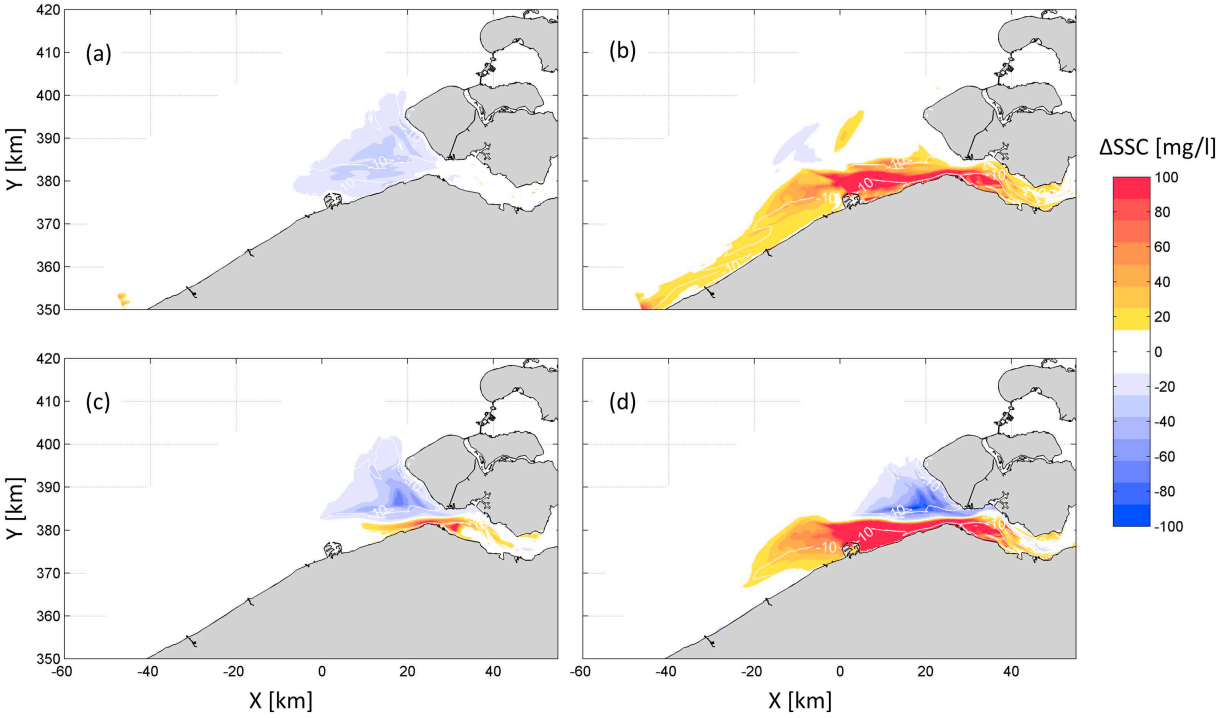

Fig. 11. Increase in near-bed SSC by (a, b) sediment-induced density effects on turbulence suppression (simulation with sediment and salinity effects minus a simulation without sediment effects but with salinity effects) and (c, d) salinity-induced density effects (simulation with sediment and salinity effects minus a simulation with sediment effects but without salinity effects). The left panels (a, c) depict simulations with the consolidated Holocene sediment source whereas the right panels (b, d) depict simulations with reduced deposition.

the turbidity maximum to a similar level of accuracy, and the underlying assumptions are important when interpreting modelled turbidity maximum dynamics; and (3) both approaches provide new insights into the formation and maintenance of the Zeebrugge Turbidity Maximum. These will be discussed in more detail below.

5.1. Near-bed sediment dynamics

The reduction in the deposition flux β is to some extent similar to the well-known and often-used Krone equation (Krone, 1962). The Krone equation only allows sedimentation below a critical user -defined parameter, and the closer the bed shear is to the critical bed shear for deposition, the lower the deposition flux (if we express reduced deposition as $\beta = (1 - \tau_b/\tau_{b,\ cr})$ for $\tau_b < \tau_{b,\ cr}$, we obtain the Krone

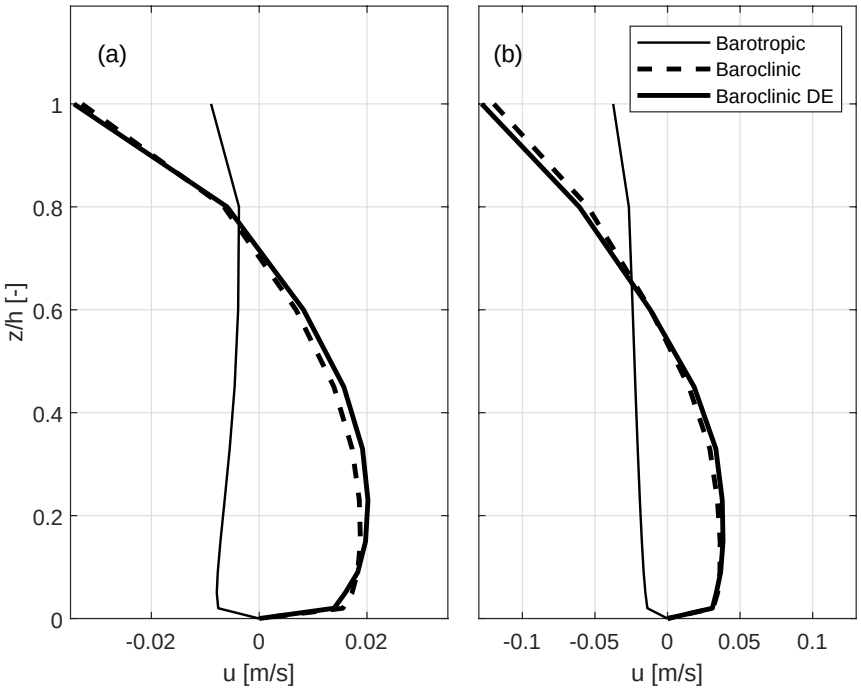

Fig. 12. Modelled flow velocity profile (averaged over one year) in the Zeebrugge entrance channel (a) and in the approach channel to the Western Scheldt (Scheur; panel b). Positive values are directed towards the port of Zeebrugge in (a) and towards the Western Scheldt in (b). The thin solid lines are velocities computed with a barotropic model excluding salinity, whereas a baroclinic model including salinity was run with deposition efficiency DE (thick solid line) and without DE (dashed line).

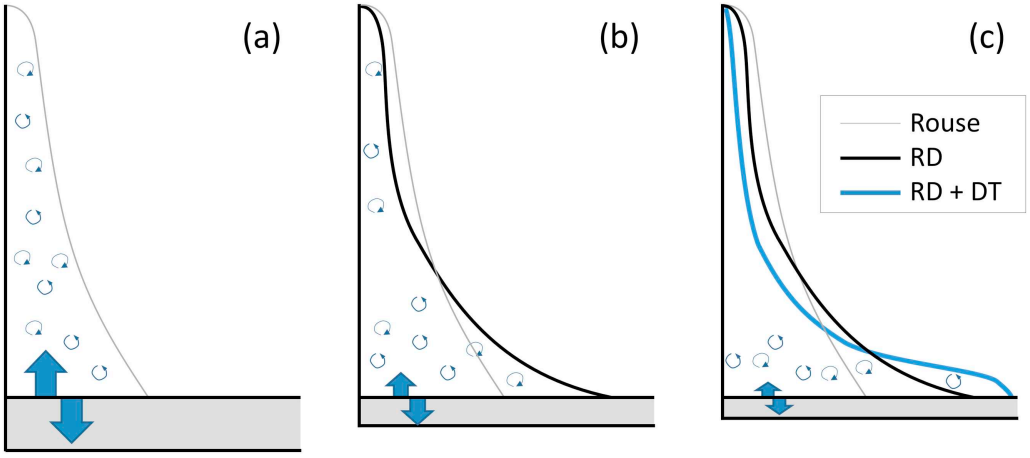

Fig. 13. Illustration of the effect of reduced deposition (RD) on a Rouse sediment concentration profile (a). Reduced deposition fluxes result in higher near-bed sediment concentrations and a lutocline-shaped profile (b), which is enhanced by turbulence suppression (DT; c).

equation). However, there are several arguments against the Krone equation. As demonstrated by Winterwerp (2007), there are no physical arguments (or proper data) to exclude mutual erosion and sedimentation as in the Krone formulation as a function of shear. Also the assumption of constant settling velocities (as implicitly in the Krone formula) is not realistic for high sediment concentrations (Mehta et al., 2014).

Reduced deposition is hypothesized to be the combined effect of vertical discretization, strength development, floc dynamics in the bed boundary layer, and local irregularities (Section 3.3). In its present form β is independent of shear, sediment concentration and settling velocity. However, there are three arguments suggesting that reduced deposition should become more pronounced at higher sediment concentrations.

First, reduced deposition leads to a steeper sediment concentration profile (Fig. 8 and Fig. 13b) which in turns leads to suppression of turbulent mixing at the lutocline (Winterwerp, 2001, 2006). With less turbulent mixing, sediment above the lutocline rapidly settles from the upper part of the water column, further steepening the concentration profile (Fig. 13c). Reduced deposition therefore favours the formation of highly concentrated near-bed layers. In the Rouse concentration profile, the sediment concentration gradients scale linearly with the sediment concentration *SSC*, and therefore the contribution of mechanism (1) to β scales with *SSC*.

Secondly, the sediment concentration influences β through consolidation. Consolidation times scale with the square thickness of the initial deposits (as follows from the diffusion term in the Gibson et al. (1967) consolidation equation). At low sediment concentrations, the deposition flux is small, and therefore all sediment on the bed consolidates instantaneously. However, sediment does not consolidate instantaneously when settling rates are large, leading to a longer period of low critical bed shear stresses. And since deposition scales linearly with the sediment concentration (as in Eq. (3)), the contribution of strength development by consolidation to β scales with SSC^2.

Thirdly, the sediment concentration influences deposition through hindered settling. It was argued in Section 3.3 that as models with low vertical resolution underestimate the near bed SSC, they underestimate hindered settling and therefore overestimate deposition. However, an underprediction of SSC also reduces the deposition flux w_sC, which would imply $\beta > 1$. Which of these two is more important, depends on the near bed concentration and the gelling concentration c_g (Fig. 14) via de formula of Richardson and Zaki (1954). Typically, c_g varies between 20 and 100 kg/m^3. For $c_g = 20$ kg/m^3, the deposition flux w_sC decreases with increasing *SSC* when *SSC* > 3 kg/m^3, hence hindered settling is dominant, requiring $\beta < 1$; for $c_g = 50$ kg/m^3 hindered settling dominates when *SSC* > 8 kg/m^3. The higher the gelling concentration, the higher the near bed sediment concentration needs to be before hindered settling becomes dominant.

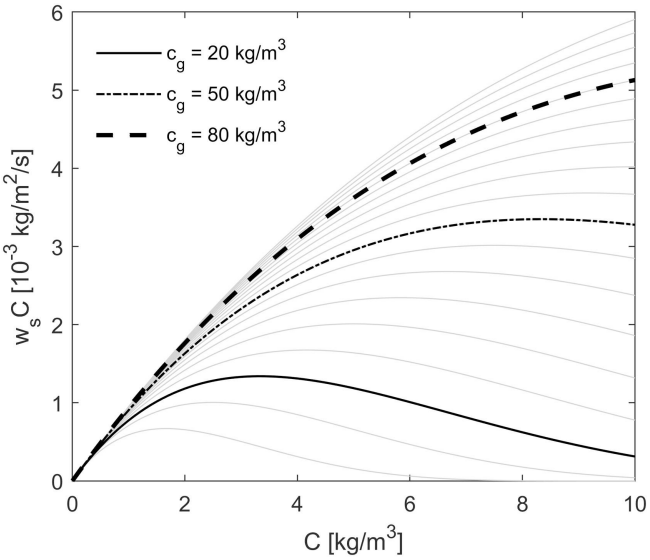

Fig. 14. Relation between deposition flux w_sC as a function of concentration C, for a gelling concentration c_g of 20, 50 and 80 kg /m^3 (black lines) and at increments of 5 kg/m^3 in-between 10 and 100 kg/m^3 (grey). *Ws* is computed using the simplified Richardson-Zaki formulation (see Section 3.3).

When the concentrations are in the hindered settling range, underprediction of the *SSC* (due to model resolution) leads to overprediction of the deposition flux (therefore $\beta < 1$). At low sediment concentrations (*SSC* less than several kg/m^3), the near-bed vertical discretization is more likely to underestimate the deposition flux (as in Spearman and Manning, 2008). This means that β should be smaller at higher sediment concentrations. In the concentration range near Zeebrugge (*SSC* several g/l near-bed) the effects of increased deposition and hindered settling are comparable, motivating a $\beta \approx 1$.

The settling velocity w_s influences β in several ways. At very low settling velocity,$\beta = 1$ because the vertical gradients are absent whereas at very high settling velocity $\beta = 1$ because particles deposit instantaneously. Hence, an optimum in w_s must exist where it maximally influences β. The settling velocity is, in turn, related to the sediment concentration through flocculation: typically, the floc size and therefore w_s increases with the sediment concentration. However, w_s also depends on shear. Dyer et al. (2002) and Manning et al. (2007) observe that the settling velocity in a highly concentrated near-bed suspension in the Tamar Estuary increases, due to damping of turbulent

energy in the lutocline. On the other hand, floc size has been observed to decrease in the bottom boundary layer due to high velocity shear (Hill et al., 2001; Safak et al., 2012; Wang et al., 2013). This apparent contradiction hypothetically introduces another concentration-dependence: at low SSC velocity shear is maximal in the bottom boundary layer (thereby destroying flocs) whereas at high SSC velocity shear is maximal at the lutocline.

The discussion above illustrates that there is great need for a better quantitative understanding of near-bed exchange processes, in particular settling behaviour and the effect of sediment concentration, settling velocity, and shear thereon, to better understand and predict sediment dynamics in turbid environments. Strength development and near-bed floc dynamics probably provide the greatest challenges: both are well studied in low-dynamic laboratory conditions, but not in more dynamic field conditions. This is further complicated by turbulent fluctuations of bed shear around the mean (see Van Prooijen and Winterwerp, 2010). Unfortunately, collecting near-bed concentration data (< 0.3 mab) is logistically difficult, especially in energetic environments at greater water depths. In data-model comparisons published in literature there is a strong bias towards observations collected at a greater height above the bed. This is especially true for environments with high sediment concentrations (van Maren et al., 2015b; Toublanc et al., 2016; Grasso et al., 2018; Hesse et al., 2019).

In turbid environments with high near-bed sediment concentrations, the intratidal SSC levels at heights exceeding 1 m.a.b. may both result from vertical mixing or sediment resuspension. Determining which one of these two processes is more important requires near-bed observations which are generally not available. This introduces uncertainty in model behaviour: turbidity maxima computed with a model assuming the TM results from local resuspension of bed sediments behaves very differently from a TM resulting from density-driven processes. The first TM is static, responding only limitedly to subtle changes in the hydrodynamic forcing. The second approach to modelling the TM responds, in contrast, much more dynamically (exemplified with the effect of salinity in Fig. 11). Consequently, more frequent collection of near-bed observations in turbid environments is crucial for (1) better understanding of complex bed exchange processes (and therefore setup of models), but also (2) calibration of models.

5.2. Uncertainty

The fact that two model alternatives which more or less equally well reproduce observational data leads to different model behaviour can be interpreted in two ways. It may suggest the model's predictive capacity is limited (as in Oreskes et al., 1994), what would imply that the model has limited use. On the other hand, it also points to the strong and weak points of the numerical model, which is essential for the decision-making process for which the models are typically designed for in the first place. For instance, both model approaches suggest that salinity effects reduce the turbidity in the estuary mouth, strengthening confidence that salinity indeed locally influences turbidity (although how much depends on the model approach). On the other hand, only the reduced deposition approach suggests that salinity- or sediment-induced density effects strengthen the TM. This weakens our confidence on the predicted role of density-induced effects on the formation of the TM.

Numerical simulation models in earth sciences have several sources of uncertainty. Aleatory uncertainty relates to the stochastic nature of the physical processes and epistemic uncertainty to limitations in understanding the physics and in quantifying its input parameters (e.g. Walker et al., 2003). Variability in input parameters typically has a limited impact on complex sediment transport models (where the amount of model realisations is limited by computational effort), both through equifinal (as van Maren and Cronin, 2016) or stochastic (e.g. van der Wegen and Jaffe, 2013) approaches. Limitations in understanding the actual physics, or conceptual uncertainty, have a much larger impact. Refsgaard et al. (2006) point out that conceptual uncertainty is often acknowledged as the main source of uncertainty, but rarely considered in environmental modelling. Our study is an example of an environmental study where conceptual uncertainty is acknowledged as the most important source of uncertainty. Most attention is given here to the role of near-bed exchange, but the same applies to the role of biology on erosion and settling (leading to seasonal variations typically not addressed in numerical models) and sand-mud interaction in general. This is important to realise, because including part of the uncertainties (for instance, a stochastic analysis of the consolidated Holocene mud bed approach) while ignoring others (role of vertical mixing and highly concentrated near-bed suspensions) may lead to results that are not only incorrect but also severely misleading for the decision maker, and therefore lead to unintended and undesirable management decisions (Uusitalo et al., 2015). Reducing the uncertainty near the Port of Zeebrugge requires at least more detailed and quantitative knowledge on the near-bed exchange processes.

5.3. Formation and persistence of the Zeebrugge TM

The numerical models do not conclusively reveal which mechanisms are responsible for the formation and persistence of the Zeebrugge TM, but do provide valuable new insights into the physical mechanisms related to the formation and persistence of the ETM compared to earlier studies. We synthesize these mechanisms into a conceptual model which identifies four consecutive phases, i.e. erosion of consolidated Holocene mud by harbour extension works, increase of the SSC, sediment-induced stratification and sediment trapping (Fig. 15).

I. Erosion of consolidated Holocene mud by harbour extension works

A large amount of sediment was brought in suspension as a direct result of the enlargement of the Port of Zeebrugge in the 1980's. Bathymetric surveys suggest that > 50 million m^3 was eroded nearby the Port of Zeebrugge after its expansion, and at least double that amount over a larger area (see Fig. 3). Large anthropogenic changes in sources and sinks may have significant impacts on the suspended sediment concentration (van Maren et al., 2016). Although the sediment concentration in the Belgian Coastal Zone has always been high (e.g. Fettweis et al., 2009a), it is likely to have changed in response to the seabed erosion following the Port of Zeebrugge expansion.

II. IIncreasing SSC in the TM

Assuming a dry density of 1 t/m^3 (representing consolidated sediment), more sediment was eroded around the Port of Zeebrugge than annually supplied by nearby river systems such as the Loire, Rhine, Seine, Elbe, and Weser (varying between 0.33 and 1.5 million tonnes; Milliman and Syvitski, 1992). Such a large amount of sediment is expected to generate an increase in suspended sediment concentrations as is commonly observed near river mouths. SSC was not monitored in the Belgian Coastal Zone during harbour extension works. However, the suspended sediment concentration in a large part of the Dutch coastal zone was significantly higher for a short period in the early 1980's (Dronkers, 2005). This anomaly has not yet been explained; but northeastward transport of the large amount of mud eroded from the Belgian coastal zone is a potential explanation.

III. Sediment induced stratification

Larger suspended sediment concentrations in the Zeebrugge TM lead to more pronounced interactions between sediments and hydrodynamics. These interactions include direct damping of turbulent mixing, sediment-induced density currents, and reduced deposition of suspended sediments to the bed. Such sediment-induced turbulence damping occurs already at concentrations of only several 100 mg/l

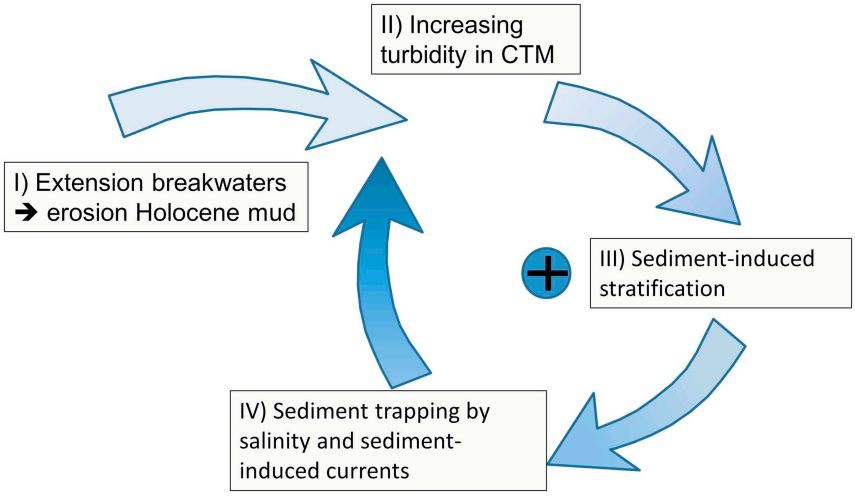

Fig. 15. Positive feedback loop hypothesizing the relation between human interventions, erosion of the consolidated Holocene mud layer and sediment-induced buoyancy effects responsible for the present-day Zeebrugge TM.

(Winterwerp, 2001) and may have strong impacts on mud transport and sediment deposition patterns (e.g. Winterwerp and van Kessel, 2003), which is confirmed by the present work.

IV. Sediment trapping

Sediment is trapped by the above-mentioned sediment-induced density effects (where the steeper sediment concentration profile makes it more susceptible to salinity-driven flows - see Section 4.3) but also by the sediment concentration effects on limited sediment deposition (Section 5.1). As a result, erosion of bed sediments (phase I) leads to conditions where sediments become more easily trapped. Enhanced trapping in turn leads to higher sediment concentrations (phase II) and stronger sediment-induced density effects (phase III), resulting in a positive feedback where the TM becomes increasingly more pronounced.

The model with a consolidated Holocene sediment source is indicative for phase I and II (realistically modelling phase I and II requires a historical bathymetry including detailed information on bed composition, which is not available), whereas the model with reduced exchange between the bed and the water column represents phase III and IV. The complete feedback loop has not been reproduced within one single model because of (1) limitations in our understanding of physical processes occurring near the bed (and especially its concentration-dependence) and (2) the timescales (30–50 years) associated with such transitions are too long to simulate with computational intensive numerical models.

Such positive feedback mechanisms have already been described for estuaries (Winterwerp and Wang, 2013; Winterwerp et al., 2013) and have been quantified using numerical (van Maren et al., 2015b) or semi-analytical models (Dijkstra et al., 2019). Once an estuary becomes too turbid (often as a result of deepening), positive feedback mechanisms lead to further increase in the turbidity. As long as the concentrations are high, sediment convergence therefore continue to trap sediment (even if the mechanism responsible for the initial increase, such as deepening, no longer exist). The Zeebrugge TM provides a first non-estuarine example where this sediment-induced trapping mechanism is hypothesized as an important factor.

6. Conclusions

A large amount of fine-grained bed sediment was eroded in response to the expansion of the Port of Zeebrugge in 1979–1986. Although direct observational evidence is missing, this has likely led to an increase in suspended sediments up to the Dutch coast. The extension of the port may have also provided a trigger for a positive feedback mechanism strengthening sediment convergence in the Zeebrugge TM through formation of highly concentrated near-bed sediment suspensions. The contribution of a local sediment source (erosion) and of the positive feedback mechanisms has been evaluated using two separate model approaches. In the one model approach, the increase in SSC is caused by erosion of consolidated Holocene mud. In the other approach, the deposition from the water column to the bed is reduced with a simple parameterization, resulting in larger near-bed SSC and larger effects of salinity-driven and sediment-induced density currents. The latter approach provides a positive feedback mechanism, where sediment convergence increases with higher sediment concentrations, thereby maintaining the Zeebrugge TM. The reduced deposition is based on physical arguments and circumstantial evidence provided by observational data, and is likely important for fluid mud formation in general. Responsible transport mechanisms, including dependencies on setting velocity, sediment concentration, and bed shear stress, need to be quantified in more detail through detailed field observations. Both model approaches (local source and reduced deposition) reproduce available observations comparably well, but for different reasons. The response of the model in a scenario analysis context is, therefore, also very different, resulting in a source of uncertainty.

Supplementary data to this article can be found online at https://doi.org/10.1016/j.margeo.2020.106186.

Declaration of competing interest

There is no conflict of interest.

Acknowledgements

This work has been mainly carried out as part of the vision for the Flemish Coastal Zone (Complex Project Kustvisie) and by the MOMO project (both funded by the Maritime Access Division of the Flemish Ministry of Mobility and Public Works) and the Scheldt Applied Research Programme of Deltares. We acknowledge the following agencies, ministries and institutes for providing the observational data: Flemish Ministry of Mobility and Public Works (wave, currents, water elevation), Dutch Ministry of Public Works (currents, water elevation, bathymetry, salinity), the Royal Belgian Institute of Natural Sciences (in situ and remote sensing suspended sediment concentrations) and the Royal Dutch Meteorological Institute (KNMI, for wind data). Three anonymous reviewers are acknowledged for their critical comments,

which have led to a significant improvement of the manuscript.

References

Adriaens, R., Zeelmaekers, E., Fettweis, M., Vanlierde, E., Vanlede, J., Stassen, P., Elsen, J., Środoń, J., Vandenberghe, N., 2018. Quantitative clay mineralogy as provenance indicator for recent muds in the southern North Sea. Mar. Geol. https://doi.org/10.1016/j.margeo.2017.12.011.

Allen, G.P., Salmon, J.C., Bassoullet, P., Du Penhoat, Y., De Grandpre, C., 1980. Effects of tides on mixing and suspended sediment transport in macrotidal estuaries. Sed Geol 26, 69–90.

Bastin, A., 1974. Regionale sedimentologie en morfologie van de zuidelijke Noordzee en van het Schelde estuarium. Ph.D. Thesis. Geography-Geology Department, Katholieke Universiteit Leuven, Belgium.

Beardsley, R.C., Limeburner, R., Yu, H., Cannon, G.A., 1985. Discharge of the Changjiang (Yangtze River) into the East China Sea. Cont. Shelf Res. 4 (1–2), 57–76.

Booij, N., Ris, R.C., Holthuisen, L.H., 1999. A third-generation wave model for coastal regions: 1. Model description and validation. J. Geophys. Res. 104, 7649–7666.

Burchard, H., Flöser, G., Staneva, J.V., Badewien, T.H., Riethmüller, R., 2008. Impact of density gradients on Net Sediment Transport into the Wadden Sea. J. Phys. Oceanogr. 38, 566–587.

Burchard, H., Schuttelaars, H.M., Ralston, D.K., 2018. Sediment trapping in estuaries. Annu. Rev. Mar. Sci. 10, 371–395. https://doi.org/10.1146/annurev-marine-010816-060535.

De Boer, G.J., Pietrzak, J.D., Winterwerp, J.C., 2009. SST observations of upwelling induced by tidal straining in the Rhine ROFI. Cont. Shelf Res. 29, 263–277. https://doi.org/10.1016/j.csr.2007.06.011.

De Maerschalck, B., Vanlede, J., 2013. Zeebrugge harbour sediment transport model. In: Bonneton, P. (Ed.), Extended Abstracts of Coastal Dynamics 2013: Coastal Dynamics Research Emphasizing Practical Applications, pp. 477–486.

de Nijs, M.J., Pietrzak, J.D., 2012. Saltwater intrusion and ETM dynamics in a tidally-energetic stratified estuary. Ocean Modell 49 (2012), 60–85. https://doi.org/10.1016/j.ocemod.2012.03.004.

Dijkstra, Y.M., Schuttelaars, H.M., Schramkowski, G.P., Brouwer, R.L., 2019. Modeling the transition to high sediment concentrations as a response to channel deepening in the Ems River Estuary. Journal of Geophysical Research: Oceans 124. https://doi.org/10.1029/2018JC014367.

Dronkers, J., 2005. Natural and Human Impacts on Sedimentation in the Wadden Sea: An Analysis of Historical Data. Unpublished report by. the Dutch Ministry of Public Works (47 p).

Dyer, K.R., 1994. Estuarine sediment transport and deposition. In: Pye, K. (Ed.), Sediment Transport and Depositional Processes. Blackwell Scientific Publications, Oxford, pp. 193–218.

Dyer, K.R., Bale, A.J., Christie, M.C., Feates, N., Jones, S., Manning, A.J., 2002. The turbidity maximum in a mesotidal estuary, the Tamar Estuary, UK. Part I: dynamics of suspended sediment. In: Winterwerp, J.C., Kranenburg, C. (Eds.), Fine Sediment Dynamics in the Marine Environment: Proc. in Marine Science 5. Elsevier, Amsterdam, 0-444-51136-9, pp. 203–218.

Eisma, D., Irion, G., 1988. Suspended matter and sediment transport. In: Salomons, W., Bayne, W.L., Duursma, E.K., Forstner, U. (Eds.), Pollution of the North Sea: An Assessment. Springer, Berlin, pp. 20–35.

Fettweis, M., Baeye, M., 2015. Seasonal variation in concentration, size, and settling velocity of muddy marine flocs in the benthic boundary layer. J. Geophys. Res. Oceans 120, 5648–5667. https://doi.org/10.1002/2014JC010644.

Fettweis, M., Van den Eynde, D., 2003. The mud deposits and the high turbidity in the Belgian–Dutch coastal zone, Southern bight of the North Sea. Cont. Shelf Res. 23, 669–691.

Fettweis, M., Sas, M., Monbaliu, J., 1998. Seasonal, neap- spring and tidal variation of cohesive sediment concentration in the Scheldt Estuary, Belgium. Estuar. Coast. Shelf Sci. 47, 21–36.

Fettweis, M., Francken, F., Pison, V., Van den Eynde, D., 2006. Suspended particulate matter dynamics and aggregate sizes in a high turbidity area. Mar. Geol. 235, 63–74.

Fettweis, M., Nechad, B., Van den Eynde, D., 2007. An estimate of the suspended particulate matter (SPM) transport in the southern North Sea using SeaWiFS images, in situ measurements and numerical model results. Cont. Shelf Res. 27, 1568e1583.

Fettweis, M., Houziaux, J.-S., Du Four, I., Van Lancker, V., Baeteman, C., Mathys, M., Van den Eynde, D., Francken, F., Wartel, S., 2009a. Long-term influence of maritime access works on the distribution of cohesive sediment: analysis of historical and recent data from the Belgian nearshore area (southern North Sea). Geo-Mar. Lett. 29, 321–330.

Fettweis, M., Van den Eynde, D., Francken, F., Van Lancker, V., 2009b. MOnitoring en MOdellering van het cohesieve sedimenttransport en evaluatie van de effecten op het mariene ecosysteem ten gevolge van bagger- en stortoperatie (MOMO). (Rapport MOMO/4/MF/200912/NL/AR/2, 31 p).

Fettweis, M., Francken, F., Van den Eynde, D., Verwaest, T., Janssens, J., Van Lancker, V., 2010. Storm influence on SPM concentrations in a coastal turbidity maximum area with high anthropogenic impact (southern North Sea). Cont. Shelf Res. 30, 1417–1427.

Fettweis, M., Baeye, M., Francken, F., Lauwaert, B., Van den Eynde, D., Van Lancker, V., Martens, C., Michielsen, T., 2011. Monitoring the effects of disposal of fine sediments from maintenance dredging on suspended particulate matter concentration in the Belgian nearshore area (southern North Sea). Mar Poll Bull 62, 258–268. https://doi.org/10.1016/j.marpolbul.2010.11.002.

Fettweis, M., Baeye, M., Cardoso, C., Dujardin, A., Lauwaert, B., Van den Eynde, D., Van Hoestenberghe, T., Vanlede, J., Van Poucke, L., Velez, C., Martens, C., 2016. The impact of disposal of fine grained sediments from maintenance dredging works on SPM concentration and fluid mud in and outside the harbor of Zeebrugge. Ocean Dyn. 66, 1497–1516.

Friedrichs, C.T., Armbrust, B.A., de Swart, H.E., 1998. Hydrodynamics and equilibrium sediment dynamics of shallow, funnel-shaped tidal estuaries. In: Dronkers, J., Scheffers, M. (Eds.), Physics of Estuaries and Coastal Seas. Balkema, Rotterdam, pp. 315–328.

Gibson, R.E., England, G.L., Hussey, M.J.L., 1967. The theory of one-dimensional consolidation of saturated clays. Geotechnique 17 (3), 261–273.

Grasso, F., Verney, R., Le Hir, P., Thouvenin, B., Schulz, E., Kervella, Y., Khojasteh Pour Fard, I., Lemoine, J.-P., Dumas, F., Garnier, V., 2018. Suspended sediment dynamics in the macrotidal seine estuary (France). 1. Numerical modeling of turbidity maximum dynamics. J Geophys Res Oceans 123 (1), 558–577.

Hasselman, S., Hasselman, K., Allender, J.H., Barnett, T.P., 1985. Computations and parameterizations of the linear energy transfer in a gravity wave spectrum: II. Parameterization of the nonlinear transfer for application in wave models. J. Phys. Oceanogr. 15, 1378–1391.

Hesse, R.F., Zondt, A., Fröhle, P., 2019. Modelling dynamics of the estuarine turbidity maximum and local net deposition. Ocean Dyn. https://doi.org/10.1007/s10236-019-01250-w.

Hill, P.S., Voulgaris, G., Trowbridge, J.H., 2001. Controls on floc size in a continental shelf bottom boundary layer. J. Geophys. Res. 106 (C5), 9543–9549.

Howarth, M.J., Dyer, K.R., Joint, I.R., Hydes, D.J., Purdie, D.A., Edmunds, H., Jones, J.E., Lowry, R.K., Moffat, T.J., Pomroy, A.J., Proctor, R., 1993. Seasonal cycles and their spatial variability. Philos. Trans. R. Soc. London A 343, 383–403.

Irion, G., Zollmer, V., 1999. Clay mineral associations in fine grained surface sediments of the North Sea. J. Sea Res. 41, 119–128.

Jago, C.F., Kennaway, G.M., Novarino, G., Jones, S.E., 2007. Size and settling velocity of suspended flocs during a phaeocystis bloom in the tidally stirred Irish Sea, NW European Shelf. Mar. Ecol. Prog. Ser. 345, 51–62. https://doi.org/10.3354/meps07006.

Jay, D.A., Musiak, J.D., 1994. Particle trapping in estuarine tidal flows. J. Geophys. Res. 99, 445–461.

Kineke, G.C., Sternberg, R.W., Trowbridge, J.H., Geyer, W.R., 1996. Fluid-mud processes on the Amazon continental shelf. Cont. Shelf Res. 16 (Issues 5–6), 667–696. ISSN 0278-4343. https://doi.org/10.1016/0278-4343(95)00050-X.

Kornman, B.A., De Deckere, E.M.G.T., 1998. Temporal variation in sediment erodibility and suspended sediment dynamics in the Dollard estuary. In: Black, K.S., Paterson, D.M., Cramp, A. (Eds.), Sedimentary Processes in the Intertidal Zone. Geological Society London Special Publications, vol. 139. pp. 231–241.

Krone, R.B., 1962. Flume Studies of the Transport of Sediment in Estuarial Shoaling Processes. Final Report. Hydraulic Engineering Laboratory and Sanitary Engineering Research Laboratory. University of California, Berkeley.

Lacroix, G., Lancelot, C., Ruddick, K., Spitz, Y., Gypens, N., 2004. Modelling the Relative Impact of the Rivers Scheldt, Rhine, Meuse and Seine on the Availability of Nutrients in Belgian Waters (Southern North Sea) Using the 3D Coupled Physical-Biological Model MIRO&CO-3D. ICES CM 2004/P:08. (2004). ICES Annual Sciences Conference (ASC), Vigo, Spain, pp. 22–25 22-25 September 2004.

Lafite, R., Shimwell, S.J., Nash, L.A., Dupont, J.P., Huault, M.F., Grochowski, N.T.L., Lamboy, J.M., Collins, M.B., 1993. Sub-Task S1: suspended material fluxes through the Strait of Dover, hydrodynamics and biogeochemical fluxes in the Eastern Channel: fluxes into the North Sea. In: FLUXMANCHE I Second Annual Report, MAST 0053-C (EDB), pp. 81–106.

Lerczak, J.A., Geyer, W.R., 2004. Modeling the lateral circulation in straight, stratified estuaries. J. Phys. Oceanogr. 34, 1410–1428.

Lesser, G.R., Roelvink, J.A., Van Kester, J.A.T.M., Stelling, G.S., 2004. Development and validation of a three-dimensional morphological model. Coast. Eng. 51, 883–915.

Malarkey, J., Baas, J.H., Hope, J.A., Aspden, R.J., Parsons, D.R., Peakall, J., Paterson, D.M., Schindler, R.J., Ye, L., Lichtman, I.D., Bass, S.J., Davies, A.G., Manning, A.J., Thorne, P.D., 2015. The pervasive role of biological cohesion in bedform development. Nat. Commun. https://doi.org/10.1038/ncomms7257.

Manning, A.J., Dyer, K.R., 2007. Mass settling flux of fine sediments in northern European estuaries: measurements and predictions. Mar. Geol. 245, 107–122.

Manning, A.J., Bass, S.J., Dyer, K.R., 2007. Preliminary findings from a study of the upper reaches of the Tamar Estuary, UK, throughout a complete tidal cycle: Part II. In-situ floc spectra observations. In: Maa, J.P.-Y., Sanford, L.P., Schoellhamer, D.H. (Eds.), Coastal and Estuarine Fine Sediment Processes: Proc. in Marine Science 8. Elsevier, Amsterdam, 0-444-52238-7, pp. 15–33.

Manning, A.J., Baugh, J.V., Spearman, J., Whitehouse, R.J.S., 2010. Flocculation settling characteristics of mud:sand mixtures. Ocean Dyn. https://doi.org/10.1007/s10236-009-0251-0.

Manning, A.J., Baugh, J.V., Spearman, J.R., Pidduck, E.L., Whitehouse, R.J.S., 2011. The settling dynamics of flocculating mud:sand mixtures: part 1 – empirical algorithm development. In: Ocean Dynamics, INTERCOH 2009 Special Issue, https://doi.org/10.1007/s10236-011-0394-7.

McManus, J.P., Prandle, D., 1997. Development of a model to reproduce observed suspended sediment distributions in the southern North Sea using principal component analysis and multiple linear regression. Cont. Shelf Res. 17, 761–778.

McSweeney, J.M., Chant, R., Sommerfield, C.K., 2016. Lateral variability of sediment transport in the Delaware Estuary. Journal of Geophysical Research: Oceans 121, 725–744. https://doi.org/10.1002/2015 JC010974.

Mehta, A.J.A., Manning, J., Khare, Y.P., 2014. A note on the Krone deposition equation and significance of floc aggregation. Mar. Geol. 354, 34–39.

Mietta, F., Chassagne, C., Winterwerp, J.C., 2009. Shear-induced flocculation of a suspension of kaolinite as function of pH and salt concentration. J. Colloid Interface Sci. 336, 134–141.

Milliman, J.D., Syvitski, J.P.M., 1992. Geomorphic/tectonic control of sediment discharge to the ocean: the importance of small mountainous rivers. The Journal of Geology 100, no 5 (September), 525–544. https://doi.org/10.1086/629606.
Mitchener, H.J., Torfs, H., Whitehouse, R.J.S., 1996. Erosion of mud/sand mixtures. Coast. Eng. 29, 1–25.
Nechad, B., Ruddick, K., Park, Y., 2010. Calibration and validation of a generic multisensor algorithm for mapping of total suspended matter in turbid waters. Remote Sens. Environ. 114, 854–866.
Nihoul, J.C.J., 1975. Effect of tidal stress on residual circulation and mud deposition in the Southern Bight of the North Sea. Review of Pure and Applied Geophysics 113, 577–581.
Oreskes, N., Shrader-Frechette, K., Belitz, K., 1994. Verification, validation, and confirmation of numerical models in the earth sciences. Science 263 (5147), 641–646.
Parsons, D.R., Schindler, R.J., Hope, J.A., Malarkey, J., Baas, J.H., Peakall, J., Manning, A.J., Ye, L., Simmons, S., Paterson, D.M., Aspden, R.J., Bass, S.J., Davies, A.G., Lichtman, I.D., Thorne, P.D., 2016. The role of biophysical cohesion on subaqueous bed form size. Geophys. Res. Lett. 43. https://doi.org/10.1002/2016GL067667.
Paterson, D.M., Hagerthey, S.E., 2001. Microphytobenthos in contrasting coastal ecosystems: biology and dynamics. In: Reise, K. (Ed.), Ecological Comparisons of Sedimentary Shores. Ecological studiespp. 105–125.
Postma, H., 1967. Sediment transport and sedimentation in the estuarine environment. In: Lauff, G.H. (Ed.), Estuaries, American Association for the Advancement of Science Special Publication. vol. 83. pp. 158–179.
Ralston, D.K., Geyer, W.R., Warner, J.C., 2012. Bathymetric controls on sediment transport in the Hudson River estuary: lateral asymmetry and frontal trapping. J. Geophys. Res. 117, C10013. https://doi.org/10.1029/2012JC008124.
Refsgaard, J.C., van der Sluijs, J.P., Brown, J., van der Keur, P., 2006. A framework for dealing with uncertainty due to model structure error. Adv. Water Resour. 29 (11), 1586–1597. https://doi.org/10.1016/j.advwatres.2005.11.013. ISBN 0309-1708.
Richardson, J.F., Zaki, W.N., 1954. Sedimentation and fluidization—part I. Trans., Inst. Chem. Engng. 32, 35–53.
Safak, I., Allison, M.A., Sheremet, A., 2012. Floc variability under changing turbulent stresses and sediment availability on a wave-energetic muddy shelf. Cont. Shelf Res. https://doi.org/10.1016/j.csr.2012.11.015.
Simpson, J.H., Brown, J., Matthews, J., Allen, G., 1990. Tidal straining, density currents, and stirring in the control of estuarine stratification. Estuaries 13 (2), 125–132.
Spearman, J., Manning, A.J., 2008. On the significance of mud transport algorithms for the modelling of intertidal flats. In: Kudusa, T., Yamanishi, H., Spearman, J., Gailani, J.Z. (Eds.), Sediment and Ecohydraulics - Proc. in Marine Science 9. Elsevier, Amsterdam, 978-0-444-53184-1, pp. 411–430.
Toublanc, F., Brenon, I., Coulombier, T., 2016. Formation and structure of the turbidity maximum in the macrotidal Charente estuary (France): influence of fluvial and tidal forcing. Estuar. Coast. Shelf Sci. 169, 1–14. https://doi.org/10.1016/j.ecss.2015.11.019.
Uusitalo, L., Lehikoinen, A., Helle, I., Myrberg, K., 2015. An overview of methods to evaluate uncertainty of deterministic models in decision support. Environ. Model. Softw. 63, 24–31.
Van Alphen, J.S.L.J., 1990. A mud balance for Belgian–Dutch coastal waters between 1969 and 1986. Neth. J. Sea Res. 25, 19–30.
Van der Hout, C.M., Gerkema, T., Nauw, J.J., Ridderinkhof, H., 2015. Observations of a narrow zone of high suspended particulate matter (SPM) concentrations along the Dutch coast. Cont. Shelf Res. 95, 27–38. https://doi.org/10.1016/j.csr.2015.01.
van der Hout, C.M., Duineveld, G.C.A., Rozemeijer, M.J.C., Bergman, M.J.N., Duineveld, G.C.A., Rozemeijer, M.J.C., Gerkema, T., 2017. Dynamics of suspended particulate matter (SPM) and chlorophyll-a from intratidal to annual time scales in a coastal turbidity maximum. J. Sea Res. 127 (September 2017), 105–118.
van der Wegen, M., Jaffe, B.E., 2013. Towards a probabilistic assessment of process-based, morphodynamic models. Coast. Eng. 75 (2013), 52–63.
Van Kessel, T., van Maren, D.S., 2013. Far-field and long-term dispersion of released dredged material. In: Proceedings of the XXth WODCON Conference, (9p).
Van Kessel, T., Vanlede, J., 2009. Impact of harbour basins on mud dynamics in the Scheldt estuary. In: Deltares & Flanders Hydraulics Report No. 1200253, Delft, the Netherlands.
Van Kessel, T., Winterwerp, J.C., van Prooijen, B., van Ledden, M., Borst, W., 2011a. Modelling the seasonal dynamics of SPM with a simple algorithm for the buffering of fines in a sandy seabed. Cont. Shelf Res. 31, S124–S134. https://doi.org/10.1016/j.csr.2010.04.008.
Van Kessel, T., Vanlede, J., de Kok, J.M., 2011b. Development of a mud transport model for the Scheldt estuary. Cont. Shelf Res. 31, S165–S181. https://doi.org/10.1016/j.csr.2010.12.006.
van Ledden, M., van Kesteren, W.G.M., Winterwerp, J., 2004. A conceptual framework for the erosion behaviour of sand-mud mixtures. Cont. Shelf Res. 24 (1), 1–11.
van Maren, D.S., Cronin, K., 2016. Uncertainty in complex three-dimensional sediment transport models: equifinality in a model application of the Ems Estuary, the Netherlands. Ocean Dyn. https://doi.org/10.1007/s10236-016-1000-9.
van Maren, D.S., van Kessel, T., Cronin, K., Sittoni, L., 2015a. The impact of channel deepening and dredging on estuarine sediment concentration. Cont. Shelf Res. 95, 1–14. https://doi.org/10.1016/j.csr.2014.12.010.
van Maren, D.S., Winterwerp, J.C., Vroom, J., 2015b. Fine sediment transport into the hyperturbid lower Ems River: the role of channel deepening and sediment-induced drag reduction. Ocean Dyn. https://doi.org/10.1007/s10236-015-0821-2.
van Maren, D.S., Oost, A.P., Wang, Z.B., Vos, P.C., 2016. The effect of land reclamations and sediment extraction on the suspended sediment concentration in the Ems Estuary. Mar. Geol. 376, 147–157.
Van Mierlo, C.-J., 1899. La carte lithologique de la partie méridionale de la mer du Nord. In: Bulletin de la Société Belge de Géologie, Paléontologie et Hydrologie, XII, 2i e me série III, pp. 219–265.
Van Prooijen, B.C., Winterwerp, J.C., 2010. A stochastic formulation for erosion of cohesive sediments. J. Geophys. Res. 115, C01005. https://doi.org/10.1029/2008JC005189.
van Rijn, L.C., 2007a. A unified view of sediment transport by currents and waves. Part I: initiation of motion, bed roughness and bed load transport. J. Hydraul. Eng. 133 (6), 649–667.
van Rijn, L.C., 2007b. A unified view of sediment transport by currents and waves. Part II: suspended transport. J. Hydraul. Eng. 133 (6), 668–689.
Vanlede, J., Dujardin, A., 2014. A geometric method to study water and sediment exchange in tidal harbors. Ocean Dyn. 64 (2014), 1631–1641. https://doi.org/10.1007/s10236-014-0767-9.
Velegrakis, A.F., Bishop, C., Lafite, R., Oikonomou, E.K., Lecouturier, M., Collins, M.B., 1997. Sub-Task S3: Investigation of Meso- and Macro-Scale Sediment Transport, Hydrodynamics Biogeochemical Processes and Fluxes in the Channel. FLUXMANCHE II Final Report, MAST II, MAS2CT940089. pp. 128–143.
Vroom, J., Schrijvershof, R., 2015. Summary of Human Interventions in the Western Scheldt and Mouth Area in the Period 1985–2014 (in Dutch). Deltares Report 1210301–001-ZKS-0005. (40 p).
Walker, W.E., Harremoes, P., Rotmans, J., van der Sluijs, J.P., van Asselt, M.B.A., Janssen, P., Krayer von Kross, M.P., 2003. Defining uncertainty. A conceptual basis for uncertainty mangement in model-based decision support. Integr. Assess. 4 (1), 5–17.
Wang, Y.P., Voulgaris, G., Li, Y., Yang, Y., Gao, J., Chen, J., Gao, S., 2013. Sediment resuspension, flocculation, and settling in a macrotidal estuary. J. Geophys. Res. Oceans 118, 5591–5608. https://doi.org/10.1002/jgrc.20340.
Widdows, J., Friend, P.L., Bale, A.J., Brinsley, M.D., Pope, N.D., Thompson, C.E.L., 2007. Inter-comparison between five devices for determining erodibility of intertidal sediments. Cont. Shelf Res. 27, 1174–1189.
Winterwerp, J.C., 2001. Stratification effects by cohesive and non-cohesive sediment. Journal of Geophys Research 106 (C10), 22,559–22,574.
Winterwerp, J.C., 2006. Stratification effects by fine suspended sediment at low, medium and very high concentrations. J. Geophys. Res. 111. https://doi.org/10.1029/2005JC003019.
Winterwerp, J.C., 2007. On the deposition flux of cohesive sediment. In: Maa, J., Sanford, L., Schoelhamer, D. (Eds.), Proceedings of the 8th International Conference on Nearshore and Estuarine Cohesive Sediment Transport Processes, INTERCOH-2003, Gloucester Point, USA, pp. 209–226.
Winterwerp, J.C., van Kessel, T., 2003. Siltation by sediment-induced density currents. Ocean Dyn. 53, 186–196.
Winterwerp, J.C., Wang, Z.B., 2013. Man-induced regime shifts in small estuaries – I: theory. Ocean Dyn. 63 (11–12), 1279–1292.
Winterwerp, J.C., Wang, Z.B., van Braeckel, A., van Holland, G., Kösters, F., 2013. Man-induced regime shifts in small estuaries – I: a comparison of rivers. Ocean Dyn. 63 (11–12), 1293–1306.
Zijl, F., Verlaan, M., Gerritsen, H., 2015. Improved water-level forecasting for the Northwest European Shelf and North Sea through direct modelling of tide, surge and non-linear interaction. Ocean Dyn. 63, 823–847.